AR-R.1166 ISSUE A

(2)

MODAL TEST OF SIMULATED SOLAR ARRAY

SPAR

SPAR-R.1166 **ISSUE** A

(2)

MODAL TEST OF SIMULATED SOLAR ARRAY

PREPARED BY S. Draisey and M. Elzeki

REASON FOR RE-ISSUE _____

DATE October, 1983

APPROVALS

P.J. Smith Group Leader Structures P.J. Smith
A.S. Jones Manager, Mechanical Engineering
F. Koop Manager Product Design F. Koop
P.A. McIntyre P.A. McIntyre Director, Engineering

AMENDMENTS

NUMBER	REASON FOR AMENDMENT	SIGNATURE	DATE

Spar Aerospace Limited
Remote Manipulator Systems Division
1700 Ormont Drive, Weston, Ontario, Canada M9L 2W7

SPAR Space & Electronics Group

TEL (416) 745-9680 TELEX 065-27360 SPARORM TOR TWX 610-491-1503 CABLE-SPARORM TOR

Government of Canada / Gouvernement du Canada

Department of Communications

DOC CONTRACTOR REPORT DOC-CR-SP-83-057

DEPARTMENT OF COMMUNICATIONS - OTTAWA - CANADA

SPACE PROGRAM

TITLE: MODAL TEST OF SIMULATED SOLAR ARRAY

AUTHOR(S): S. Draisey

ISSUED BY CONTRACTOR AS REPORT NO:

PREPARED BY: SPAR AEROSPACE LIMITED
Remote Manipulator Systems Division
1700 Ormont Drive
Weston, Ontario
M9L 2W7

DEPARTMENT OF SUPPLY AND SERVICES CONTRACT NO: 01ST.36001-2-1794
Serial No. 1ST82-00137

DOC SCIENTIFIC AUTHORITY: F.R. Vigneron

CLASSIFICATION: Unclassified

DATE:

TABLE OF CONTENTS

TABLE OF CONTENTS - continued

TABLE OF CONTENTS - continued

LIST OF SYMBOLS

This list includes only the symbols used in the report, which are not defined within the text.

c	damping
C_{CR}	critical damping
f	frequency, Hz
g	gravitational acceleration
k	stiffness
m	mass
p	load
t	time
v	output displacement
$\ddot{v}_b$	base acceleration
w	frequency, rad/sec
x	input displacement
y	output displacement
Y	generalized coordinate, output displacement
ζ	damping ratio C/C_{CR}
ϕ	phase angle
ϕ_n	mode shape of mode n
ν	kinematic viscosity

LIST OF FIGURES

LIST OF FIGURES - continued

LIST OF TABLES

LIST OF TABLES - continued

ABSTRACT

MODAL TEST OF A SIMULATED SOLAR ARRAY

by

S. Draisey

This report describes the design and test of structure similar to a deployed flexible solar array.

The testing consisted mainly of modal analysis testing of the simulated array in vacuum and in air. Three excitation techniques were used-base sine, base random and step relaxation.

To compile complete natural frequency information for all modes, all three excitation frequency response functions were required. The mode shape information obtained from the testing was not sufficient to define all modes, mainly because, not enough points on the structure were instrumented to sufficiently define the geometry (insufficient degrees of freedom).

In addition to modal testing, a damper unit was designed and built to increase array damping characteristics. The damper unit did not perform well on the simulated array model, because the unit was too rigid to allow the stroke necessary for damping.

1.0 INTRODUCTION

The work described in this report has been funded under DSS Contract OIST.36001-2-1794, S/N 82-00137 and covers the objectives described in Spar Proposal P.879, Issue B (Ref. 9). In summary, the objectives included:

(a) Developing and assessing the modal analysis test method, based on the software resident in the David Florida Laboratory (Structural Dynamics Research Corporation, Modal Plus, Version 7, see Ref: 10).

(b) Demonstrate methods to alter damping and frequency characteristics of a solar array type structure.

(c) Measure frequency, mode shapes and damping of a large flexible, lightweight structure - a solar array.

(d) Compare measured data to mathematical model.

A similar exercise to the one reported here was undertaken to test the Hermes solar array (Refs: 3 and 6). At that time, modal analysis was not available, so this report constitutes an exercise in upgrading solar array testing techniques.

Deployable solar arrays are becoming widely accepted as the means of powering satellites that need large amounts of energy over many years. Power levels of current generation spacecraft are in the area of 2 kilowatts, with 8 kilowatt arrays already on drawing boards. As power level requirements climb, so do array sizes. To optimize the design of future arrays, more detailed knowledge of their behaviour becomes necessary.

Solar arrays can be divided into two structural groups. One is known as a rigid panel array, the other a flexible array. For the purposes of this study, solar array implies a flexible solar array. A flexible solar array is a solar blanket (kapton sheet, with solar cells covering it) tensioned between two panels which are deployed and supported by some form of boom or mast.

The normal operating environment of a deployed solar array cannot be achieved on earth. The vacuum environment can be simulated on earth, for moderately sized structures. Solar arrays are rapidly outgrowing these size constraints, so that vacuum testing is not possible for most arrays being built today. The zero gravity environment cannot be achieved, in all directions, simultaneously. As arrays continue to get larger and heavier, their ability to support themselves in our 1-G environment decreases. Obtaining accurate test results in a 1-G environment becomes more difficult as structural mass increases. At the

same time, the vibration levels that the arrays can withstand and are to see in space must decrease to very low levels. To input, control or measure such small vibration levels is very difficult.

The objective in this study of lightwight spacecraft structures was to design and test a model of a solar array which represents many of the structural properties of an actual solar array. The model was such that some of its parameters could be varied slightly. In particular, the effects of introducing additional damping into the structure were to be examined.

Flexible structures have high sensitivities to any added mass or stiffness (such as accelerometers, or their cables). They are also very sensitive to acceleration or displacements levels. For this reason, they present a special class of testing problems. A variety of test methods have been examined in this study to establish an appropriate technique for such structures.

Modal analysis is based on linear theory. A flexible, tensioned solar array is not a linear structure. It is the intent of this study to determine the linearized structural characteristics of a solar array and the applicability of modal analysis techniques in this area.

Of the four objectives described in the proposal, it was only possible to completly satisfy the first. Attempts to alter the frequency and damping characteristics of the structure did not lead to improvements, due to problems with vacuum approval of the damping device and a conflict between relative motion (required to generate damping force) and structural stiffness. The frequencies, modes shapes and damping of the array were measured but the mode shapes are poorly defined (time constraints limited the number of accelerometer locations) and the damping values show large scatter. Comparisons between measured and mathematical model data have been made, but the mathematical modelling had not been completed at the time this report was written.

The two most important factors to realize for future testing are that mathematical modelling should be completed prior to testing and more testing degrees of freedom are necessary to adequately define the mode shapes. Mathematical modelling is important for linear structures. For non-linear structures, an understanding of the type of non-linear nature is even more important.

This report describes the simulated solar array model and damper which was built for the test. The hardware and software which was used to do the testing as well as method and results of the various test techniques is outlined. A brief theoretical development of modal analysis is included to provide an understanding of the software objectives and potential improvements.

Just prior to the testing done for this contract, a similar test, on an astromast, was done by CRC personnel. The results which were pertinent to the array test are included as background.

2.0 DESCRIPTION OF HARDWARE AND OVERALL TEST CONFIGURATION

The test article, referred to known as the solar array consisted of three main components: the astromast, the solar blanket and the tension damper rod. There were two different tension damper rods used in testing. The tension damper rod was a new concept in flexible solar array design. For that reason, it is described in more detail than the other components, in Section 2.2.

2.1 Solar Array

Figure 2.1.1 shows the solar array configuration. The array consists of three main components, the astromast, the tension damper rod (for details, Section 2.2) and the solar blanket. The astromast (purchased from Astro Research) is a 9 inch diameter, fibreglass beam-like structure 20 feet long. It is made up of an arrangement of longerons (3, running parallel to the longitudinal axis, each with a 120° twist from base to tip), batons (joining longerons in triangular formation, dividing the structure into 'bays') and diagonals (crossing each external face of a bay, inducing the compression in the batons which provides additional stiffness characteristics to the structure). Figure 2-1.2 depicts two bays of the astromast, with an accelerometer mount. A more detailed treatment of the astromast static and dynamic characteristics is covered in Reference 1.

The solar blanket is made up of a kapton sheet (4' x 20'), two aluminum tube hanger rods and attachment brackers. The solar blanket is tensioned (to provide geometric stiffness) by the tension damper rod. The array was tested with two different levels of tension; 3.3 lb and 4.6 lb. The tension levels in the blanket were measured by a load cell (Interface SM-50) installed between the tip hanger rod and the tension damper rod. The tension level in the blanket was the sum of the load cell reading and the weight of components between it and the blanket. The actual tension in the blanket was not constant over its length, due to the effects of gravity. The quoted value is a minimum. The solar array was mounted for testing in a vertical position, with the tip at the bottom. Thus the tension level at the base of the blanket is the quoted value plus the weight of the blanket.

Table 2-1.1 lists the structural characteristics of the solar array components.

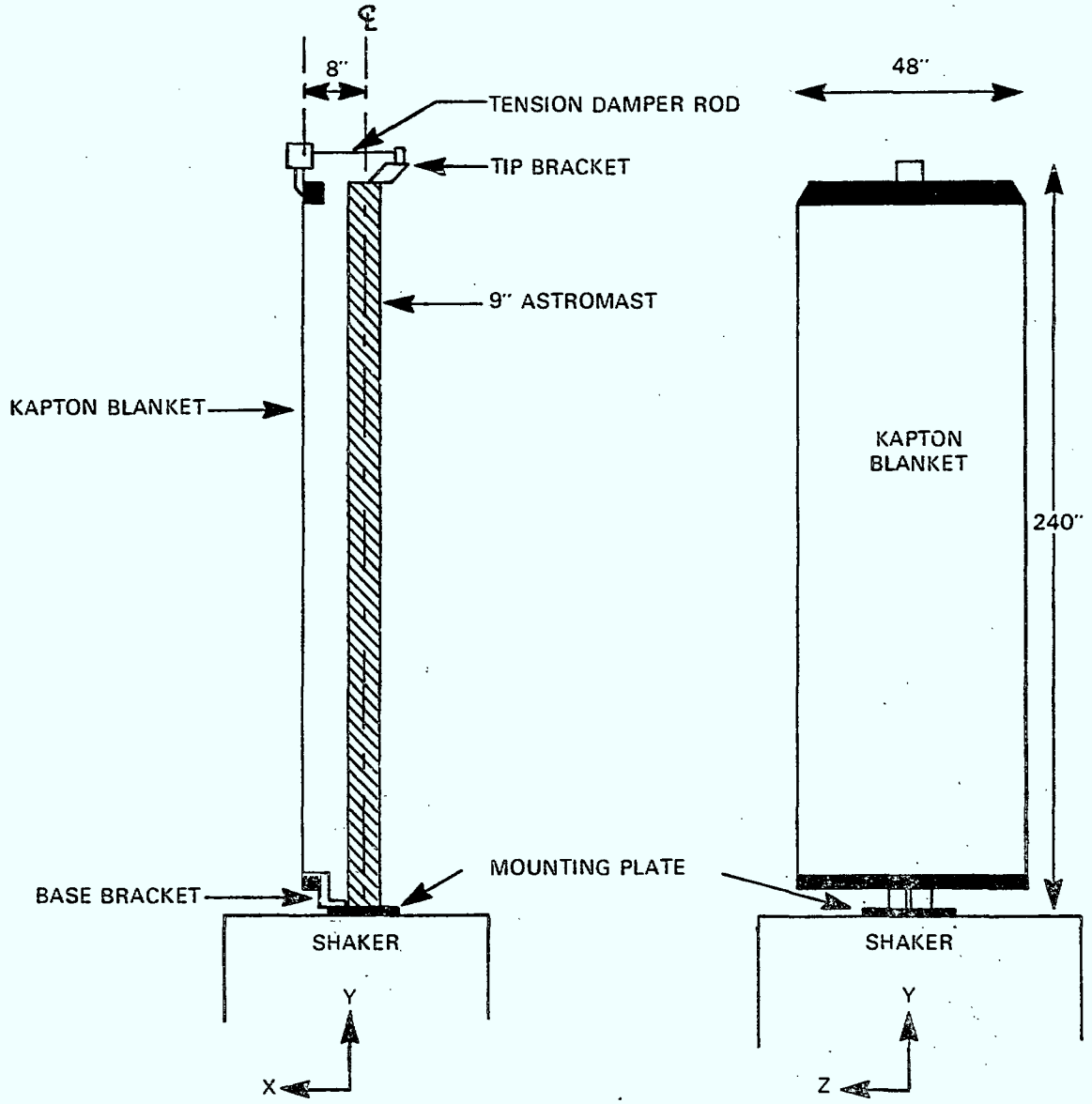

FIGURE 2-1.1 SOLAR ARRAY CONFIGURATION

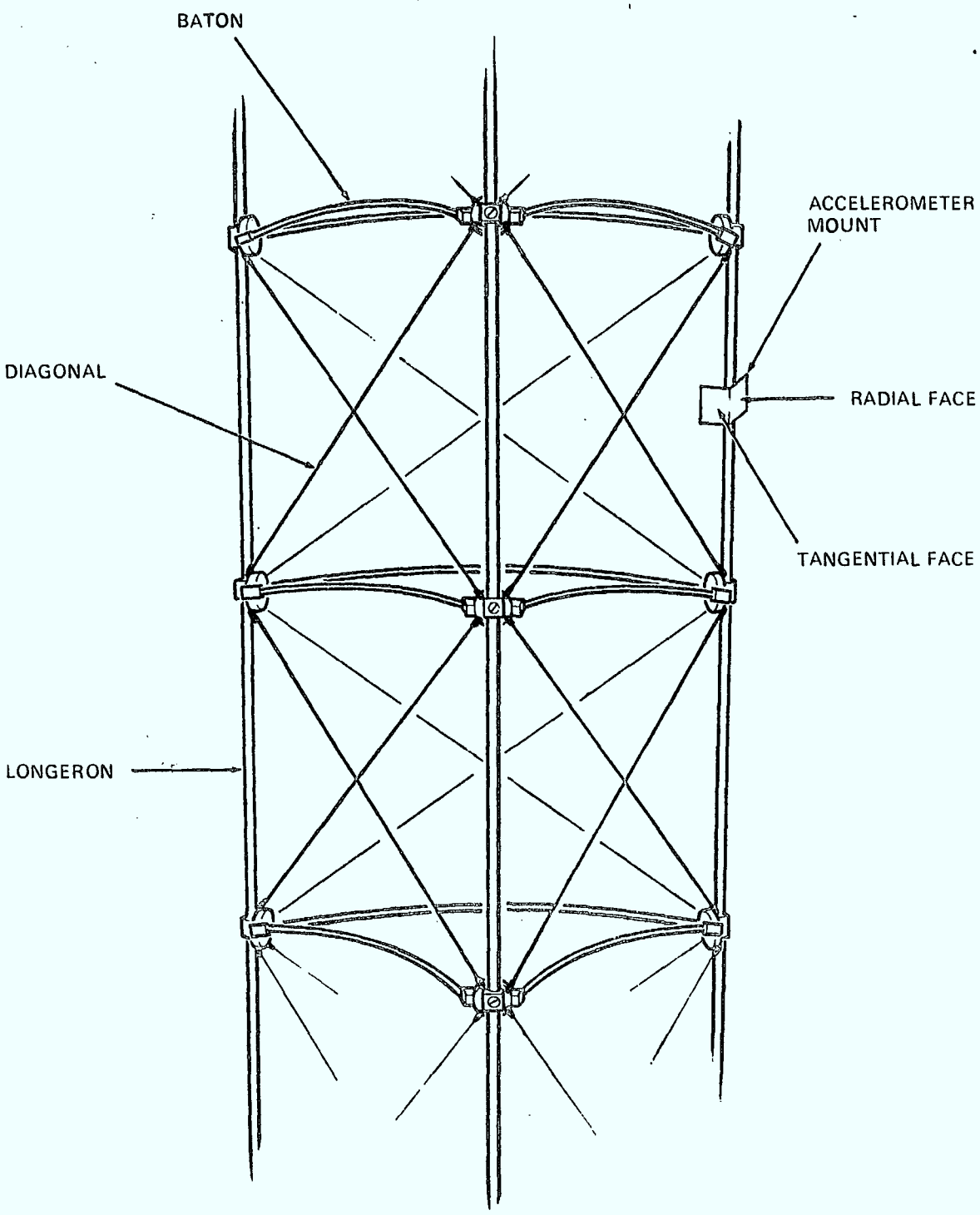

FIGURE 2.1.2 ASTROMAST BAYS

TABLE 2-1.1

ITEM	WEIGHT	LENGTH	STIFFNESS
Astromast + Top Plate	4.0 lb	240"	1.5 lb/in
Hanger Rods	4.06 lb	48"	521 lb/in
TDR and Brackets	2.33 lb or 3.04 lb	N/A	28 lb/in or 40 lb/in
Kapton Blanket	2.72 lb	240"	N/A

2.2 TDR Design Concept and Hardware

2.2.1 Damping Advantages -The ability to control large flexible structures in space is dependent on the damping characteristics. Solar arrays are an example of a difficult control problem. Although the array mass is small compared to the spacecraft total mass, its geometry means that it has a large moment of inertia about the spacecraft centroid. For this reason, the array motions have a considerble effect on the reaction control system (RCS).

Designs of solar arrays aim for high minimum natural frequencies to minimize the vibration strain energy. These frequency requirements often result in higher mass and increased costs (e.g., use of advanced materials). These requirements, however, can be relaxed if the strain energy imparted to the structure during attitude control manoeuvres can be quickly suppressed by damping. Thus an improvement in solar array damping will result in lighter structures and possibly allow for increased flexibility in future space structures.

2.2.2 Damping Options and the Selected Design -In this contract, an initial step towards damping improvement has been attempted. A damper has been designed and integrated on a solar array test model. The intension of the device was to increase damping without significantly reducing the structure's natural frequencies or increasing its mass.

2.2.2.1 Damper Position -The structure of a solar array is basically that of a cantilever. Design constraints allow for additional components only at the tip and base of the array. At the base of the array it is possible to install a torsional spring damper suspension system to react bending modes (in and out of plane).

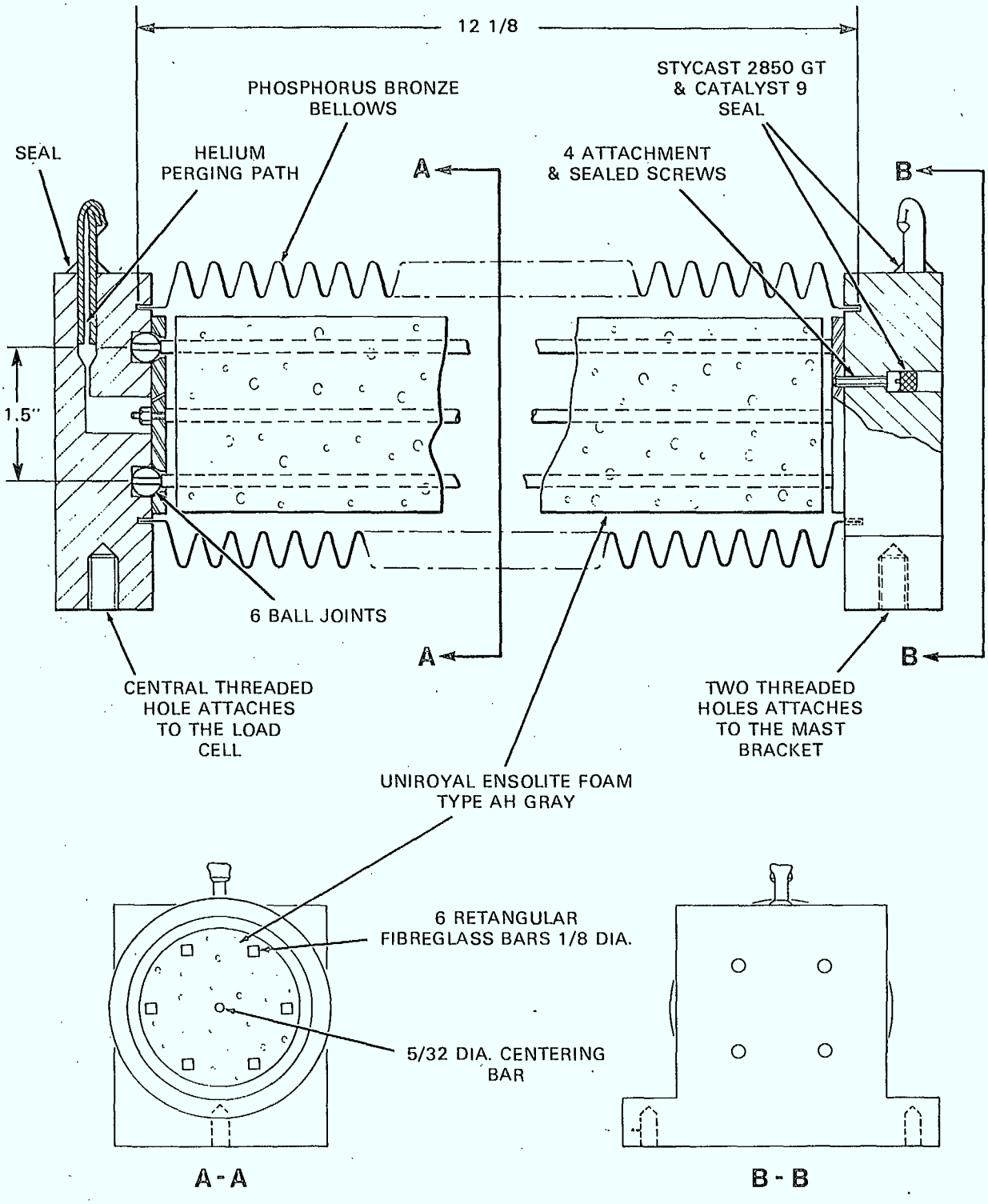

FIGURE 2-2.1 THE DAMPER ROD DESIGN

At the tip two damping mechanism options are possible. The first option is to integrate a damper to the tip tension mechanism and have a multi-purpose unit design. The other option is to have an add-on damper at the tip which resonates near the natural frequency of the structure.

2.2.2.2 **Damper Assessment** -Three types of dampers were considered. They can be summarized as follows:

1. Base Suspension Damper,
2. Tip Suspension Damper,
3. Add-on Tip Damper.

Although the base suspension damper could be effective in damping out all the bending modes, it would have to work with a very small stroke. In practice, high damping forces are difficult to achieve with small stroke. The clearance and backlash characteristics of such a system provide non-linearities that would complicate assessment of the damper.

The tip suspension damper is applicable to flexible solar arrays because, unlike rigid panel arrays, the structural continuity can be interrupted between the mast and the blanket tip plate (e.g., tip tension mechanism). In order to introduce damping at this position, there must be relative motion. The introduction of relative motion may weaken the structure and the damper itself will have a significant inertia with respect to the SAD point (Solar Array Drive). Nevertheless the tip is the position where maximum velocities occur. Therefore a damper with realistic stroke can be designed.

The final option is the add on tip damper. It is probably the optimum design to eliminate a specific mode. It is rather difficult to tune, since its natural frequency should match the structure frequency. Like the tip suspension damper, it adds a large inertia to the structure.

2.2.3 **Damper Concept** -The tip suspension damper was selected as an initial step to increase solar array damping. The criterion by which it was chosen was weight. The damper was to be included in the tip tension mechanism, therefore no additional weight would have to be added. The combined tip tension mechanism and tip suspension damper is referred to as the tension damper rod (TDR). The intension of the design was to introduce relative motion between the tip of the mast and tip of the blanket. The risk in this concept was that the relative motion allowance would increase the flexibility of the array and could result in larger amplitude responses to low frequency excitation. A priori knowledge of the damper characteristics would have eliminated some of the potential risk.

The hardware consisted of a two-dimensional parallel mechanism, self centered by a cantilever bar. The mechanism rods were bonded to a visco-elastic foam

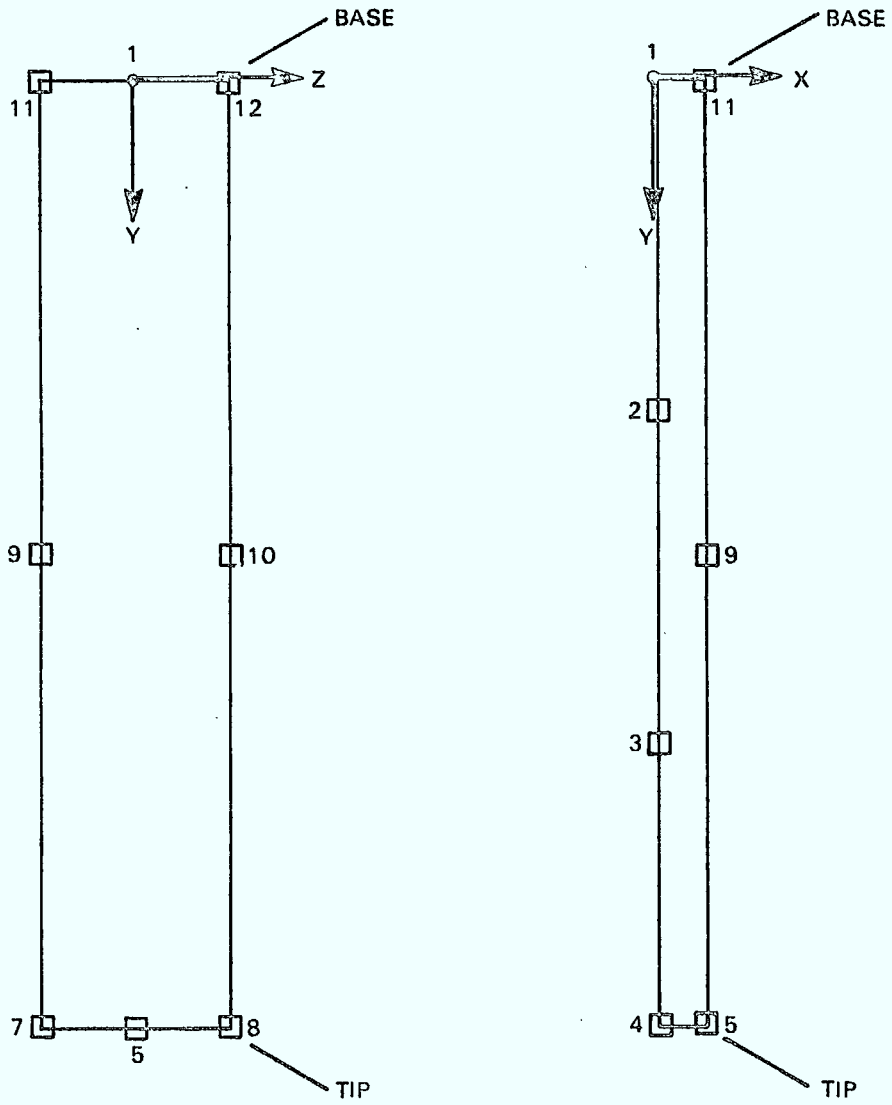

ACCELEROMETER LOCATIONS

RANDOM TEST

REFERENCE POINT 1

2	RADIAL, TANGENTIAL
3	RADIAL, TANGENTIAL
4	X, Y, Z
5	X, Y, Z
7	X, Z
8	X, Z
9	X
10	X
11	X, Z
12	X, Z

STEP RELAXATION & SINE TEST

REF PT. (1 FOR SINE; 4 FOR STEP RELAXATION)

2	RADIAL, TANGENTIAL
3	RADIAL, TANGENTIAL
4	X, Z
5	X OR Z

FIGURE 2-3.0 ARRAY CONFIGURATION & ACCELEROMETER LOCATIONS

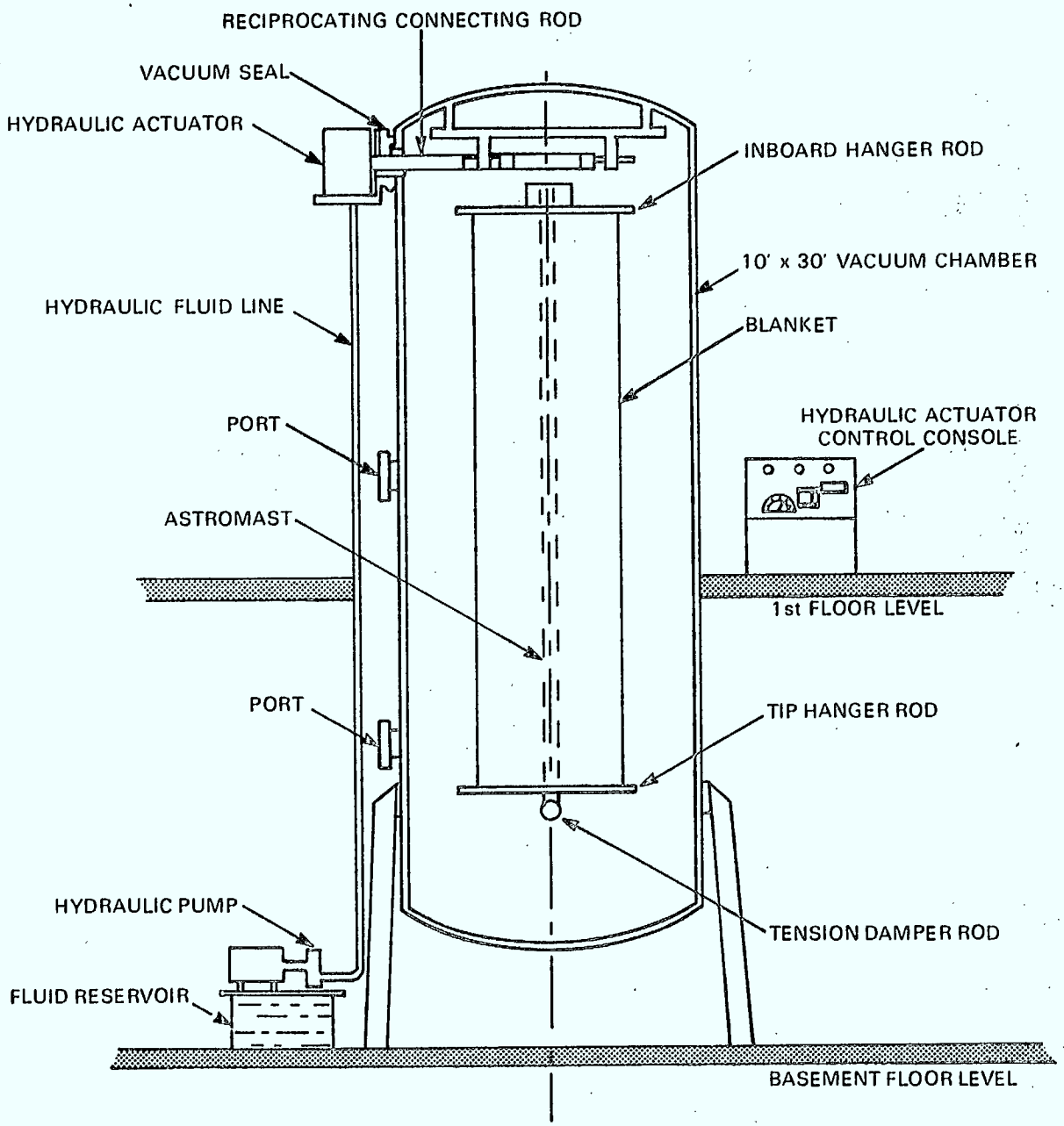

FIGURE 2-3.1 VACUUM TEST CONFIGURATION

DRIVING FREQUENCY = 5 HZ
AMPLITUDE = 0.01 G's INPUT

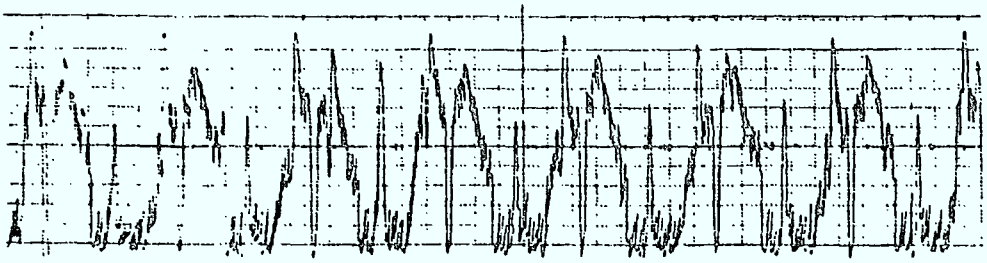

DRIVING FREQUENCY = .5 HZ
AMPLITUDE = 0.01 G's INPUT

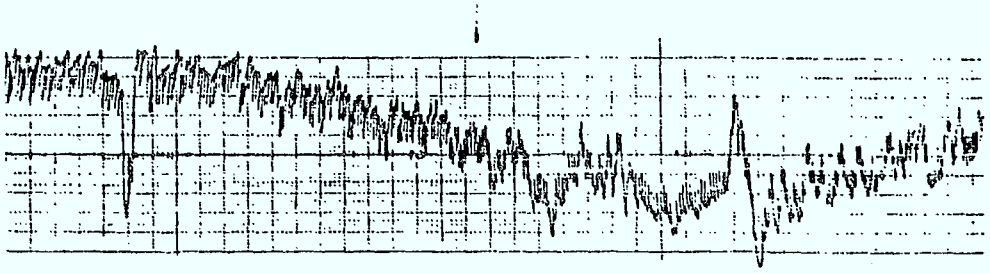

FIGUER 2.3.2 HYDRAULIC SHAKER OUTPUT

(Ensolite-Uniroyal-AH gray). The material was chosen for its high shock absorption properties. The ensolite was neither space nor vacuum approved. Thus some vacuum testing was done on it. The tests showed that the unit would have to be sealed. Figure 2-2.1 shows a sketch of the sealed damper design.

To summarize the design concept - a point of flexibility was introduced in the array structure and a damping unit of maximized but known damping value was installed. The intension was to achieve low structural amplifications (Q). This was done by damping the vibrations passing between the mast and blanket. Section 6.2 presents test evaluation of the three damping specimens that were produced.

2.3 Test Equipment and Configuration

Figure 2-3.0 shows the array configuration and accelerometer locations. The testing was done inside the 10' x 30' vacuum chamber, which is described in Section 2.3.1. The solar array was excited by a hydraulic shaker (Section 2.3.2) and by a step relaxation mechanism (Section 2.3.3). Data gathering and reduction is described in Section 2.3.5.

2.3.1 Vacuum Chamber -The testing took place within the 10' x 30' DFL vacuum chamber, at ambient temperature conditions. Some tests were performed in air, but most of them took place at 2-4 torr. Figure 2-3.1 shows the vacuum test configuration.

2.3.2 Hydraulic Shaker -An hydraulic shaker, built by CRC/DFL personnel for the purpose of testing solar array type structures in the 10' x 30' vacuum chamber was used as a means of excitation. The hydraulic shaker is included in Figure 2-3.1 vacuum test configuration. In principal, excitation to DC levels should be possible with this shaker. However, noise in the shaker starts to become a problem below 0.5 Hz. Figure 2-3.2 is a strip chart recording of the shaker output. Extensive rework would have been required to achieve acceptable results below about .5 Hz. (The limitation was actually amplitude rather than frequency dependent - for constant displacement at low frequency, acceleration levels are very low). The solar array being tested for this contract did not require input below .5 Hz., so the work was not done.

A linear voltage displacement transducer (LVDT) was used to control inputs to the shaker table, while an accelerometer at the base of the structure measured the levels for control and calculation purposes.

2.3.3 Step Relaxation Mechanism -The step relaxation mechanism was a device, built by CRC personnel, to deflect the structure, measure the resultant force and then release the structure. The sudden release provided a form of transient excitation to the structure.

For each test configuration, a minimum of four deflection/release cycles were required. To accomplish this in vacuum in a reasonable time, the mechanism was designed to reload itself. The mechanism was composed of two solenoids - one to load the structure, the other to release (conventional solenoids were used). In vacuum, there is no convection cooling, so AC power was used to reduce the overheating. Initially this created RF problems - a secondary load signal was generated electronically, invalidating the input load signal. To eliminate this problem, the device was altered so that activation took place as the current passed through a zero value.

Figure 2-3.3 shows the mechanical concept for the Step Relaxation Mechanism.

2.3.4 Transducers

2.3.4.1 Load Cells -There were two different load cells used. One was an Interface SM-50 used to monitor tension levels in the blanket. It weighed 90 gms and had a capacity of 50 lbs.

The second load cell was built by CRC personnel to measure the load level input of the step relaxation mechanism. Typical load levels for the step relaxation test were 2 lb.

2.3.4.2 Accelerometers -The accelerometers used for the testing were ENDEVCO (Series 7265) piezoresisive accelerometers. This type of accelerometer can respond to DC levels, unlike piezoelectric accelerometers. Each accelerometer weights 5 gm. Minimum weight characteristics were very important. Two of the accelerometers were mounted on the blanket. Prior to this solar array test, the astromast was tested (see Report, Ref: 1). At that time, it was determined that the accelerometer masses had no significant effect on the astromast.

Although the blanket response was probably altered significantly by the presence of the accelerometers on it, the effect was not large enough to show up on other parts of the structure.

2.3.5 Software -Figure 2-3.5 shows a simplified view of the test flow.

The hydraulic shaker is subject to software control, which is described in Section 2.3.5.1. The test data processing is described in Section 2.3.5.2.

2.3.5.1 Shaker Control -The DFL Vibration Test Facility has two vibration control systems, an HP 5427A and a Gen Rad 2503. The Gen Rad system is also used for data acquisition in the DATM software (see Section 2.3.5.2). Both systems are capable of open and closed loop sine and random control required for the solar array testing. In addition, they can provide control for shock inputs. The details of their operating procedure are described in Ref. 1, Section 3.2.2.

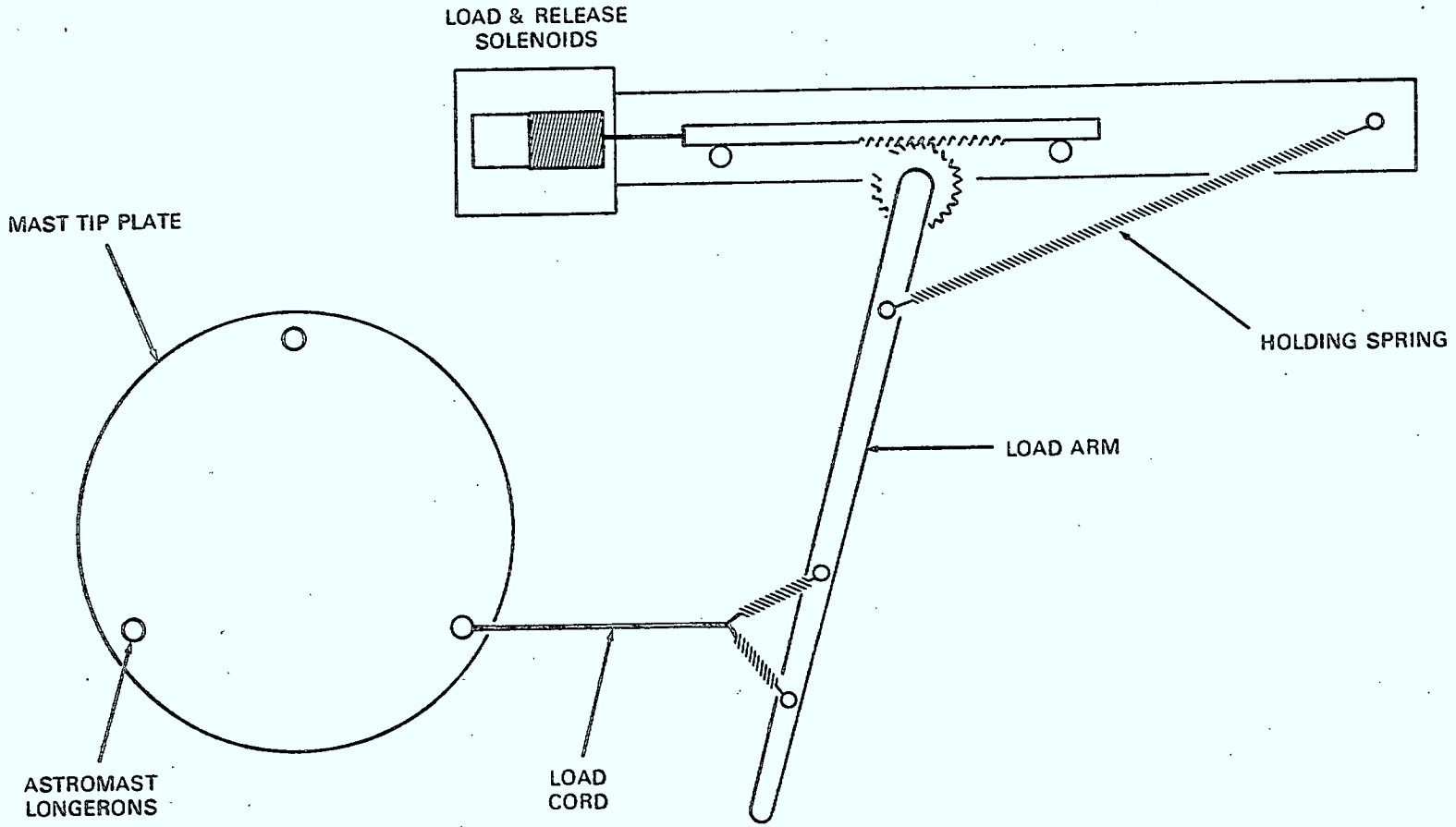

FIGURE 2.3.3 STEP RELAXATION MECHANISM

Figure 2.3.5

MODAL TEST FLOW

SPAR

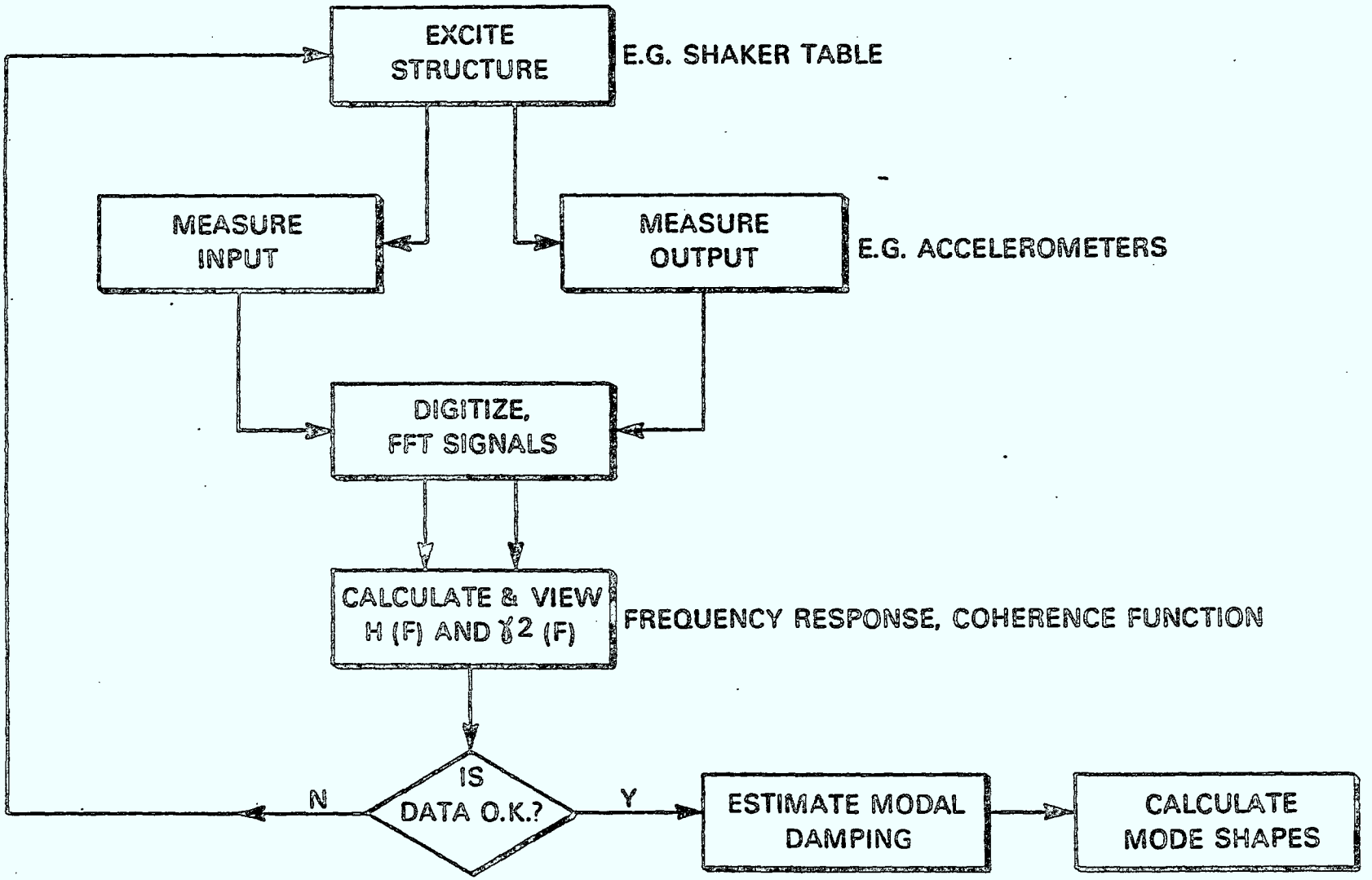

3-0-124

2.3.5.2 Test Processing Software (SDRC) -The Gen Rad 2503 system operating on a PDP 11/34 computer is used for the data acquisition (spectral analysis) program DATM and the mode shape and parameter estimation program MPLUS (Ref. 10).

The test data is stored on analogue tape. Data acquisition (by the DATM software) can be done in parallel with the data storage, or at some later time, the data can be acquired from the analogue tape.

The two SDRC software programs, DATM and MPLUS are complementary packages which share data files.

The software is capable of acquiring up to 16 channels of data at a time, but the current hardware configurations limit the acquisition to 4 channels at one time.

The Modal-Plus software (which combines DATM and MPLUS) calculates the modal parameters - natural frequency, modal damping coefficients, mode shapes, modal mass and modal stiffness. Examples of some of the output are included in Section 6.1.2. A more detailed description of the software operations and capabilities are included in Ref. 1, Sections 3.2.2 and 3.2.3.

3.0 THEORETICAL DEVELOPMENT

The theory outlined in this section extends beyond that used for the solar array covered in this contract. The multi-shaker information (Secton 3.1.3 has been briefly described, for completeness - in view of recommendations for future testing).

3.1 Modal Analysis

Modal Analysis can be performed in the time or the frequency domain. A brief discussion of the time domain concept is included in Section 3.2. An example of a time domain modal analysis is known as the Ibrahim Time Domain Technique.

Most commercially available modal analysis software operates in the frequency domain. The first step in this type of analysis consists of converting time data to frequency (this is referred to as Spectral Analysis). The change from time to frequency is done via Fast Fourier Transform hardware (discussed in Section 3.1.1). The second step (referred to as Modal Identification) in its simplest form deals with data produced from a single point of excitation. Modal Identification of single point excitation data is discussed in Section 3.1.2. An extension of single point excitation is the multipoint excitation technique. This is dealt with Section 3.1.3. The Solar Array testing done for this project used single point and base excitation. Base excitation requires a special type of multipoint processing (see Section 3.1.3.3).

3.1.1 Spectral Analysis (Ref: 13) -The test processing of solar array results makes use of the aspects of spectral analysis covered here, with the exception of multiple and partial coherence.

The concept of mode shapes (see Section 3.1.1.2) can be viewed as a transformation to a new coordiante system. Real mode shapes are orthogonal to one another. There are as many mode shapes as there are degrees of freedom. Each mode shape is associated with a particular natural frequency. It is this frequency association that makes spectral analysis useful as a first step in modal anlaysis.

The dynamic characteristics of a constant parameter linear system can be described by a weighting function $h(\tilde{\tau})$, which is defined as the output of the system at any time to a unit impulse input applied a time $\tilde{\tau}$ before. For any arbitrary input x(t), the system output y(t) is given by the convolution integral

$$y(t) = \int_{-\infty}^{\infty} h(\tilde{\tau})\, x(t-\tilde{\tau})\, d\tilde{\tau} \qquad (3.1)$$

To be physically realizable it is necessary that the system respond only to past inputs, i.e., $h(\tilde{\tau}) = 0$ for $\tilde{\tau} < 0$.

A constant parameter linear system can also be characterized by a transfer function H(p), which is defined as the Laplace transform of $h(\tilde{\tau})$.

$$H(\rho) = \int_0^\infty h(\tilde{\tau}) \exp(-\rho\tilde{\tau})\, d\tilde{\tau} \tag{3.2}$$

If a constant parameter linear system is physically realizable and stable, then the dynamic characteristics of the system can be described by a frequency response function H(f); which is the Fourier transform of $h(\tilde{\tau})$

$$H(f) = \int_0^\infty h(\tilde{\tau}) \exp(-2\pi f\tilde{\tau})\, d\tilde{\tau} \tag{3.3}$$

The frequency response function is a special case of the transfer function where, in the exponent $p = a+jb$, $a = 0$ and $b = 2\,f$.

Taking the Fourier transform of both sides of Equation (3.1)

$$Y(f) = H(f)\, X(f) \tag{3.4}$$

Thus the dynamic characteristics of a system can be defined by the ratio of the Fourier transforms of the output and input of the system.

$$H(f) = Y(f)/X(f) \tag{3.5}$$

The frequency response function can be thought of in terms of a magnitude (gain factor) and an associated phase angle (phase factor)

$$H(f) = |H(f)|\, \exp(-j\phi(f)) \tag{3.6}$$

The form of the frequency response function depends on the type of system input. As an example, consider the single degree of freedom system of Figures 3-1.1.1(a) and (b).

The frequency response functions for the two systems are:

(a) $H(f)_{force} = \dfrac{1}{k-(2\pi f)^2 m + j2\pi fc}$ magnification factor (3.8)

(b) $H(f)_{base} = \dfrac{k + j2\pi fc}{k-(2\pi f)^2 m + j2\pi fc}$ transmissibility function (3.10)

Examples of the gain and phase factor of each system are illustrated in Figure 3-1.1.2 and 3-1.1.3.

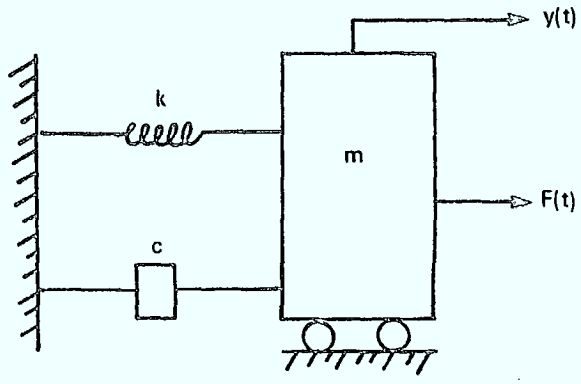

EQUATION OF MOTION

$$m\ddot{y}(t) + c\dot{y}(t) + ky(t) = F(t) \quad (3.7)$$

FIGURE 3.1.1.1a SYSTEM WITH FORCE INPUT

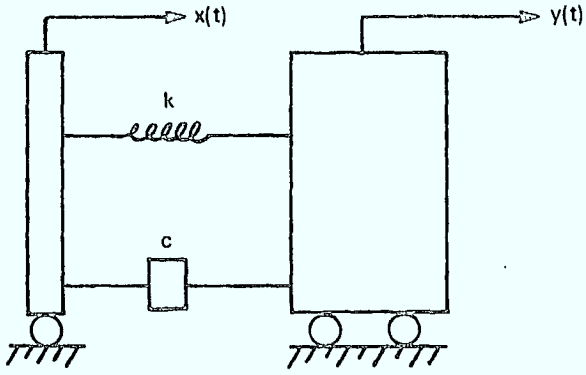

EQUATION OF MOTION

$$m\ddot{y}(t) + c\dot{y}(t) + ky(t) = kx(t) + c\dot{x}(t) \quad (3.8)$$

FIGURE 3.1.1.1b SYSTEM WITH BASE MOTION INPUT

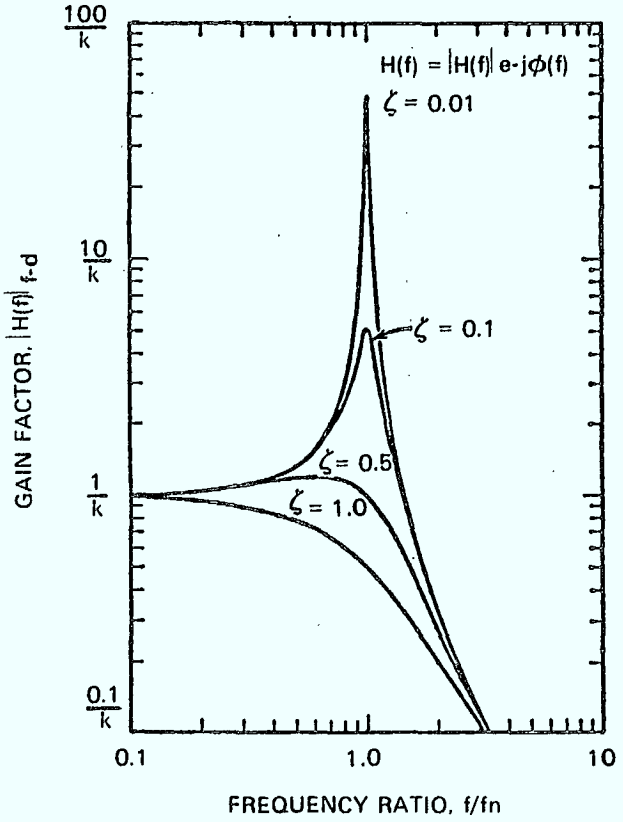

(a)

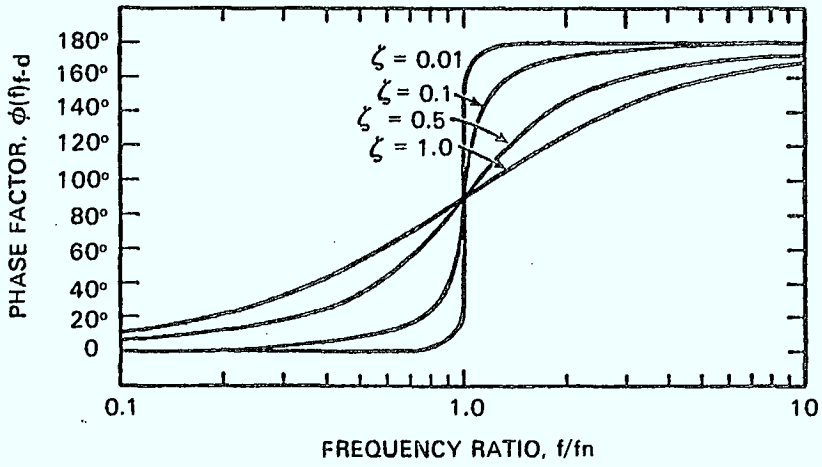

(b)

FIGURE 3.1.1.2 FREQUENCY RESPONSE FUNCTION OF MECHANICAL SYSTEM WITH FORCE INPUT. (a) GAIN FACTOR. (b) PHASE FACTOR

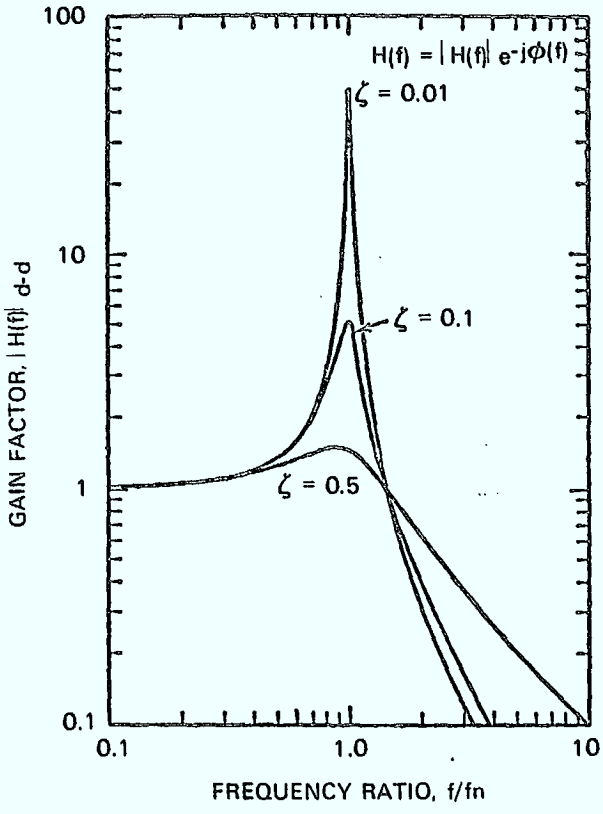

(a)

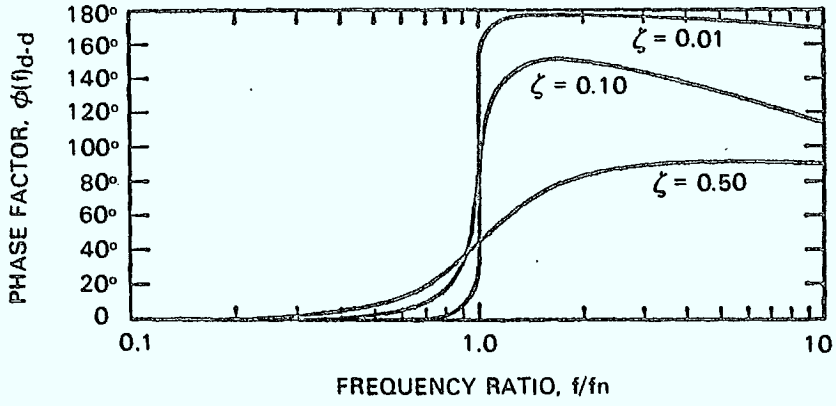

(b)

FIGURE 3.1.1.3 FREQUENCY RESPONSE FUNCTION OF MECHANICAL SYSTEM WITH BASE MOTION INPUT. (a) GAIN FACTOR. (b) PHASE FACTOR.

To improve estimates of a system frequency response function, the following spectral density relations are useful (the spectra involve expected values of transformed input and output values).

$$G_y(f) = |H(f)|^2 G_x(f) \quad (3.11)$$

$$G_{xy}(f) = |H(f)| G_x(f) \quad (3.12)$$

$$|G_{xy}(f)| = |H(f)| G_x(f) \quad (3.13)$$

$$\theta_{xy}(f) = \phi(f) \quad (3.14)$$

where

$G_y(f)$ = auto spectra of output

$G_x(f)$ = auto spectra of input

$G_{xy}(f)$ = cross spectra between input and output

In order to determine the complete frequency response function of the system, the cross-spectral density function is required. (Equation (3.11) does not include the system phase factor $\phi(f)$).

The coherence function (ordinary coherence function) is used as an indicator of data quality. It is defined as

$$\gamma^2_{xy}(f) = |G_{xy}(f)|^2/(G_x(f)G_y(f) \quad (3.15)$$

For linear systems, the coherence function $\gamma_{xy}^2(f)$ can be interpreted as the fractional portion of the mean square value at the output y(t) which is contributed by the input x(t) at the frequency f.

For an ideal constant parameter linear system $\gamma_{xy}^2(f) \rightarrow 1$. If the input and output are completely unrelated $\gamma_{xy}^2 \rightarrow 0$. If the coherence function lies between one and zero, three possible situations exist:

(a) extraneous noise is present in the system,

(b) the system is not linear,

(c) the output is due to more than the one measured input.

The ordinary coherence function is actually a special case of the multiple coherence function. The multiple coherence function is used for systems of

multiple inputs and is being applied to modal analysis techniques being developed by the University of Cincinnatti group. It describes the possible causal relationship between an output and all known inputs. For multiple input problems with uncorrelated inputs, the equation reduces to

$$\gamma^2_{y\,x(f)} = \frac{\sum_{i=1}^{q} H_i(f)\, G_{Yi}(f)}{G_{YY}(f)} \qquad (3.16)$$

q is the number of inputs

For the case of two uncorrelated inputs, the effect of each input on the output reduces to

$$H_{Y1} = \frac{G_{Y1}}{G_{11}}$$

$$H_{Y2} = \frac{G_{Y2}}{G_{22}}$$

where H_{y1} is the FRF (Frequency Response Function) of the output due to input at point 1

G_{y1} is the cross-spectra between output and input at point 1

G_{11} is the auto-spectra of input 1

This is the technique used to separate the effects of multiple inputs - multiple coherence is the function which determines if indeed enough inputs have been considered.

Figure 3-1.1.4 illustrates the assumed multiple input problem.

The partial coherence function (which is useful when some inputs are unknown) between $x_1(t)$ and $y(t)$, when $x_2(t)$ is removed from both $x_1(t)$ and $y(t)$ is

$$\gamma^2_{1y\cdot 2(f)} = \frac{|G_{1y\cdot 2(f)}|^2}{G_{11\cdot 2(f)} G_{yy\cdot 2}} \qquad (3.17)$$

3.1.2 Modal Identification (SPE) -The second phase of modal analysis consists of taking the frequency response functions, for a collection of points and estimating the structural characteristics of the system under consideration. The structural characteristics are: natural frequencies, mode shapes, modal mass and damping values. Section 3.1.2.1 deals with the estimation techniques for single reference point (single point excitation) experimental results. Section 3.1.2.2 outlines the theory of mode shapes.

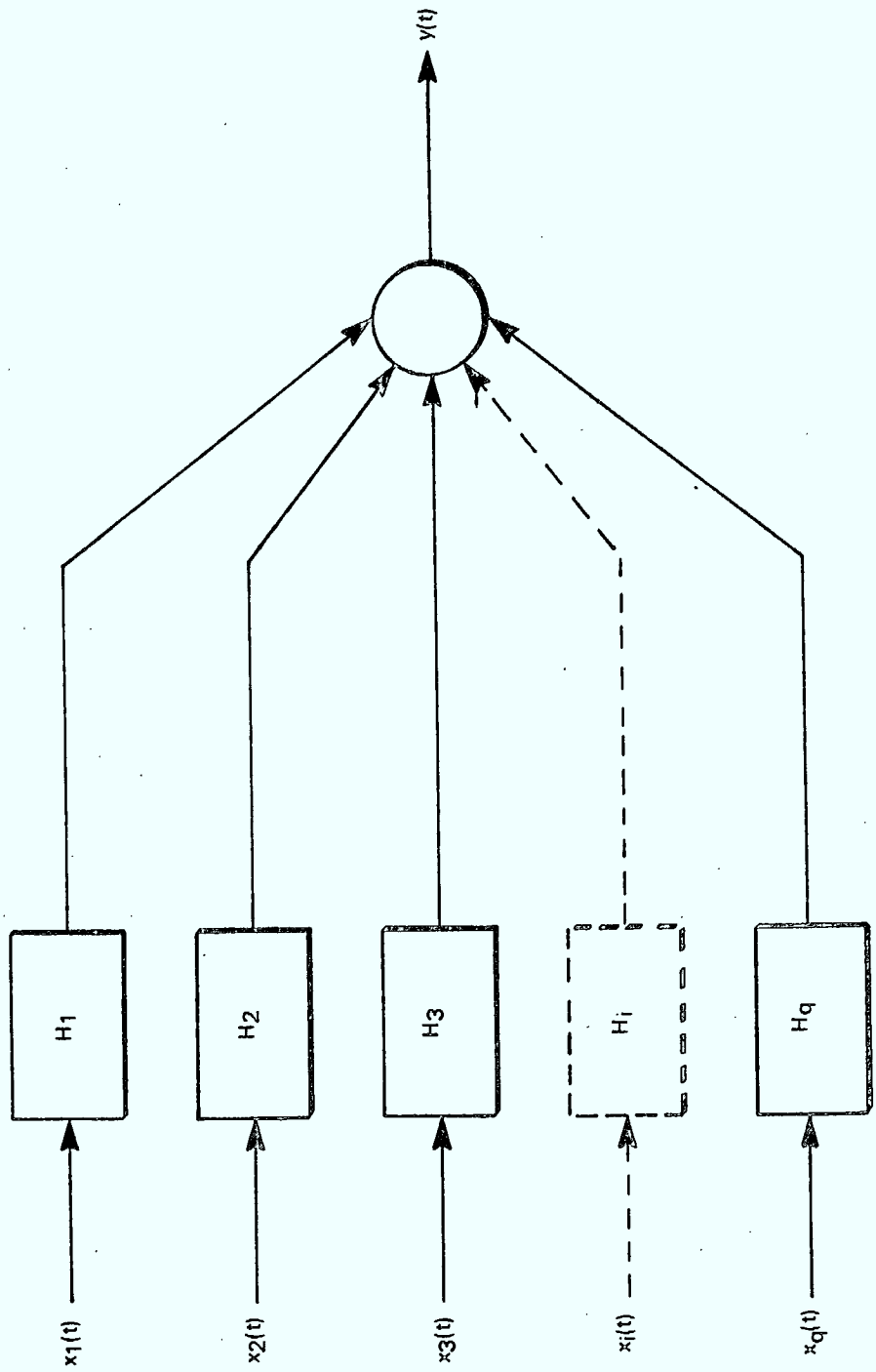

FIGURE 3.1.1.4 MULTIPLE INPUT/OUTPUT MODEL

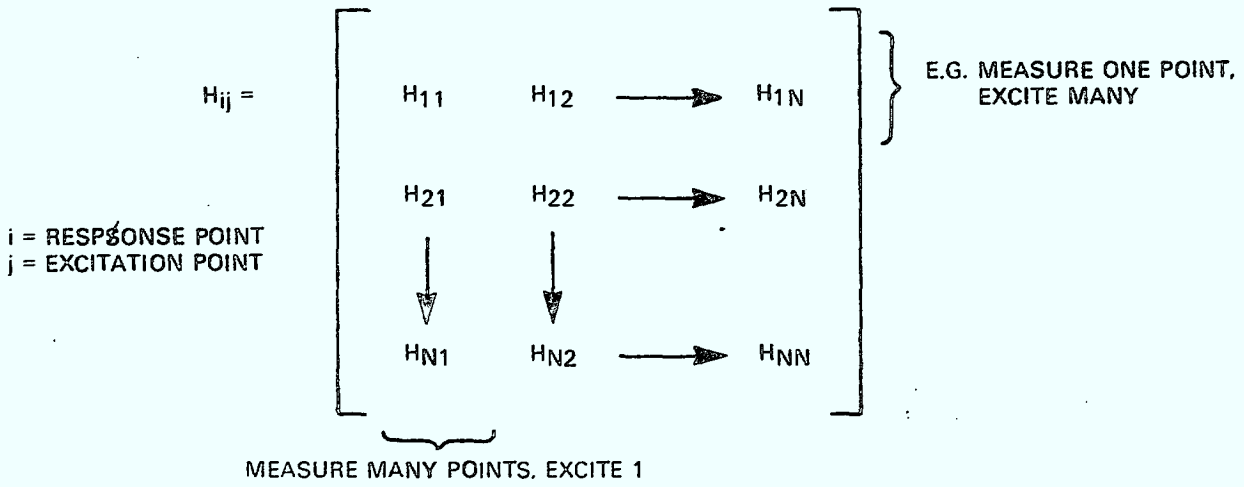

FIGURE 3.1.2 COMPLETE FREQUENCY RESPONSE FUNCTION MATRIX

Single point excitation (or single reference point) means that all frequency response functions have a common reference. The reference can be either a response point or an excitation point. The following discussion will assume a common excitation point. Figure 3.1.2 presents a complete frequency response function matrix. It presumes that there is a response and excitation point for each of the n degrees of freedom of the system.

A linear structure can be completely defined (w.r.t. frequency response functions) by either one row or one column of the frequency response matrix. Multipoint modal analysis techniques improve experimental estimates by producing redundant data (filling in more components of the frequency response function matrix).

3.1.2.1 Parameter Estimation -The first stage of parameter estimation is to pick the resonant frequencies of the structure. This can be done automatically (by some software systems) or manually. Manual input, to at least check the automatic 'peak picking' process, is preferable to a totally automated system.

Manual 'peak picking' consists of looking for peaks in the frequency response function of each point. At resonant frequencies there is also a phase shift, which helps to identify the resonance. Global (as opposed to local) modes have peaks at the same frequency for several or all points.

The techniques to calculate damping (for lightly damped structure) are:

(1) Quadrature Peak Picking Algorithm (Half Power Method)

$$\zeta = \frac{1}{2}\left\{\frac{f_u - f_l}{f_d}\right\}$$

where

f_u and f_l are the frequencies at the half power point on either side of the damped natural frequency f of the structure (see Figure 3-1.2.1(a)).

(2) Circle Fitting Algorithm

At a system resonance, a Nyquist plot (plot of imaginary vs. real components of frequency response will appear as a circle (see Figure 3-1.2.1(b)). The circle can be used to estimate the damping value $\zeta = a/c$ and the damped natural frequency. This technique is limited to lightly damped, well spaced modes.

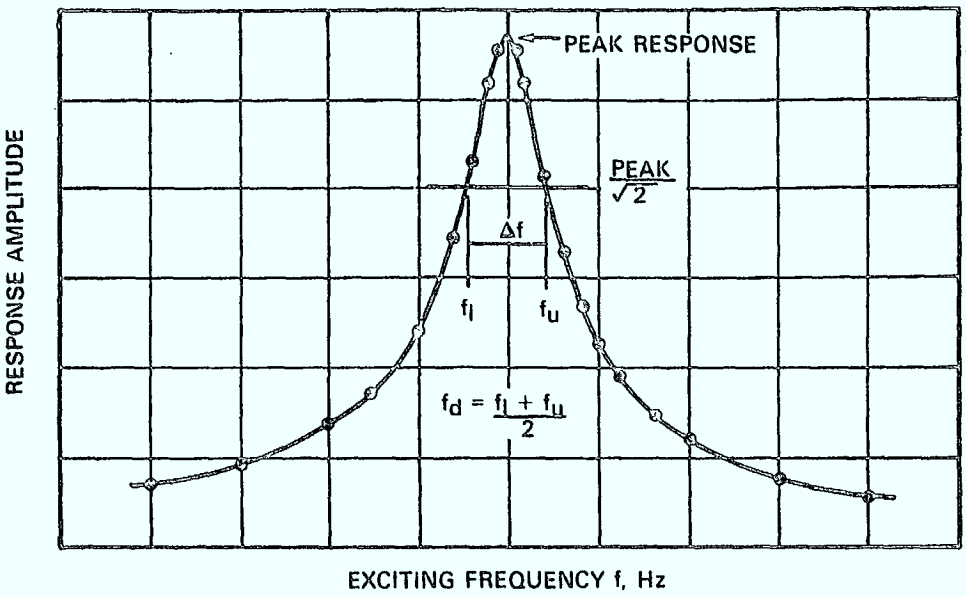

FIGURE 3.1.2.1a HALF POWER METHOD

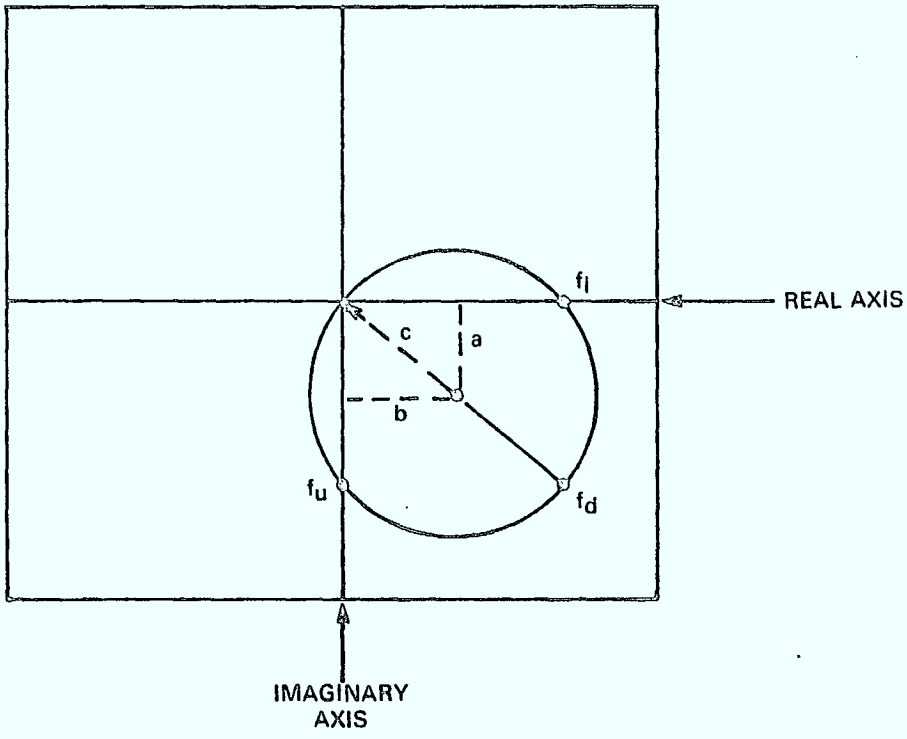

FIGURE 3.1.2.1b CIRCLE FIT

(3) Frequency Response Curve Fit

The frequency response function is defined by complex amplitude which is converted to a residue (R) by factoring out 2j, damped natural frequency (w_n) and damping value $\sigma = \left\{ \frac{w_d^2 \zeta^2}{1-\zeta^2} \right\}^{1/2}$

$$H(j\omega) = \frac{1}{2} \left\{ \frac{R}{(\omega_d - \omega) + j\sigma} - \frac{R^*}{j\sigma - (\omega_d + \omega)} \right\} \qquad (3.18)$$

The system parameters can be extracted by estimation and least squares fit comparison to the experimental values.

3.1.2.2 Mode Shapes -The mode shapes of an n degrees of freedom system constitute n independent displacement patterns. The amplitudes serve as coordinates to express any form of displacement (see Figure 3-1.2.2). Each mode shape is orthogonal with respect to all other mode shapes.

The equations of motion

$$m\ddot{v} + c\dot{v} + kv = p(t) \qquad (3.19)$$

can be decoupled using the normal coordinate transformation to

$$\phi_n^T m \phi_n \ddot{Y} + \phi_n^T c \phi_n \dot{Y} + \phi_n^T k \phi_n = \phi_n^T p(t)$$

$$\left.\begin{aligned} \phi_q^T m \phi_n &= 0 \\ \phi_q^T k \phi_n &= 0 \\ \phi_q^T c \phi_n &= 0 \end{aligned}\right\} \; q \neq n$$

thus

$$M_n\ddot{Y} + C_nY_n + K_nY_n = P_n(t) \qquad (3.20)$$

where

M_n = generalized mass $\phi_n^T m \phi_n$

K_n = generalized stiffness $\phi_n^T k \phi_n$

C_n = generalized damping $\phi_n^T c \phi_n$

P_n = generalized force $\phi_n^T p(t)$

$\mathcal{L}_n$ = participation factor $\phi_n^T m$ for constant acceleration over structure

MODE SHAPE, ϕ $\qquad V_n = \phi_n Y_n$

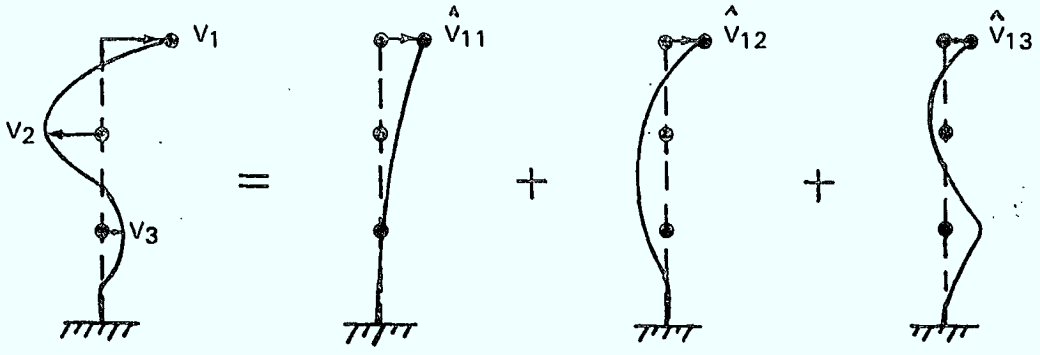

$V = \phi Y \qquad \hat{V}_1 = \phi_1 Y_1 \qquad \hat{V}_2 = \phi_2 Y_2 \qquad \hat{V}_3 = \phi_3 Y_3$

$$V = \phi_1 Y_1 + \phi_2 Y_2 + \phi_3 Y_3$$

$$= \sum_{n=1}^{N} \phi_n Y_n$$

FIGURE 3.1.2.2

Modal damping assumes that damping $c = a_{0m} + a_1 k$, i.e., damping proportional to mass and/or stiffness (Rayleigh or Structural Damping). This type of damping is a reasonable model for a system where the damping is distributed throughout the structure. For systems with a point damper, modal damping is not a good estimate. Many of the modal analysis software systems provide the option to use complex eigenvalue solutions, which allow for a completely general representation of damping in the solution.

3.1.3 **Multipoint Excitation** - The solar array test work did not include any multipoint processing but future work should incorporate it. Multipoint excitation implies simultaneous excitation of the structure at more than one point. There are two principal purposes to doing this, just as there are two techniques involved in doing it. One aim is to reduce test time, the other is to improve the results obtained - particularly to separate closely spaced modes. The random excitation multipoint technique (Section 3.1.3.1) is primarily to reduce test time, though it can also be used to improve test data. The sine dwell multipoint technique (Section 3.1.3.2) is to separate closely spaced modes. Base excitation (Section 3.1.3.3) is not physically a multipoint excitation technique, but the mathematical model requires that it be treated as such, because the constant acceleration over the structure effectively means that each mass excites itself.

3.1.3.1 **Random, Multipoint Excitation** - Random, multipoint excitation makes use of the redundancy of the frequency response function matrix to improve estimates of modal parameters. It allows some mode shapes to be highlighted while suppressing others by geometric combination of mode shapes (see Figure 3-1.3.1). The points to be combined should be excited at the same levels. This can be achieved by exciting at more than one position, though not necessarily at the same time. Simultaneous excitation improves the results by maintaining stationarity and it reduces test time.

When the structure is being excited by more than one input, it is necessary (to calculate frequency response functions) to be able to assess what part of a response is due to each input. The multiple coherence function (discussed in Section 3.1.1) is used to identify each input.

An extension of mode shape enhancement (termed Polyreference Technique, by SDRC) involves correlations between redundant components of the frequency response function matrix.

Modal Analysis is a linear type of analysis. The mode shape enchancement techniques depend more heavily on structural linearity and test stationarity than the single point techniques. To check for structural linearity, two frequency response functions (input and output points transposed) should be compared. Stationarity is guaranteed for simultaneous excitations - which is one of the key advantages to simultaneous excitation.

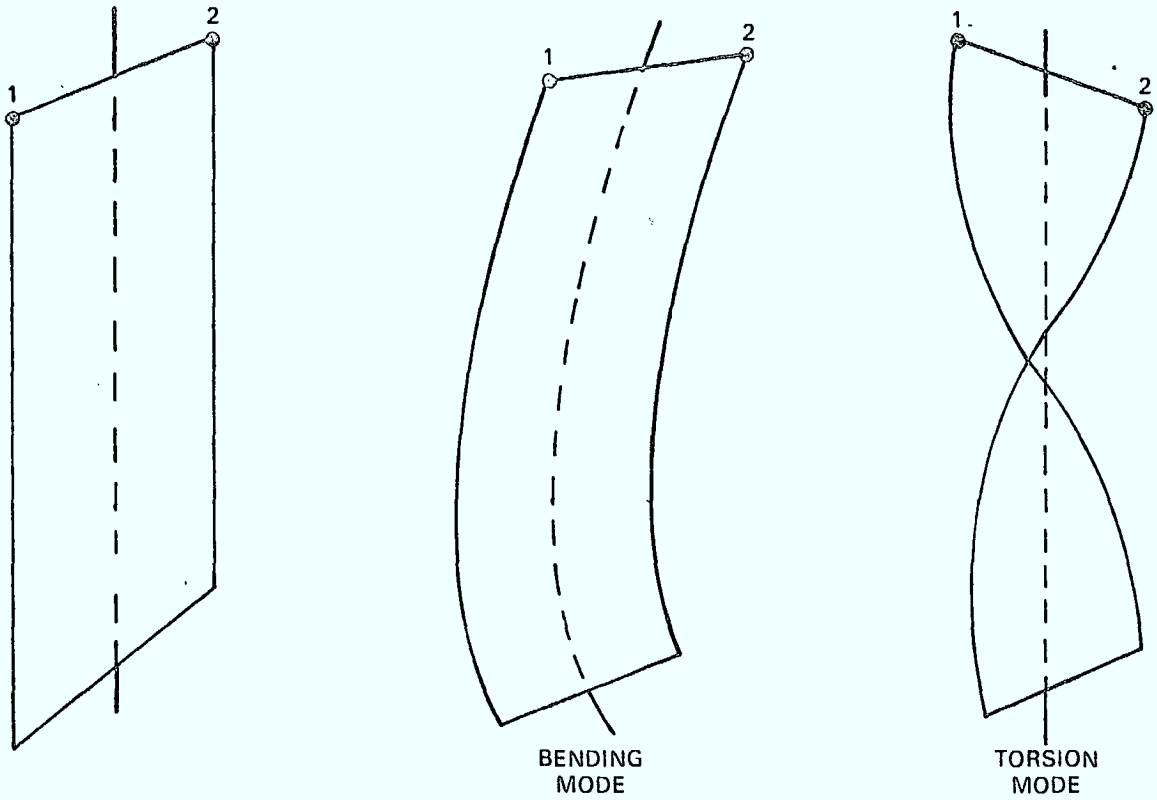

FIGURE 3.1.3.1 MODE SHAPE ENHANCEMENT

3.1.3.2 Sine Dwell, Multipoint Excitation -The object of a sine dwell multipoint test is to coordinate the excitation so that one mode is excited, while all others are suppressed. The modal tuning is accomplished in a variety of ways. The mode shapes of the structure are initially estimated (either analytically or experimentally with single point exciters). The forcing functions are all in phase (or 180°) and their ratios are initially determined from the estimated mode shapes. The structure is then tuned to a single mode by adjusting force ratios, force locations and frequency. There are a variety of techniques used to tune the structure.

To assure pure mode shapes, there should be as many excitation points as there are degrees of freedom. As this is not possible (2 to 16 exciters are typical), iterative procedures are used to ensure that modes close to the mode of interest are suppressed. If there are n exciters, then n-1 modes can be suppressed.

3.1.3.3 Base Acceleration Excitation -The equation of motion for a structure excited at the base (as in the case of a building in an earthquake, a spacecraft on a shaker table or a solar array subjected to S/C motion) is

$$M_n\ddot{Y}_n + C_n\dot{Y}_n + K_nY_n = P_n(t) \qquad (3.20) \text{ from Section 3.1.2.2}$$

$$P_n(t) = \ddot{v}_b(t)\,\phi_n^T m$$

This effectively means that each lumped mass of the structure provides part of the exciting force. There does not seem to be commercially available software that deals with this type of excitation yet. (Reference 2, page 11 summarizes the equations in terms of modal parameters).

3.2 Time Domain Techniques

Time Domain Techniques make use of the decay form of structural oscillations to determine parameters. Complete modal characterization of a structure is possible using the Ibrahim Time Domain Technique, Section 3.2.1. The Polyreference Technique used by SDRC involves a similar approach.

3.2.1 Complex Exponential Decay -This technique (also known as IDT, Prony Method) can be applied to free decay resulting from random or impact input. The SDRC Modal Plus Version 7 software uses a similar type of parameter estimation (Polyreference) though the data acquisition phase is actually a spectral analysis approach (Reference 11 and 12). Response for a number of points is measured simultaneously, sampled at equally spaced intervals. This data is used to form a matrix. A second matrix is formed from the same decay data, shifting the sampling points by Δt.

The technique is fast - a complete test can be run in about 20 minutes. There is virtually no judgement required on the part of operator in processing the test results. The technique does require a mainframe computer to process the results and provides little physical insight to the structural properties.

If the noise levels present in the data are small and modal damping factors are not equal, closely spaced modes can be identified using this technique.

The Polyreference technique employed by SDRC uses the same type of parameter estimation method. The decay data is generated from impulse response functions formed from the frequency response function data. By making use of FRF's it provides more visibility into the physical problem.

3.2.2 Hilbert Transform -Damping values can be estiamted from a decaying free vibration. The log decrement technique is one of the most common ways of doing this. By making use of the Hilbert transform of sine and cosine functions, an improved estimate of damping can be made from the same decay data.

The decaying signal is assumed to be of the form

$$v(t) = A\, e^{-\zeta\omega t} \cos(wt) \quad \text{(see Figure 3-2.2(a))}$$

The Hilbert transform of the signal is then

$$H[v(t)] = Ae^{-\zeta\omega t} \sin(wt)$$

If the signal and its Hilbert transform are squared and added, the result is

$$A^2e^{-2\zeta t} \sin^2(wt) + A^2e^{-2\zeta\omega t} \cos(wt) = A^2\, e^{-2\zeta\omega t}$$

Taking the natural log of the result:

$$\ln(A^2) - 2\zeta\, wt$$

and plotting as a function of time will produce a straight line, with w as the slope (see Figure 3-2.2(b)).

A routine to calculate the Hilbert transform is included in Appendix H.

Excitation of the structure should be a sine dwell at a resonant frequency. The data sample rate for the routine listed in the Appendix should be from 4 to 8 samples per cycle.

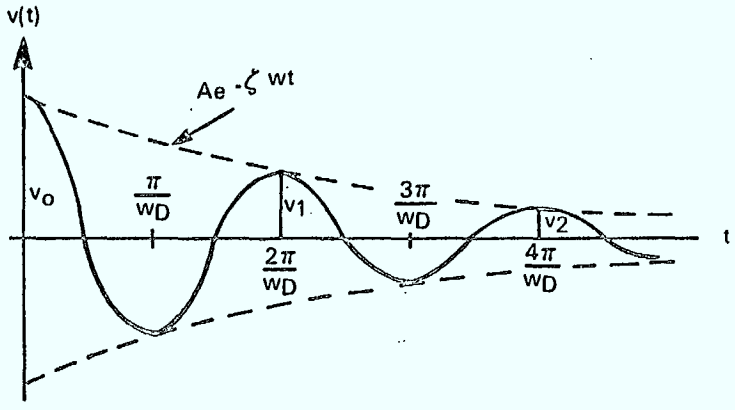

FIGURE 3.2.2a DECAYING FREE VIBRATION

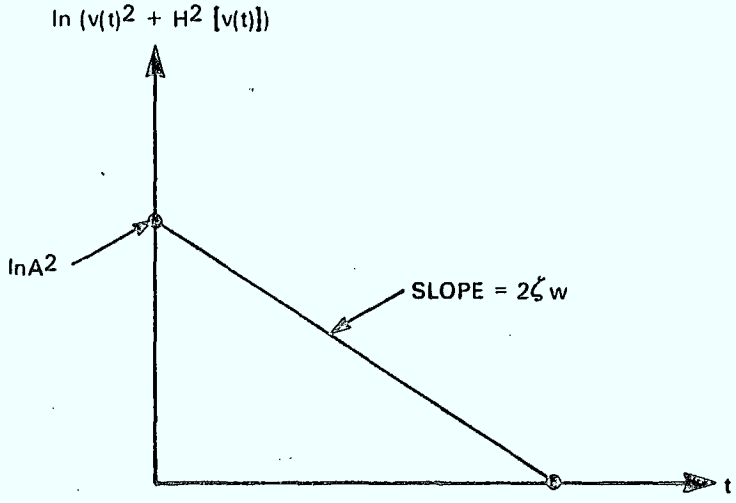

FIGURE 3.2.2b RELATION BETWEEN DAMPING AND PROCESSED SIGNAL, VS TIME

4.0 ANALYTICAL MODEL

The analytical predictions described in this chapter have been calculated using a computer program written by CRC personnel (originally by F. Vigneron, S.J. Zurawski and R.E. Cloutier - subsequently modified to include damping by K. Lips).

The computer program employs a mathematical model which describes the structural mechanics of a flexible solar array in terms of variational principles and continuum mechanics methods. Modes and frequencies can be calculated for a 1-g test state and compared to corresponding ones for the 0-g on-orbit state. The details of the program are covered in Refrences 3 and 4. Figure 4 illustrates degrees of freedom and damping types of the math model.

Section 4.1 outlines the input parameters for the two solar array configurations which are tested. Section 4.2 discusses the output frequencies and mode shapes. Section 4.3 compares the calculated frequencies with those obtained from testing.

4.1 Solar Array Parameters

The solar array parameters are presented in Table 4-1. There are two configurations considered. The first is called the undamped case (it does not involve any attempt to increase damping over that inherent to the structure). The second configuration is referred to as the damped case (a mechanism to increase damping has been used).

4.2 Analytical Predictions

Analytical predictions were made for the damped and undamped configurations tested. Tables 4-2.1 and 4-2.4 list the predictions. The difference between the two configurations was the tension level, the TDR stiffness and the TDR Weight. The effects of tension and weight have been estimated and the results listed in Tables 4-2.2 and 4-2.3.

The effects of gravity have been assessed by running cases for 1-g and 0-g. The in-plane modes seem to be unaffected by gravity, but the twist and out of plane modes are significantly effected.

The change in blanket tension seems to affect only the twist modes.

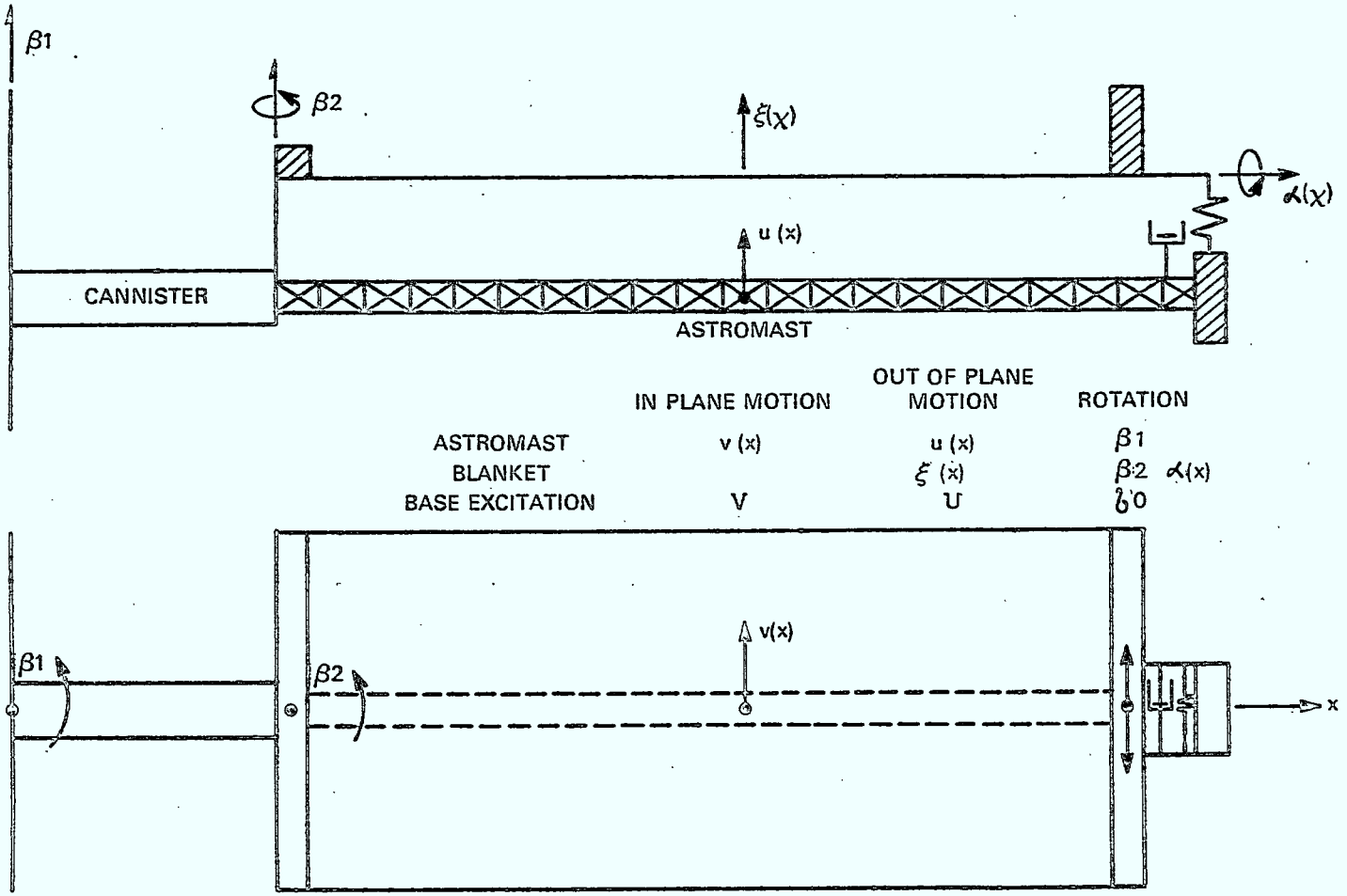

FIGURE 4-0 COORDINATES SPECIFYING MAST DEFORMATIONS

TABLE 4-1

MODELLING PARAMETERS

	CONFIGURATION 1	CONFIGURATION 2
Tension Level	3.3 lb	4.6 lb
Astromast Stiffness		
Bending	.75 lb/in	.75 lb/in
Torsion	5.6 lb-in/degree	5.6 lb-in/degree
Astromast Weight	4.0 lb	4.0 lb
Blanket Weight	2.2 lb	2.2 lb
Hanger Rod Stiffness	521 lb/in	521 lb/in
Hanger Rod Weight	2.03 lb	2.03 lb
TDR Stiffness		
Bending	28 lb/in (calc)	40 lb/in (measured)
Axial	1.E5 lb/in (calc)	1.E6 lb/in (est)
Torsion	100 lb-in/rad (calc)	200 lb-in/rad (est)
TDR Damping	N/A	12.5%
TDR Weight	1.83 lb	2.74 lb
Mast Tip Bracket Weight	0.50 lb	0.50 lb

TABLE 4-2-1

ANALYTICAL PREDICTIONS

UNDAMPED CONFIGURATION
TDR WEIGHT = 1.8 lb
T = 3.3 lb

MODE	FREQUENCY (Hz)	
	g = 32.2 ft/sec	g = 0
In-plane 1	1.02	-
In-plane 2	11.0	-
In-plane 3	15.7	-
Twist 1	1.57	-
Twist 2	2.35	-
Twist 3	3.61	-
Out of plane 1	0.93	-
Out of plane 2	1.23	-
Out of plane 3	2.24	-

TABLE 4-2-2

ANALYTICAL PREDICTIONS

DAMPED CONFIGURATION
TDR WEIGHT = 2.74 lb
T = 3.3 lb

MODE	FREQUENCY (Hz)	
	g = 32.2 ft/sec	g = 0
In-plane 1	1.29	-
In-plane 2	10.32	-
In-plane 3	15.3	-
Twist 1	1.58	-
Twist 2	2.27	-
Twist 3	3.74	-
Out of plane 1	0.91	-
Out of plane 2	1.22	-

TABLE 4-2-3

ANALYTICAL PREDICTIONS

DAMPED CONFIGURATION
TDR WEIGHT = 2.74 lb
T = 4.5 lb

MODE	FREQUENCY (Hz)	
	g = 32.2 ft/sec	g = 0
In-plane 1	0.96	0.94
In-plane 2	11.7	11.6
In-plane 3	15.8	15.7
Twist 1	1.52	1.16
Twist 2	2.2	1.97
Twist 3	3.5	2.53
Out of plane 1	0.92	0.77
Out of plane 2	1.28	1.03
Out of plane 3	2.46	1.70

TABLE 4-2-4

DAMPED CONFIGURATION
TDR WEIGHT = 2.74 lb
T = 4.6 lb

MODE	FREQUENCY (Hz)	
	g = 32.2 ft/sec	g = 0
In-plane 1	0.96	0.94
In-plane 2	11.7	11.6
In-plane 3	15.8	15.7
Twist 1	1.63	1.16
Twist 2	2.35	1.97
Twist 3	3.97	2.53
Out of plane 1	0.925	0.77
Out of plane 2	1.29	1.03
Out of plane 3	2.48	1.70

Analytical Undamped Mode Shapes

Damped Configuration

OUT-OF-PLANE MODE SHAPES

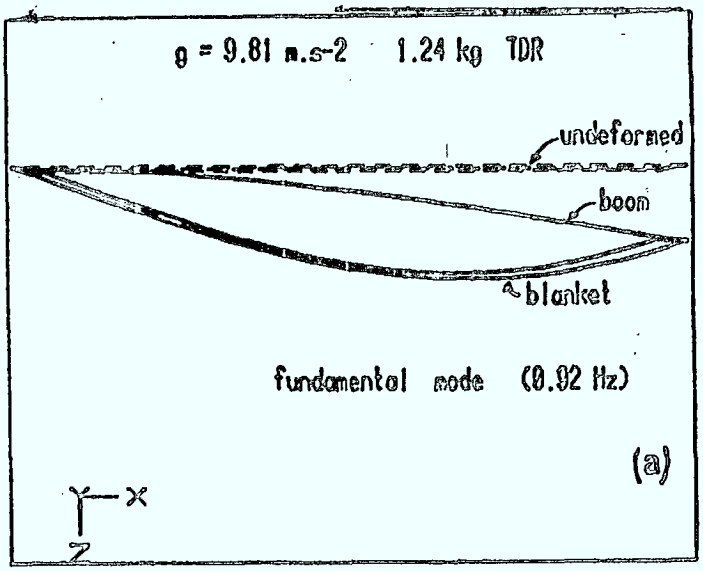

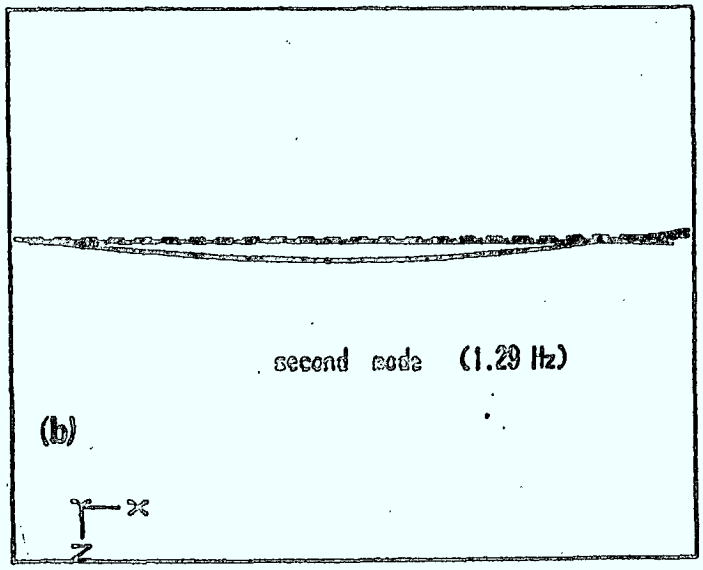

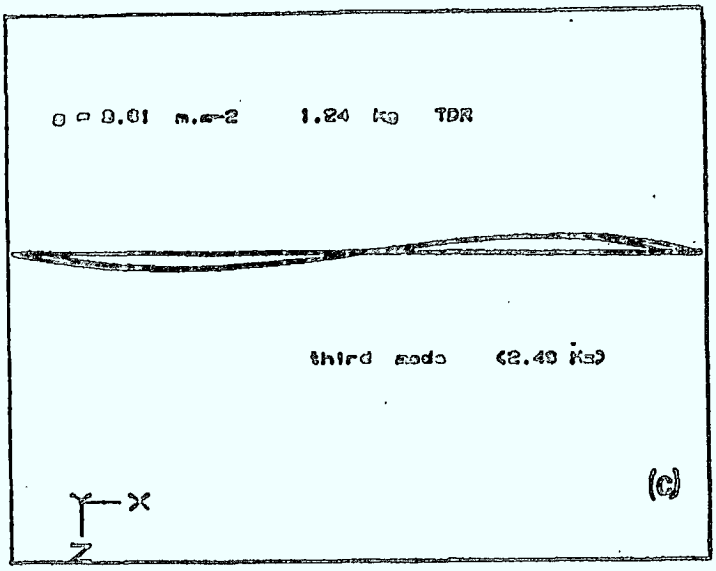

Figure A2

Analytical Undamped Mode Shapes

Damped Configuration

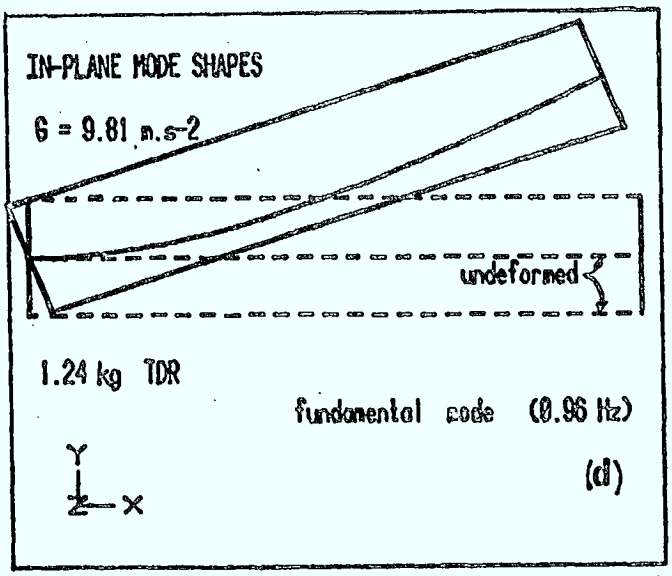

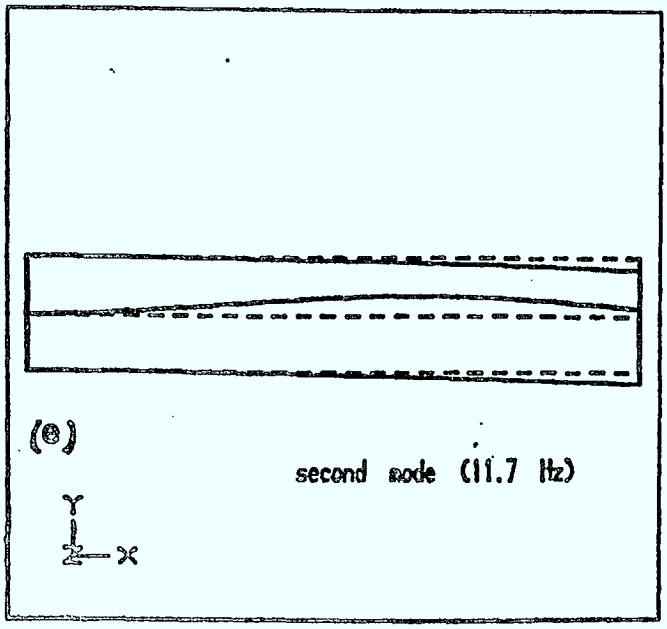

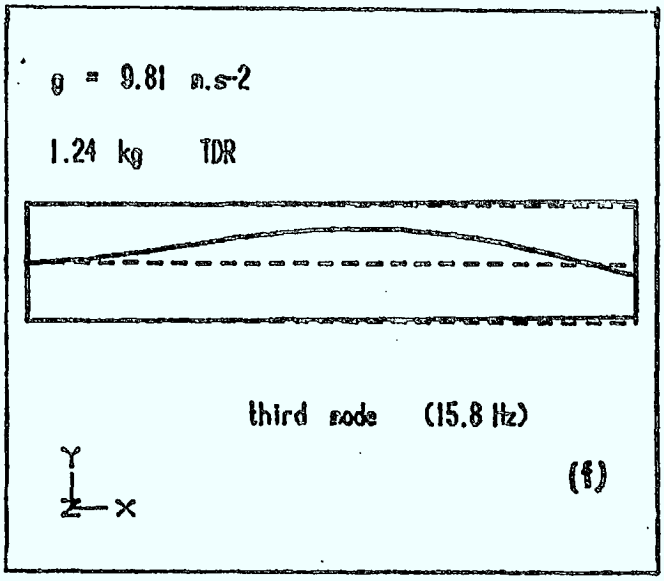

Figure 4.2

Analytical Undamped Mode Shapes

Damped Configuration

TWIST MODE SHAPES

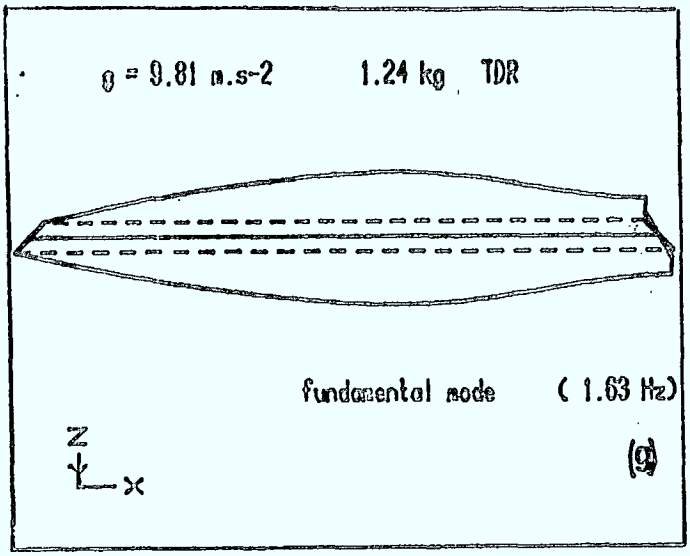

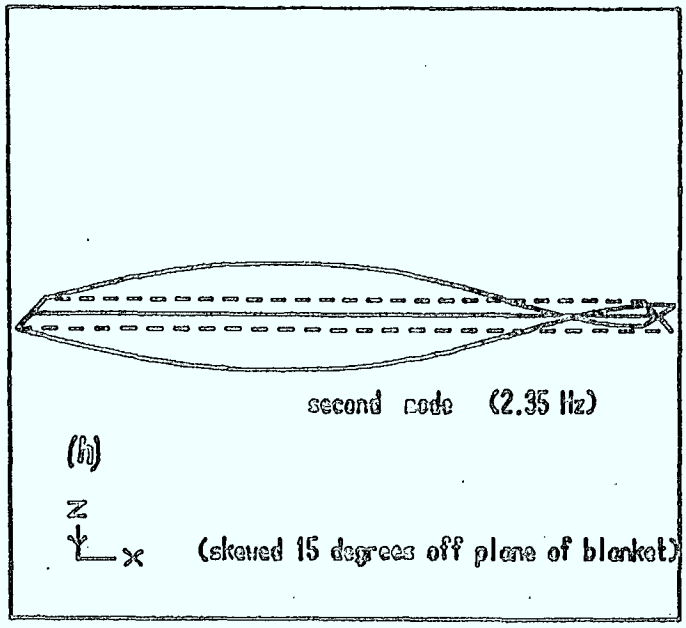

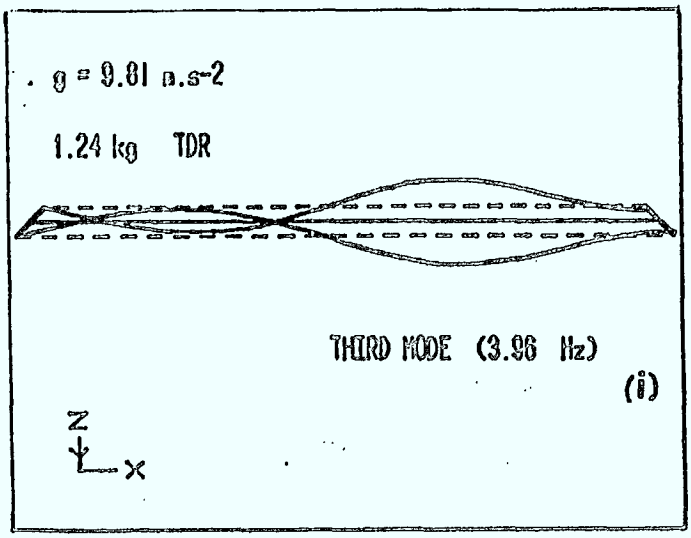

Figure 4.2

TABLE 4-3-1

COMPARISON OF ANALYTICAL AND TEST RESULTS
UNDAMPED CONFIGURATION

MODE	FREQUENCY (Hz)	
	Analysis	**Test**
In-plane 1	1.02	.88-.92
In-plane 2	11.0	
In-plane 3	15.9	12.5-12.7
Twist 1	1.55	.98-.99
Twist 2	2.34	1.08-1.10
Twist 3	3.61	1.44-1.56
		1.85-1.91
		9.6 -9.8
Out of plane 1	0.94	.9 -.98
Out of plane 2	1.24	1.45-1.56
Out of plane 3	2.22	5.6 -5.8

TABLE 4-3-2

COMPARISON OF ANALYTICAL AND TEST RESULTS
DAMPED CONFIGURATION

MODE	FREQUENCY (Hz)	
	Analysis	Test
In-plane 1	0.96	.86 - .88
In-plane 2	11.7	
In-plane 3	15.8	
Twist 1	1.63	1.20-1.21
Twist 2	2.35	1.72-1.77
Twist 3	3.97	2.34-2.39
Out of plane 1	0.925	.81- .86
Out of plane 2	1.29	.97-1.01
Out of plane 3	2.48	4.1

The undamped mode shapes for the damped array configuration in 1-g are shown in Figure 4-2(a-i).

A study to determine the effects of blanket damping is in progress. Preliminary results indicated that blanket damping may cause the natural frequency to increase slightly. The work done so far has shown 2% increase in frequency for a fundamental out of plane mode (damping value of 10^{-4}). Not all modes increase in frequency, some decrease and others are completely eliminated.

An increase in frequency was noted in the test results of some modes tested in air, over those in vacuum.

5.0 TEST DESCRIPTION

Three types of testing were done on the solar array (test plan described in Reference 8) and a fourth test was done for the tension damper rod alone. Section 5.1, the random testing was done in vacuum only. Section 5.2 the sine sweep testing was also done in vacuum only, on only the undamped configuration of the solar array. The step relaxation testing, Section 5.3, was done in both air and vacuum for the undamped array and in vacuum only for the damped array configuration.

The number of accelerometers present on the array at one time was limited to 7. Astromast testing, (see Ref. 1) had been done with 3 at one time (after a study to assess effects). The ratio of accelerometer and cable weight to total structure weight was not as critical for the array, since the structure was heavier. The number of accelerometers was limited by the maximum number of amplifiers available. This maximum number was chosen because of the time required for each vacuum test setup. The time required to pump the vacuum chamber down and to vent was at least two hours. The fewer the number of accelerometers per test setup, the greater number of times the chamber would have to be pumped down.

5.1 Random Test

The random, base excitation test was done for 20 accelerometer locations shown in Figure 2-3.0. The hydraulic shaker, described in Section 2.3.2 provided the input.

For the first few tests, a non-equalized random (from .5 Hz to 15 Hz) input was used. Based on astromast test results, it was considered dangerous to the structure to sustain the enforced high amplitude accelerations at low frequency, which would result from the equalized random input. Figure 5-1.1 shows the unequalized input spectrum. In fact, the solar array Q-factor was significantly lower than that of the astromast (8 compared to 45). As a result a revised (semi-equalized random) spectrum was used for the remaining tests. Figure 5-1.2 shows the revised spectrum. For each test configuration, a random test was done in the two perpendicular axes, X and Z.

Typical test duration was 15-30 minutes. The number of sample averages was 50, with an overlap factor of 4.

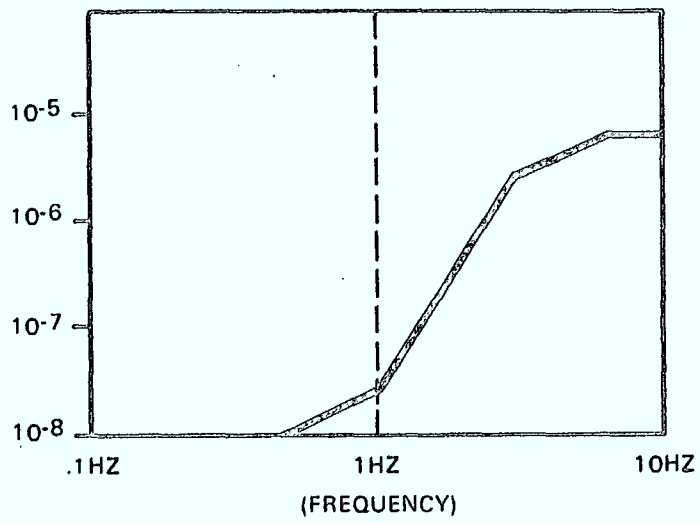

FIGURE 5.1-1 RANDOM UNEQUALIZED INPUT SPECTRUM

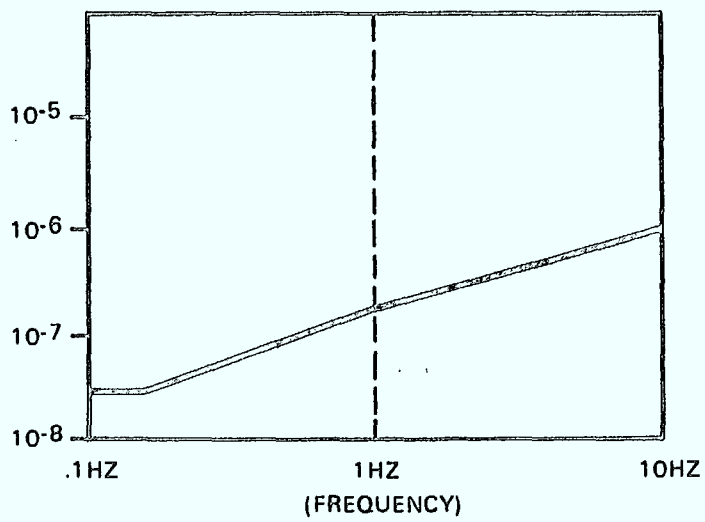

FIGURE 5.1-2 RANDOM EQUALIZED INPUT SPECTRUM

5.2 Sine Sweep Tests

The sine sweep, base excitation test was done with the 7 accelerometer locations shown in Figure 2-3.0. The input was provided by the hydraulic shaker, described in Section 2.3.2.

It had been planned that the sine sweep test should cover the range from .5 to 15 Hz. The sweep rate for such a test is extremely low.

$$\theta = \omega_n \left(\frac{\pi}{d\omega/dt} \right)^{1/2}$$

θ = Hop's sweep parameter Ref. 5 states that the sweep rate is slow enough if $\theta > 2$.

and thus, takes a great deal of time-2 hrs testing, plus setup per test. It was felt that this test did not warrant so much time. As a result, the test was cut to cover just .7 to 2.0 Hz (in fact, one test was stopped at 1.7 Hz) at a sweep rate of 3200 sec/Hz. Even this test occupied most of a morning.

The sine sweep amplitude level was .008 g's.

5.3 Step Relaxation

The step relaxation test was done with the accelerometer locations, shown in Figure 2-3.0. The step relaxation mechanism (Figure 2-3.3) provided the excitation input, at the mast tip (locations 4X and 4Z of Figure 2-3.0). Step relaxation is an impulse type of test, unlike the sine and random base inputs. Each test consisted of 4 'step relaxations' averaged to make modal estimates.

A step relaxation test was done by pulling the tip of the mast with a steady force (approximately 1 lb) to cause about a 1 inch tip deflection (if the 1 inch deflection was exceeded, longerons at the mast base would begin to buckle). The time for oscillation to die out was 1 to 2 minutes in air (slightly more in vacuum).

The test time for one configuration was of the order of 15 minutes.

5.4 Summary of Tests Done

Table 5-4 lists the testing done on the solar array model. The TDR testing consisted of static stiffness and dynamic testing of the damped TDR and two pretest units.

Table 5-4

SUMMARY OF TEST DONE

SPAR

a) STRUCTURE WITH UNDAMPED TENSION DAMPER ROD (TENSION LEVEL = 3.3 LB.)

BASE INPUT RANDOM TEST (0 TO 15 HZ, 18 DOF)	- IN PLANE EXCITATION	- VACUUM
	- OUT OF PLANE EXCITATION	- VACUUM
BASE INPUT SINE TEST (.7 TO 1.3 HZ, 7 DOF)	- IN PLANE EXCITATION	- VACUUM
	- OUT OF PLANE EXCITATION	- VACUUM
STEP RELAXATION TEST (7 DOF)	- IN PLANE EXCITATION	- VACUUM
	- OUT OF PLANE EXCITATION	- VACUUM
STEP RELAXATION TEST (7 DOF)	- IN PLANE EXCITATION	- AIR
	- OUT OF PLANE EXCITATION	- AIR

b) STRUCTURE WITH DAMPED TENSION DAMPER ROD (TENSION LEVEL = 4.6 LB)

BASE INPUT RANDOM TEST (0 TO 15 HZ, 18 DOF)	- IN PLANE EXCITATION	- VACUUM
	- OUT OF PLANE EXCITATION	- VACUUM
STEP RELAXATION TEST (7 DOF)	- IN PLANE EXCITATION	- VACUUM
	- OUT OF PLANE EXCITATION	- VACUUM

IN ADDITION TO THE ABOVE, TWO LOG DECAY TESTS WERE PERFORMED.

6.0 TEST RESULTS

The test results of the solar array, reported in this chapter are for vacuum tests only. The tests done in air are discussed in Section 9.0. There were two solar array configurations tested.

The first configuration (Section 6.1.1) is referred to as the undamped case, with blanket tension = 3.3 lb. The second configuration (Section 6.1.2) is referred to as the damped case, with blanket tension = 4.6 lb. The two configurations were changed only by the presence of the tension damper rod, which was also tested, independent of the solar array (see Section 6.2) to determine its dynamic characteristics.

6.1 Solar Array

The first solar array configuration was tested more extensively than the second. The results of the second configuration test are much clearer than the first. The increased tension level stiffened the structure such that many local modes and structural noise sources were eliminated.

There were several excitation techniques used on each configuration. The results do not appear to be independent of the type of excitation. There are three sources of difference. One is the excitation technique and software. The mode shapes for the base excitation test were not accurate because the software did not properly analyze the resuts. The frequencies and damping factors remained unaffected by this.

The second source of difference was the nonlinear nature of the structure. The structural characteristics are dependent on the amplitude of excitation. This effect, with respect to damping has been noted on the CTS Solar Array (Ref. 6). Though the overall excitation deflections were similar between tests, the amplitude for individual mode shapes would have been different.

The third source of difference also relates to the type of structure. Visual observations indicated that there were travelling waves travelling up through the blanket membrane. This type of vibration does not lend itself to modal characterization of the structure.

The resonant frequencies of the structure were not constant with respect to the accelerometer locations. The reason for this is not clear, test non-stationary, structural non-linearity or local structurally induced noise are all possibilities. In the case of random testing, three different instrumentation setups were required for one test configuration (due to a limited number of accelerometers). There would have been some mass loading effects due to the positioning of the accelerometers, but it was felt that the effect would be negligible (see Section 8.0).

The step relaxation and sine test data could not be used to determine mode shapes, because only the mast was instrumented. Only the random test data had sufficient test points to identify blanket modes. The blanket modes cannot be described in detail, due to an insufficient number of blanket accelerometers (six points).

The modal software (MPLUS) based damping and frequency estimates on individual frequency response functions. (It could make estimates from a more complete transfer function matrix, using the Polyreference technique. The Polyreference technique is extremely sensitive to non-linearity and non-stationarity. Recriprocity and stationarity checks indicated that the solar array data was not suitable for Polyreference processing).

6.1.1 **Undamped Solar Arrays: Blanket Tension = 3.3 lb** - Table 6-1.1.1 describes the modes detected by the modal analysis software used (MPLUS). Modal estimates are included for Random, Sine and Step Relaxation test data. Most modes existed for all three test types, though the frequency and damping values shifted slightly. There were modes that did not appear in all test data. The mode shape descriptions are incomplete or non-existent for many modes. These three factors made it extremely difficult to identify modes. Table 6-1.1.2 is the result of a statistical analysis of manually determined frequencies, for all test points on the structure. It allowed an estimate of realistic frequency ranges, which made it simpler to establish common modes between the test types. Figure 6-1.1.2 is a graphical illustration of the statistical results, based on the random test information, with the sine and step relaxation points plotted. The figure is a plot of the manually picked spectral peaks vs. accelerometer point (see Figure 2-3.0 for geometry).

The MPLUS estimates of frequency and damping were based on the frequency response function. The frequency range from the statistical peak peaking estimates were based on all of the test data points for a particular test configuration. The manual peak picking should have provided the best estimates of resonant frequencies. The damping values from the MPLUS estimates will be reasonable estimates, provided the modal spacing was not too close.

Table 6-1.1.3 combines the results of the MPLUS estimates and the manual statistical evaluation.

The results of the random, sine and step relaxation agreed, with the following exceptions:

1. The sine and step tests completely missed what appeared to be a strong in-plane/twist mode at 1.08 - 1.10 Hz. It has been suggested that the random results may have erroneously predicted this mode, but the consistency of the accelerometer responses, over three test runs makes that seem unlikely.

TABLE 6-1.1-1

MPLUS RESULTS - UNDAMPED CONFIGURATION VACUUM

TEST TYPE	FREQUENCY	DAMPING	MODE SHAPE DESCRIPTION
In-Plane			
Random	.909	.041	1st in-plane/torsion mode.
Random	1.145	.039	Blanket mode - twisting (about mast) and hanger blanket clapping.
Random	9.849	0.15	
Random	12.663	.040	Blank mast mode - torsion and in-plane bending.
Out of Plane			
Random	.848	.064	Mast and blanket bending (1st) out of phase with each other - slight twisting motion.
Random	1.119	.069	Blanket mode - twist; one side of blanket moves more than other; tip of mast moves slightly.
Random	1.458	.043	Blanket and mast bend (in phase) out of plane.
Random	1.557	.092	Hanger rod out of plane bending.
Random	5.840	.0029	Blanket mode out of plane.
Random	9.058	.0266	Blanket and hanger rod - clapping effect.
Random	9.665	.027	Mast twists; blanket folds.
Random	11.331	.041	Mast mode out of plane.

TABLE 6-1.1-1 - continued

TEST TYPE	FREQUENCY	DAMPING	MODE SHAPE DESCRIPTION
In-plane			
Sine	.923	.034	
Sine	1.017	.058	
Sine	1.169	.054	
Sine	1.910	.016	
Out of Plane			
Sine	.981	.054	
Sine	1.121	.050	
Sine	1.181	.090	Not a mast mode.
Sine	1.526	.009	Mast bends out of plane.
In-plane			
Step	.892	.078	1st in plane/torsion mode.
Step	9.617	.017	Mast twists (similar to random, f = 9.665 out of plane excitation).
Step	11.319	.017	Mast mode; similar to random, f = 12.663.

TABLE 6-1.1-1 - continued

TEST TYPE	FREQUENCY	DAMPING	MODE SHAPE DESCRIPTION
Out of Plane			
Step	.943	.077	Out of plane bending.
Step	1.077	.026	
Step	5.734	.007	
Step	7.950	.020	
Step	9.027	.029	
Step	9.889	.004	
Step	11.035	.015	

TABLE 6-1.1-2

STATISTICAL RESULTS
UNDAMPED CONFIGURATION
VACUUM

Spectral Peaks
T = 3.3
Vacuum

In-Plane Excitation

TEST TYPE	# SAMPLES	AVERAGE FREQUENCY	SAMPLE STANDARD DEVIATION	FREQUENCY RANGE	DESCRIPTION OF MODE
Random	4	.878	.013	.863-.893	Mast in plane response
Sine	5	.906	.022	.885-.927	Mast twist
Step	5	.916	.013	.904-.928	Mast twist
Random	8	.98	.016	.969-.991	Blanket twist/in plane response
Step	1	.996	-		Mast twist/in plane response
Sine	3	1.033	.010	1.016-1.050	Mast twist/in plane response
Random	14	1.089	.017	1.081-1.097	Mast blanket, twist/ in plane reponse
Random	8	1.461	.045	1.431-1.491	Mast and blanket twist/in plane response
Sine	2	1.517	.009	1.477-1.557	As above.
Sine	6	1.853	.065	1.80-1.906	Mast twist/in plane response

TABLE 6-1.1-2 - continued

Spectral Peaks
T = 3.3
Vacuum

In-Plane Excitation

TEST TYPE	# SAMPLES	AVERAGE FREQUENCY	SAMPLE STANDARD DEVIATION	FREQUENCY RANGE	DESCRIPTION OF MODE
Random	4	5.643	.111	5.512-5.774	Hanger rod responsse (out of plane)
Step	5	9.562	.050	9.514-9.610	Mast response
Random	8	9.594	.250	9.427-9.761	Mast and hanger rod response
Step	2	10.96	-	-	Mast tip response
Step	5	12.524	.188	12.345-12.703	Mast tip response
Random	11	12.675	.410	12.451-12.899	Mast and hanger rod response

TABLE 6-1.1-2 - continued

Spectral Peaks
T = 3.3
Vacuum

Out of-Plane Excitation

TEST TYPE	# SAMPLES	AVERAGE FREQUENCY	SAMPLE STANDARD DEVIATION	FREQUENCY RANGE	DESCRIPTION OF MODE
Random	12	.919	.026	.906-.932	1st out of plane, blanket and mast
Step	3	.951	.009	.936-.966	As above
Sine	4	.958	.017	.938-.978	As above
Random	2	1.005	-	-	
Step	1	1.039	-	-	
Sine	2	1.057	.025	.945-1.169	
Random	3	1.087	.010	1.070-1.104	
Sine	2	1.186	.050	.963-1.409	
Random	3	1.201	.026		
Random	5	1.493	.052	1.443-1.543	Out of plane blanket response
Sine	3	1.514	.008	1.501-1.527	In plane mast tip response
Random	5	5.605	.129	5.482-5.728	In plane mast tip, hanger rod response

TABLE 6-1.1-2 - continued

Spectral Peaks
T = 3.3
Vacuum

Out of-Plane Excitation

TEST TYPE	# SAMPLES	AVERAGE FREQUENCY	SAMPLE STANDARD DEVIATION	FREQUENCY RANGE	DESCRIPTION OF MODE
Step	6	5.610	.039	5.578-5.642	Mast twist response
Step	2	1.86	.094	7.440-8.280	Mast response
Random	10	8.984	.139	8.959-9.009	Mast and hanger rod response out of plane
Step	3	9.006	-	-	As above
Random	2	9.558	-	-	Mast response
Step	4	9.722	-	-	Mast response
Step	1	11.22	-	-	Mast tip in plane response
Random	7	11.456	.280	11.250-11.662	Mast and blanket out of plane response
Step	3	13.13	.064	12.992-13.238	Out of plane response (mast and tip)

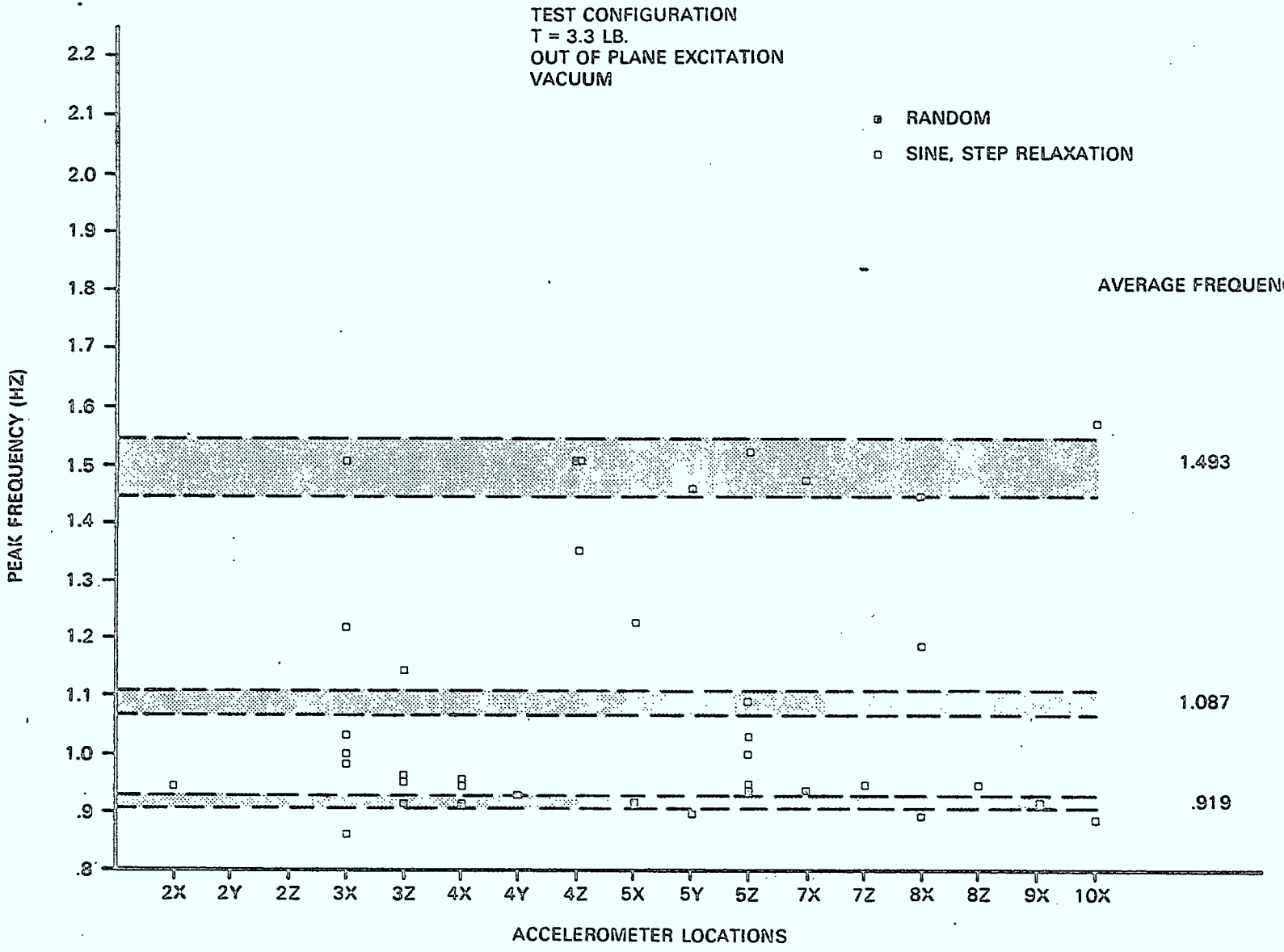

FIGURE 6.1.1-2 FREQUENCY RESPONSE FUNCTION PEAK vs ACCELEROMETER LOCATIONS

TABLE 6.1.1-3a

SUMMARY OF RESULTS
UNDAMPED TDR VACUUM TEST

EXCITATION DIRECTION	TEST TYPE	FREQUENCY RANGE (HZ)	DAMPING	MODE SHAPE DESCRIPTION
IN PLANE	RANDOM, SINE, STEP	.88-.92	.04-.08	MAST IN PLANE/TWIST RESPONSE
IN PLANE	RANDOM, SINE, STEP	.98-.99	.06	BLANKET TWIST/IN PLANE RESPONSE
IN PLANE	RANDOM	1.08-1.10	.04-.05	MAST & BLANKET; TWIST/IN PLANE RESPONSE; HANGAR RODS CLAPPING
IN PLANE	RANDOM	1.44-1.46		MAST & BLANKET; TWIST/IN PLANE RESPONSE
IN PLANE	SINE	1.56		
IN PLANE	SINE	1.85-1.91	.02	MAST TWIST/IN PLANE
IN PLANE	RANDOM, STEP	9.6-9.8	.015-.017	MAST & HANGAR ROD; TWISTING
IN PLANE	RANDOM, STEP	12.5-12.7	.04	MAST MODE; TORSION & IN PLANE BENDING

TABLE 6.1.1-3b

SUMMARY OF RESULTS
UNDAMPED TDR VACUUM TEST

SPAR

EXCITATION DIRECTION	TEST TYPE	FREQUENCY RANGE (HZ)	DAMPING	MODE SHAPE DESCRIPTION
OUT OF PLANE	RANDOM, SINE, STEP	.9-.98	.05-.08	1ST OUT OF PLANE, BLANKET & MAST RESPONSE
OUT OF PLANE	RANDOM, SINE	1.45-1.56	.04-.09	BLANKET, MAST, HANGAR ROD - OUT OF PLANE RESPONSE
OUT OF PLANE	RANDOM, STEP	5.6-5.8	.003-.007	BLANKET MODE - OUT OF PLANE; IN PLANE-MAST TIP
OUT OF PLANE	RANDOM, STEP	9.0	.027-.029	BLANKET & HANGAR ROD CLAPPING EFFECT MAST OUT OF PLANE RESPONSE
OUT OF PLANE	RANDOM, STEP	9.5-9.7	.027	MAST TWISTS; BLANKET FOLDS
OUT OF PLANE	RANDOM, STEP	11.3-11.5	.04	MAST & BLANKET; OUT OF PLANE RESPONSE
OUT OF PLANE	STEP	13.1	.06	MAST OUT OF PLANE

2. Blanket responses could only be determined from random test data (due to insufficient instrumentation).

3. For the first in-plane and bending modes, the random data frequencies were significantly lower than the sine and step relaxation tests. This phenomena has been noted in other modal analysis tests.

4. The sine data did not provide any information above 2 Hz (because the sine sweep was halted at 2 Hz).

5. The random and step data missed the in-plane/twist mode at 1.8 - 1.9 Hz. The effect of testing with sinusoidal base excitation is improved modal tuning.

6. The random test failed to detect an out-of-plane mode at 13 Hz. The emphasis was on establishing low frequency results. It is possible that this mode was not excited.

7. The sine test predicted the lowest damping values and the highest frequency estimates (also most consistent frequency values). Sine testing generally exhibits these trends.

A comparison between in and out of plane modes indicates the following:

1. First mode had slightly lower frequency for in-plane response. The damping values were similar.

2. A blanket mode exists at 5.6 Hz for the out-of-plane case. No blanket modes existed for the in-plane case from 2 to 10 Hz.

3. The highest modes for the two cases had approximately the same damping values.

The modes shapes, produced from the MPLUS program are not included. The ones that were reasonably accurate were the same as those for the damped array configuration (see Figure 6-1.2.3).

6.1.2 Damped Solar Array: Blanket Tension = 4.6 lb - Table 6-1.2.1 describes the modes detected by the modal analysis software (MPLUS). Figure 6-1.2.1 is an example of the MPLUS output which lead to these results. Modal estimates are included for Random and Step Relaxation test data. Most modes existed for both types of test data, though the frequency and damping values shifted slightly.

Figure 6-1.2.2 is an example of frequency response function peaks (picked manually) vs. accelerometer number. This helped to pick out modes or determine where closely spaced modes exist. It also served as a check on the MPLUS estimates of frequency and types of mode shapes. Table 6-1.2.2 is a statistical

TABLE 6-1.2-1

MPLUS RESULTS
DAMPED CONFIGURATON - VACUUM

TEST TYPE	DATA QUALITY	FREQUENCY	DAMPING	MODE SHAPE DESCRIPTION
In-Plane				
				Mast and Blanket
Random	Good γ^2 = .9	.885	.042	Torsion and in plane - (1st) slight torsion and out of plane blanket response.
Random	Poor γ^2 = .5	1.774	.030	Blanket mode - 1st blanket torsion.
Random	Poor γ^2 = .7	2.008	.031	Blanket mode - 2nd blanket torsion. Outer edges of blanket move in opposite direction and twist.
Random	Good γ^2 = .95	11.855	.045	Mast torsion and plane (2nd) mast looks like beam swinging mast-simply supported beam in plane excite; out of plane response blanket non-symmetric out of plane motion.
Out of Plane				
Random	Good γ^2 = .9	.831	.070	Out of plane bending (1st) blanket and mast - hanger rod (tip) and opposite phase blanket clapping effect.
Random	Poor γ^2 = .8	4.140	.019	Blanket mode - out of plane one side of blanket moves more than other.

TABLE 6-1.2-1 - continued

TEST TYPE	DATA QUALITY	FREQUENCY	DAMPING	MODE SHAPE DESCRIPTION
Out of Plane				
Random	Poor γ^2 = .8	5.638	.018	Blanket mode out of plane bending inboard hanger clapping effect.
Random	Good γ^2 = .9	11.231	.049	
In-Plane				
Step	Good	.894	.053	1st bending in plane.
Step	Good	.994	.028	Tip motion only.
Step	Good	1.166	.029	
Step	Fair	8.386	.039	
Out of Plane				
Step	Good	.838	.046	1st bending (out of plane).
Step	Good	1.090	.002	Tip motion only.

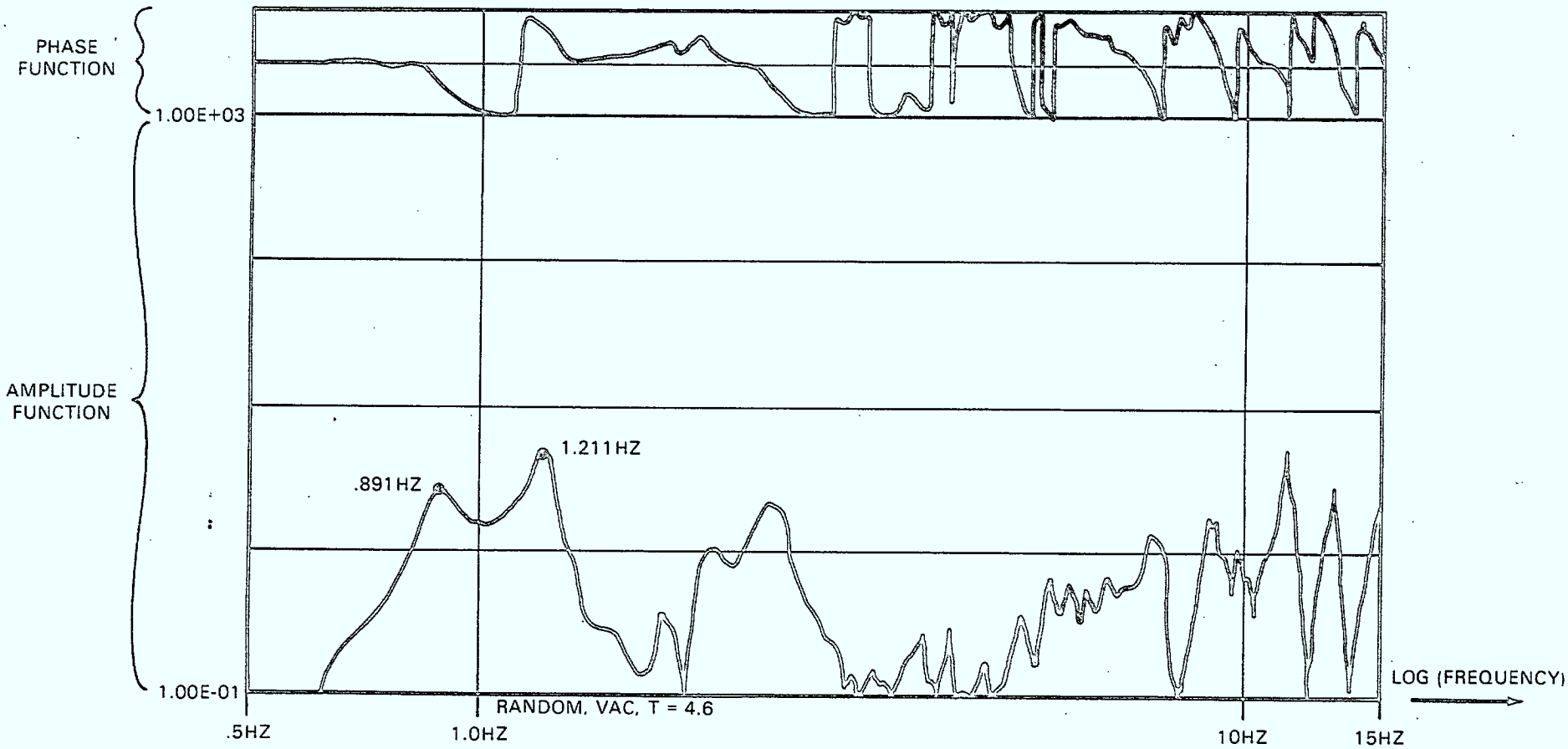

FIGURE 6.1.2-1a FREQUENCY RESPONSE FUNCTION OUT OF PLANE, BLANKET ACCELEROMETER

1) CHOOSE FREQUENCY BOUNDS FOR PARAMETER ESTIMATION (IN THIS CASE .6 TO 1.6 HZ)

2) MARK PEAKS: 1 = .90 HZ
2 = 1.21 HZ
3 = 1.25 HZ

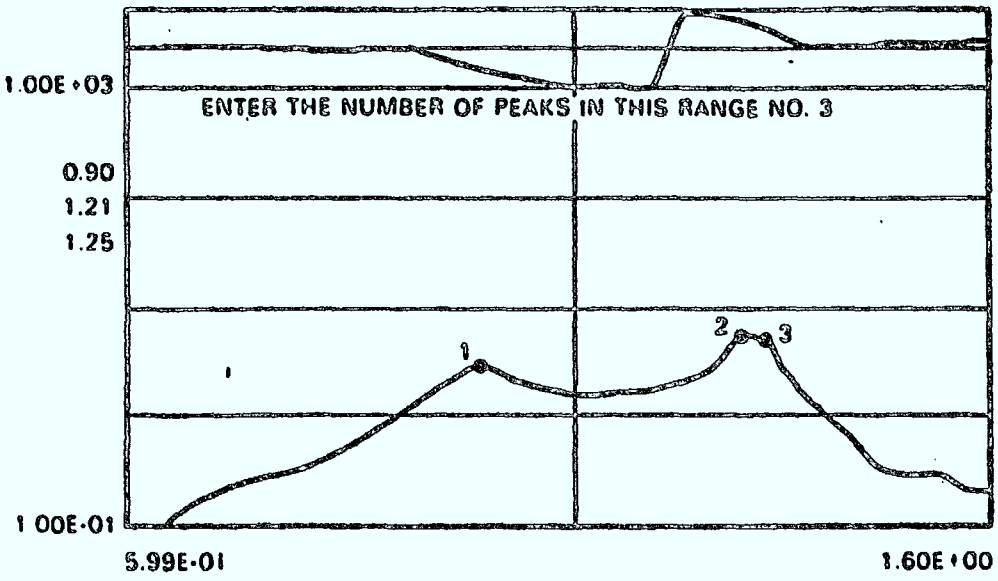

3) SOFTWARE ESTIMATES FREQUENCY AND DAMPING VALUES. THESE RESULTS ARE USED TO FORM AN ANALYTICAL CURVE. WHICH IS PLOTTED OVER EXPERIMENTAL VALUES

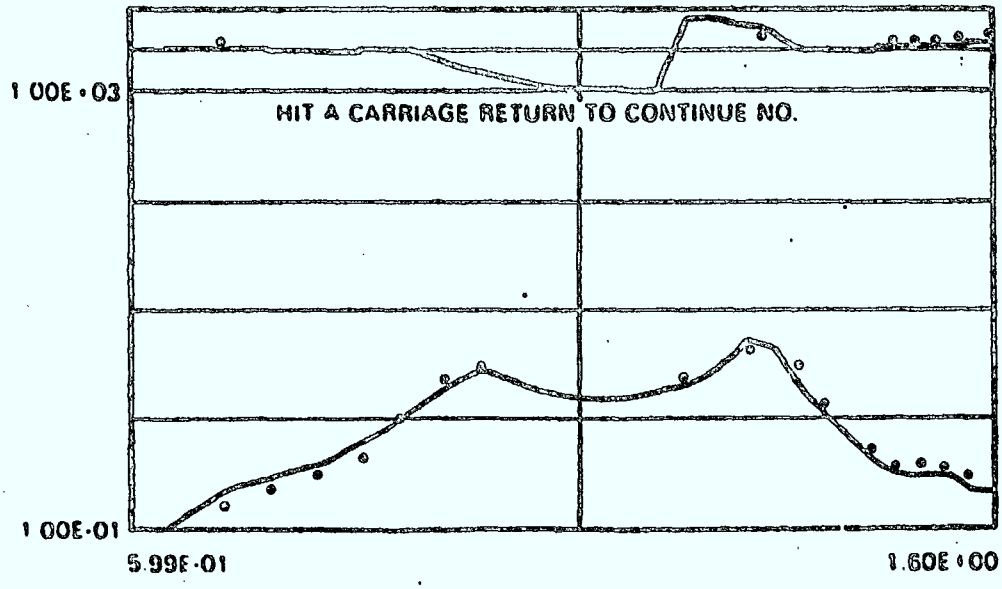

FIGURE 6.1.2-1b PARAMETER ESTIMATION

4) THE CALCULATED PARAMETERS ARE:

FREQUENCY	DAMPING	PHASE
.885	.042	1.838
1.228	.028	-1.611

5) ALL FREQUENCY RESPONSE FUNCTIONS (FOR THE SELECTED TEST CONFIGURATION) ARE SEARCHED. THEIR REAL AND IMAGINARY PEAK VALUES ARE PLOTTED (FOR FREQUENCY RANGE OF INTEREST).

FREQ. = 0.8848
DAMP = 0.4229E-01
1Z- 9X+
MODE SHAPE 0: SCALE 1.75
MODE COEFFICIENT
REAL -6.65992E-01
IMAG 2.79119E+00
AMPL 2.86955E+00
LIMITS 0.859 0.938

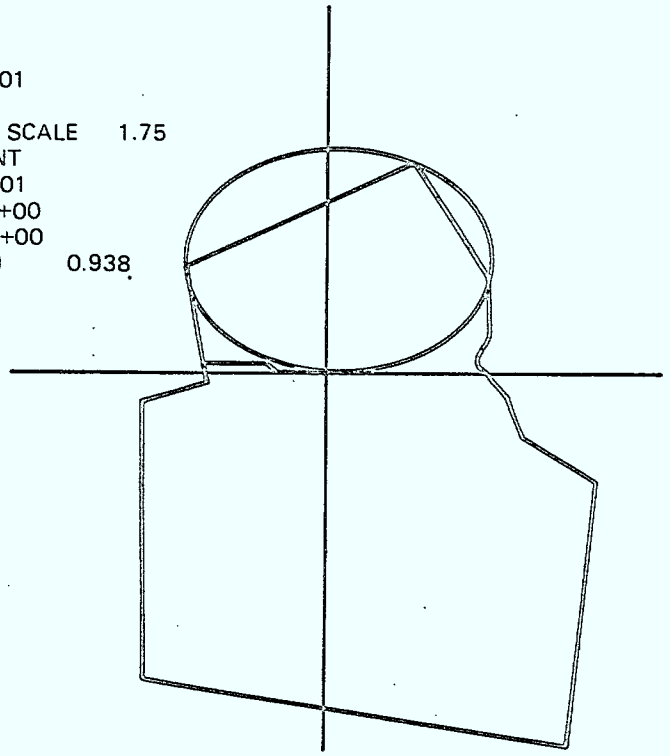

1: 1Z- COMP,F = 0.885HZ

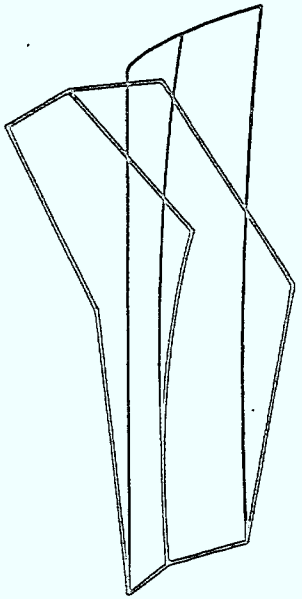

6) THE AMPLITUDE VALUES FROM THE FREQUENCY RESPONSE FUNCTION SEARCH ARE APPLIED TO THE STRUCTURES GEOMETRY FILE TO PRODUCE A MADE SHAPE.

FIGURE 6.1.2-1c MODE SHAPE ESTIMATION

TABLE 6-1.2-2

STATISTICAL RESULTS
DAMPED CONFIGURATION

Spectral Peaks
T = 4.6
Vacuum

TEST TYPE	# SAMPLES	AVERAGE FREQUENCY	SAMPLE STANDARD DEVIATION	FREQUENCY RANGE	DESCRIPTION OF MODE
In-Plane Excitation					
Step	7	.870	.009	.864-.877	Blanket and mast response lst in-plane mode.
Random	16	.870	.015	.864-.877	
Random	5	1.207	.006	1.201-1.213	Mast tip and blanket response out of plane (i.e., twist dominates).
Random	3	1.745	.015	1.720-1.770	Blanket response (out of plane).
Random	3	1.987	.012	1.967-2.007	Blanket response (out of plane).
Random	4	2.365	.025	2.336-2.394	Blanket out of plane response (centre of blanket has maximum deflection).
Random	1	3.652	-	-	Blanket centre response (one side only). (Out of plane).
Random	1	6.248	-	-	Same as above (3.652).

TABLE 6-1.2-2 - continued

TEST TYPE	# SAMPLES	AVERAGE FREQUENCY	SAMPLE STANDARD DEVIATION	FREQUENCY RANGE	DESCRIPTION OF MODE
Step	5	8.314	.080	8.24-8.39	Mast response.
Step	5	10.986	.309	10.69-11.28	Mast response (centre portion of mast has largest deflections).
Random	10	11.619	.201	11.50-11.74	Mast and blanket response - blanket response is out of plane.
Out of Plane					
Random	9	.821	.015	.812-.830	Out of plane mast and blanket response.
Step	7	.847	.013	.837-.857	Out of plane mast response.
Random	2	.891	0	N.A.	In-plane response of mast tip and one side of tip hanger.
Random	4	.988	.015	.970-1.006	In-plane response of mast tip and tip hanger rod.

TABLE 6-1.2-2 - continued

TEST TYPE	# SAMPLES	AVERAGE FREQUENCY	SAMPLE STANDARD DEVIATION	FREQUENCY RANGE	DESCRIPTION OF MODE
Random	9	10.92	.078	10.87-10.97	Mast and blanket response (blanket out of plane - light response) - mast similar to step.
Step	4	10.838	.186	10.62-11.06	Mast response (centre portion of mast deflects - tip does not).
Random	2	4.137	-	-	One side of blanket out of plane very clear response at blanket centre.
Random	1	5.594	-	-	One point on blanket centre very clear response (out of plane).

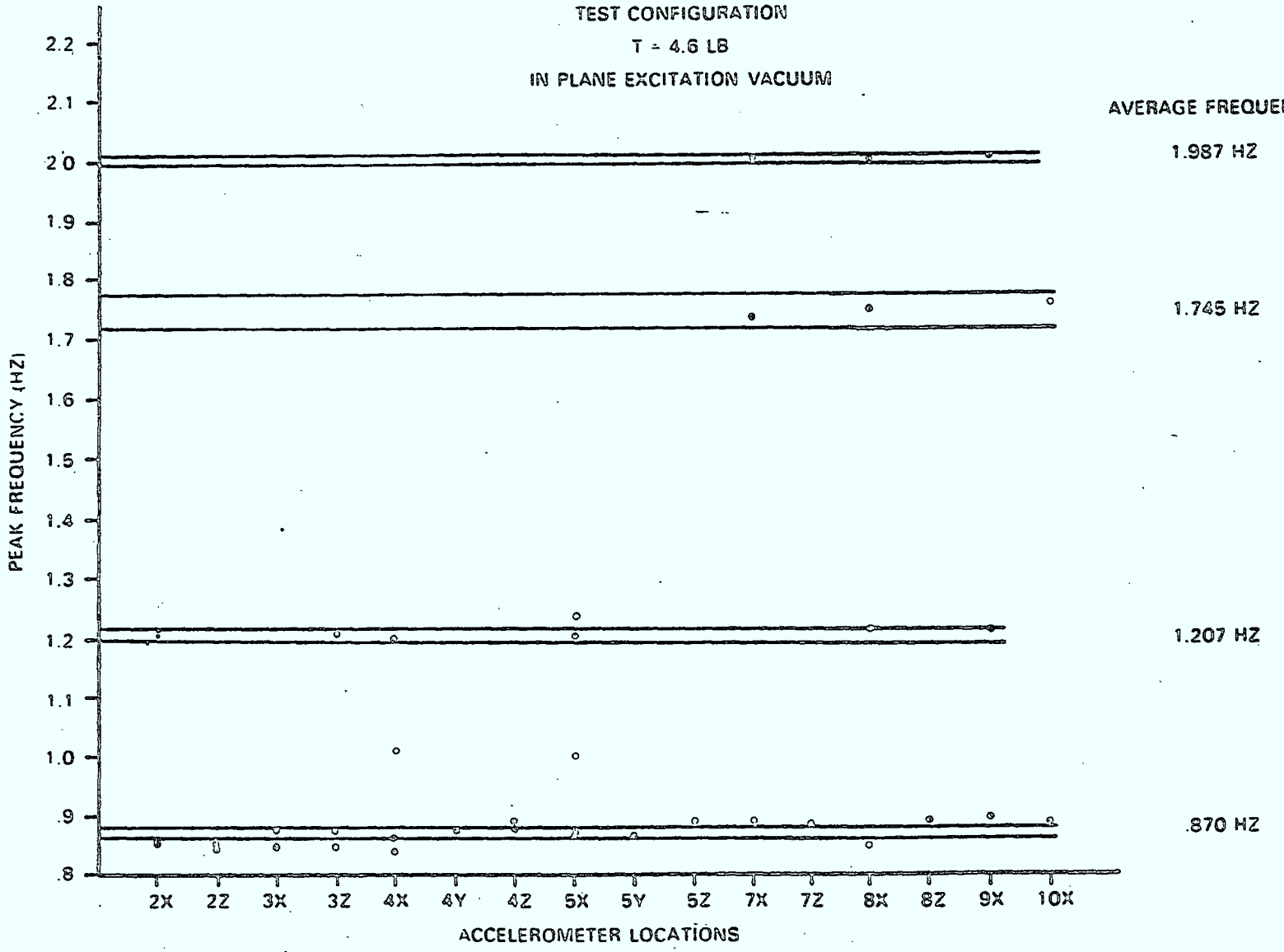

FIGURE 6.1.2-2 FREQUENCY RESPONSE FUNCTION PEAK vs ACCELEROMETER LOCATION

TABLE 6.1.2-3a

SUMMARY OF RESULTS
DAMPED TDR VACUUM TEST

SPAR

EXCITATION DIRECTION	TEST TYPE	FREQUENCY RANGE (HZ)	DAMPING	MODE SHAPE DESCRIPTION
IN PLANE	RANDOM, STEP	.86-.88	.04-.05	1ST IN PLANE/TWIST MODE-MAST & BLANKET
IN PLANE	RANDOM	1.20-1.21	.03	MAST TIP & BLANKET RESPONSE-OUT OF PLANE (i.e. TWIST DOMINATES)
IN PLANE	RANDOM, STEP	1.72-1.77	.03	BLANKET RESPONSE-OUT OF PLANE (BLANKET TORSION)
IN PLANE	RANDOM	1.97-2.01	.03	BLANKET RESPONSE-OUT OF PLANE (BLANKET TORSION)
IN PLANE	RANDOM	2.34-2.39		BLANKET RESPONSE-OUT OF PLANE
IN PLANE	RANDOM	3.65		BLANKET RESPONSE (ONE SIDE ONLY)
IN PLANE	RANDOM	6.25		BLANKET RESPONSE (ONE SIDE ONLY)
IN PLANE	STEP	8.24-8.39	.04	MAST RESPONSE
IN PLANE	STEP RANDOM	10.69-11.28 11.50-11.74	.05	MAST & BLANKET RESPONSE - BLANKET RESPONSE OUT OF PLANE (TWISTING)

TABLE 6.1.2-3b

SUMMARY OF RESULTS
DAMPED TDR VACUUM TEST

SPAR

EXCITATION DIRECTION	TEST TYPE	FREQUENCY RANGE (HZ)	DAMPING	MODE SHAPE DESCRIPTION
OUT OF PLANE	RANDOM	.81-.83	.070	OUT OF PLANE MAST & BLANKET RESPONSE (BLANKET & MAST OPPOSITE PHASE); TIP HANGAR ROD & BLANKET CLAPPING
OUT OF PLANE	STEP	.84-.86	.046	OUT OF PLANE MAST RESPONSE
OUT OF PLANE	RANDOM	.89		IN PLANE RESPONSE OF MAST TIP & ONE SIDE OF TIP HANGAR (RESULT OF BASE ACCⁿ ON TWISTED LONGERON)
OUT OF PLANE	RANDOM	.97-1.01		IN PLANE RESPONSE OF MAST TIP & TIP HANGAR
OUT OF PLANE	RANDOM	4.1	.02	BLANKET RESPONSE-OUT OF PLANE - ONE SIDE OF BLANKET MOVES MORE THAN OTHER
OUT OF PLANE	RANDOM	5.6	.02	BLANKET RESPONSE-OUT OF PLANE - BASE HANGAR CLAPPING EFFECT
OUT OF PLANE	STEP RANDOM	10.7-11.3 11.5-11.7	.05	MAST BENDING - OUT OF PLANE

TEST CONFIGURATION

T = 4.6 LB
VACUUM
RANDOM, BASE

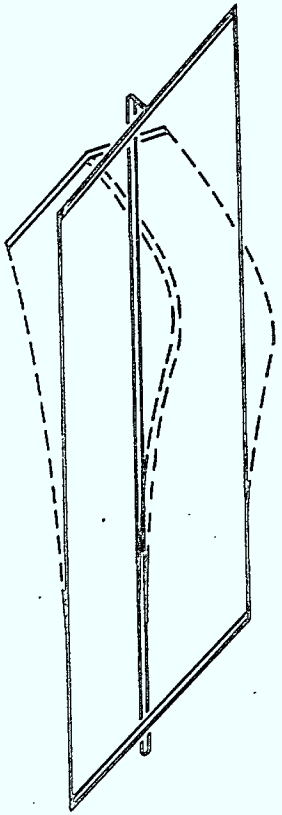

FREQUENCY: .87 HZ
EXCITATION: IN PLANE
DESCRIPTION OF MODE: 1ST IN PLANE BENDING/TORSION MODE OF MAST AND BLANKET

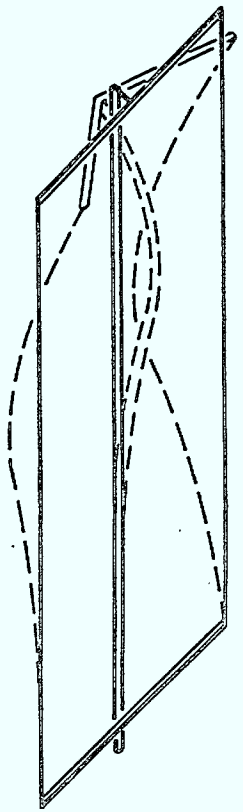

FREQUENCY: .82 HZ
EXCITATION: OUT OF PLANE
DESCRIPTION OF MODE: OUT OF PLANE BENDING OF BLANKET AND MAST
- MAST AND BLANKET HAVE OPPOSITE PHASE
- HANGER RODS AND BLANKET ENDS HAE CLAPPING EFFECT

FIGURE 6.1.2-3a **MODE SHAPES**

TEST CONFIGURATION

T = 4.6 LB

VACUUM
RANDOM, BASE

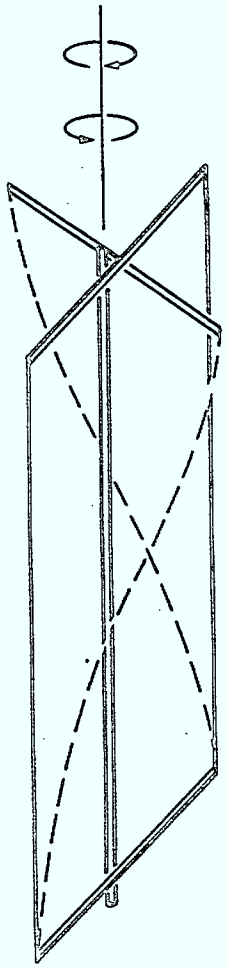

FREQUENCY: 1.7 HZ
EXCITATION: IN PLANE
DESCRIPTION OF MODE: BLANKET TORSION

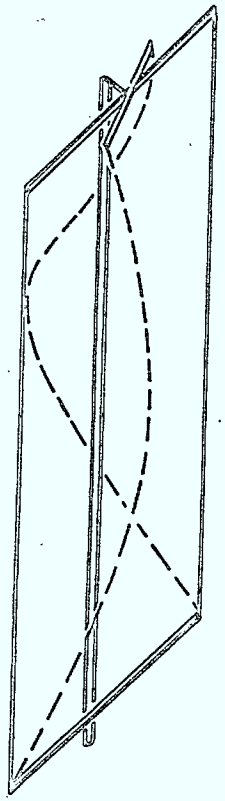

FREQUENCY: 2.0 HZ
EXCITATION: IN PLANE
DESCRIPTION OF MODE: BLANKET TORSION
- OUTER EDGES OF BLANKET ROTATE IN OPPOSITE DIRECTION

FIGURE 6.1.2-3b MODE SHAPES

TEST CONFIGURATION

T = 4.6 LB
VACUUM
RANDOM, BASE

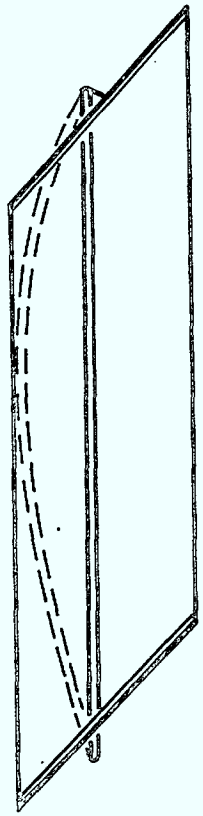

FREQUENCY: 11.6 HZ
EXCITATION: IN PLANE
DESCRIPTION OF MODE: MAST IN PLANE BENDING/TORSION
- MAST TAKES SHAPE OF SIMPLY SUPPORTED BEAM

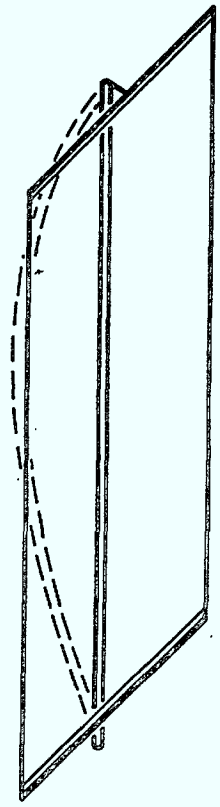

FREQUENCY: 10.9 HZ
EXCITATION: OUT OF PLANE
DESCRIPTION OF MODE: MAST OUT OF PLANE BENDING
- MAST TAKES SHAPE OF SIMPLY SUPPORTED BEAM

FIGURE 6.1.2-3c MODE SHAPES

interpretation of the manually selected peak responses. The statistics are based on the Student-t distribution (appropriate for less than 30 samples). The frequency range column is the range where there is 95% certainty that the resonant frequency actually exists.

The MPLUS estimates of frequency and damping are based on one frequency response function. The frequency range from the statistical peak picking is the average structural frequency. The damping values from the MPLUS estimates will be reasonable values, as long as there was not another mode close by. The statistical information provides a better estimate of the frequency value. The mode shapes of the structure were determined by the amplitudes of each point at the frequency value chosen within MPLUS. For this reason, the shapes will be distorted if the structural frequency and the single point estimated frequency are significantly different.

Table 6-1.2.3 incorporates the results from MPLUS and the manual statistical evaluation.

The results of the random and step relaxation agree with the following exception:

1. Blanket responses could only be determined from the random test (only the mast was instrumented for the step relaxation test).

2. The random test failed to note the mast resonance at 8.3 Hz.

3. The results of the second mast and blanket resonance (at about 11 Hz) were at slightly different frequencies for the two tests.

4. The first out-of-plane bending results are at different frequencies (.82 compared to .85) for the two techniques. The damping values were also different (.046 compared to .07).

Figure 6-1.2.3 illustrates mode shapes which are reasonably accurate.

The damping value ( ) for mast modes varies from .04 to .07 and the value for blanket modes is .02 to .03.

6.1.3 **Summary of Solar Array Results** - Two sets of solar array testing were done. The key differences between the two tests were: blanket tension level (3.3 and 4.6 lb); weight of tension mechanism (TDR) (1.8 lb to 2.7 lb) and damping characteristics of tension mechanism (TDR, Section 6.2).

The test data was not accurate enough to note differences between mode shapes for the two structures. The differences between the two configurations were as follows:

1. Damping values were not significantly different.

2. Out of plane first mode frequency values were lower for the T = 4.6 lb case. Higher modes did not change significantly.

3. More in-plane blanket modes could be identified for the T = 4.6 lb. case.

4. The first in-plane/twist modes had approximately the same frequencies. The higher mast modes had slightly lower frequencies for the T = 4.6 lb. case.

6.2 Static and Dynamic Testing of TDR

6.2.1 Introduction - The function of the Tension Damper Rod (TDR) was to absorb some of the energy of vibration. A perfect device would make the behaviour of a large, flexible solar array appear to the reaction control system as a rigid body. If this were the case, the modes would not need to be considered in control system design. In this sense, each vibration mode would be critically damped. In theory, this is possible with distributed damping such as structural damping. In practice, the structural damping is small (7% maximum) and it is not possible to artificially increase it enough. Alternatively, it is possible to integrate a two point damper within the array structure. This type of damper cannot critically damp any of the modes, since it is an internal (not grounded) but it could damp most of the modes which excite it. The efficiency of damping depends on the damping factor and the stroke length of the damper. The factor C depends on the materials used in the design.

In the TDR design, the damping material used was Ensolite (Uniroyal Type 'AH' Gray Shock Absorbing Foam). The stroke length depended on the flexibility allowed across the damper. The damper operational stroke length was designed to be 1.5 inches. The actual C, K factors were determined subsequent to the design.

6.2.2 Selection of Testing Method - Two tests were selected to characterize the TDR:

1. Static Hysteresis Test.
2. Dynamic Resonance Test.

The static tests (Figures 6-2.1.1 and 6-2.1.2) showed high non-linearities in the viscoelastic foam material. This was observed from the values of residual strain in the foam after unloading the stress in each tested unit.

A simple drop test was made for the foam. It was found that the rebound distance was less than 5% of the original drop height. This indicated that 95% of the kinetic energy was absorbed by the foam. Based on the two stiffness tests, it was concluded that the damper would exhibit nonlinear behaviour. Therefore, it

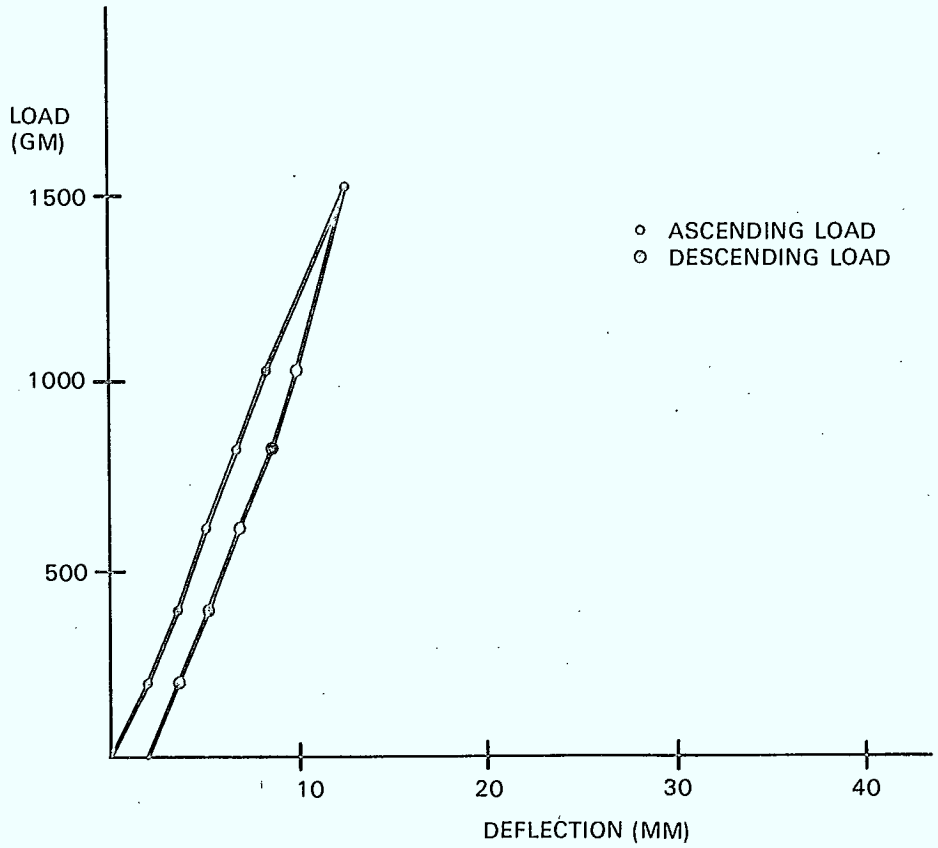

FIGURE 6.2.1-1 TENSION DAMPER ROD - SEALED UNIT
LOAD vs DEFLECTION

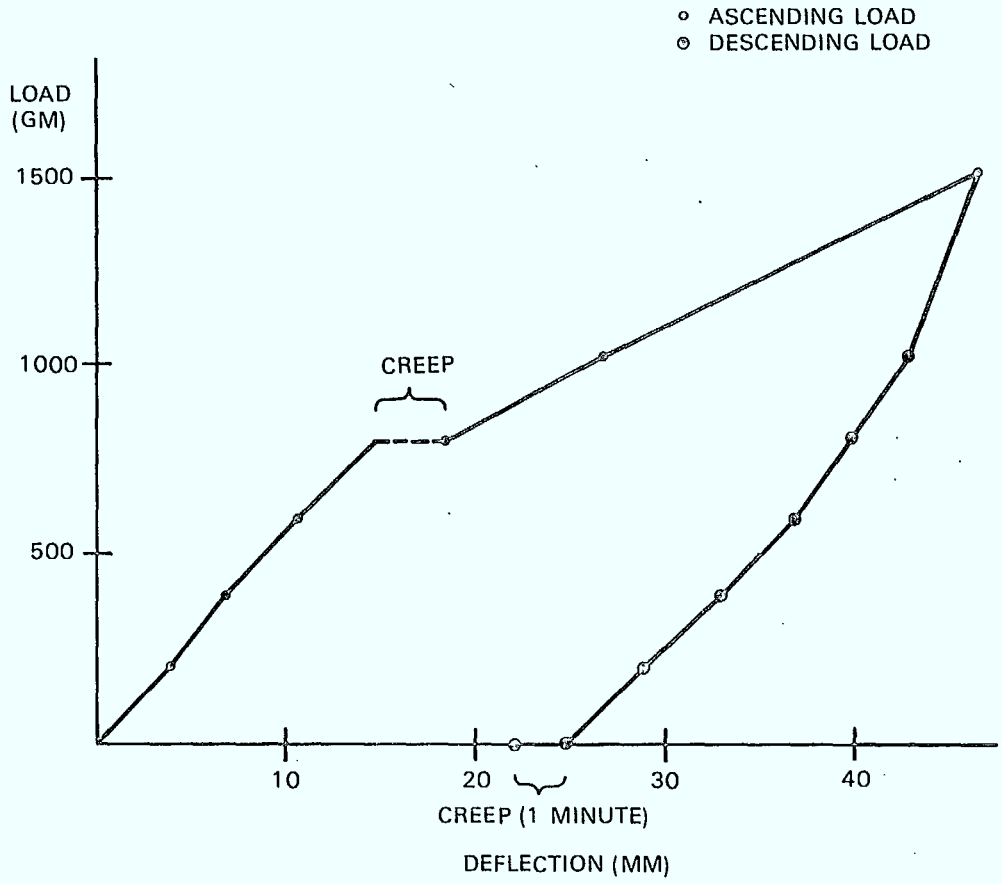

FIGURE 6.2.1-2 TENSION DAMPER ROD - PRETEST UNIT
LOAD vs DEFLECTION

was decided that a sine sweep test would be most appropriate. The sweeps were to be ascending and descending in frequency, repeated with variable amplitudes. The intentions were:

1. Identify a softening or hardening nonlinearity amplitude - if an amplitude jump phenomenon was noted during the test.

2. Identify any load dependence from the damper transfer function.

6.2.3 Test Specimens -Three specimens were used for the dynamic test. The amount of foam in each specimen was identical. The differences between the specimens were:

1. Difference in tip and total mass.

2. Difference in stiffness.

3. Difference in the foam connectivity to the TDR structure.

The specimens were:

1. A vacuum sealed unit (weight 1152 grams) purged with helium. The foam was bonded to the central rod (4mm diameter), as well as the mechanism rods. This unit was the one used on the solar array model for testing. This unit is referred to as the 'sealed unit'.

2. The second unit weighed 383 grams. The foam was bonded to all bars. The central rod diameter was 3mm (this corresponded to 42% of the sealed unit stiffness). This unit is referred to as the 'bonded unit'.

3. The third unit weighed 383 grams. The foam and the mechanism bar interface was greased. The central bar was bonded to aid the self centering motion. This unit is referred to as the 'greased unit'.

Based on linear assumptions, the expected results were:

1. Different natural frequencies and damping ratios, resulting from mass and stiffness variations.

2. Different damping ratios, . The damping coefficients 'C' were expected to be close, at least for specimens with bonded foam and for tests where identical strokes were excited. The greased specimen was expected to have a different 'C' value, due to the different damping concept.

From the corresponding test graph the value of g, Q and w are entered to the table. To calculate the values of ζ, c, E, x and S follow the equations:

$$\zeta = 1/2Q(1 - \zeta^2)^{1/2}, \quad c = 2\ wm\zeta$$

$$x = 9810/(2\pi)^2\ g/w^2, \quad S = 2(Q-1)X_i$$

$$E = \pi\ cw(x_i Q)^2 = \pi c/w\ (\ddot{x}_i Q)^2$$

6.2.4 Test Results

6.2.4.1 Summary of Results - The maximum damping force was obtained for the TDR sealed unit. The damping coefficient c was 10.0 N.sec/m, more than double the value of either of the other specimens. The maximum excited damper stroke exceeded 21mm for 1.5g load.

The dissipated energy per cycle was 0.375 Joules at its constrained frequency of 9.3 Hz. If the TDR was to have a frequency equal to the array frequency, the damped energy for the same stroke S would be 0.037 Joules/cycle. This value is approximately twice the strain energy in the Step Relaxation Test (tip deflection = 1 inch).

For optimum damping, the TDR natural frequency should be designed to be approximately equal to the solar array frequency. At resonance, it would sufficiently decouple the blanket from the mast to allow the TDR to remove most of the vibration energy.

The ratio between the TDR unit and the array structure frequencies was as high as 14. This meant that during the structure in-plane resonance (0.87 Hz) the TDR was acting as a rigid body. Nevertheless the 'C' value of 10.0 N.sec/m is sufficient to design a damper. Thus for future design a less stiff unit would be recommended so that the stroke would be larger.

Two of the results were unexpected. The first was that the TDR behaved in a dynamically linear manner, at least over the range of loads tested (.5 - 1.5 g's). The second was that the damping factor 'c' in the TDR was twice the value of the pretest bonded unit. This indicated that within the testing range its structural damping of bellows and fittings caused the difference. The foam used was identical to all units - only the structure was different.

6.2.4.2 Data Results - The test results are presented in Figures 6-2.4.1, 6-2.4.2 and 6-2.4.3. The bonded and sealed units show a decrease in natural frequency and Q factor for increasing base input.

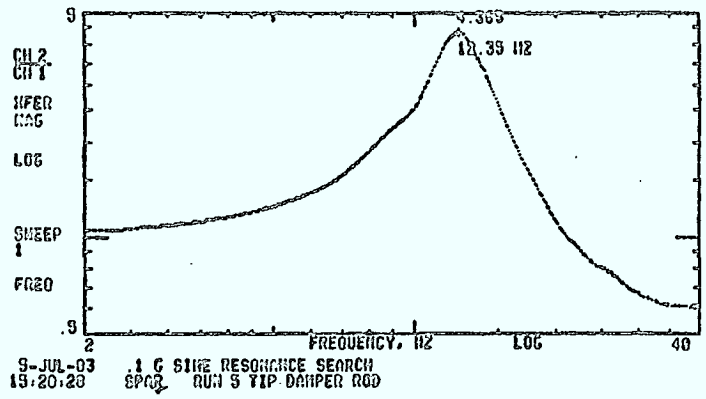

0.1 G

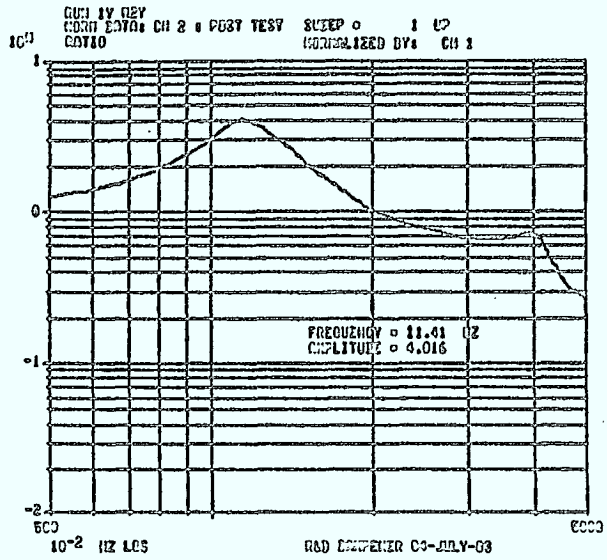

0.6 G

BASE
ACCELERATION
AMPLITUDE

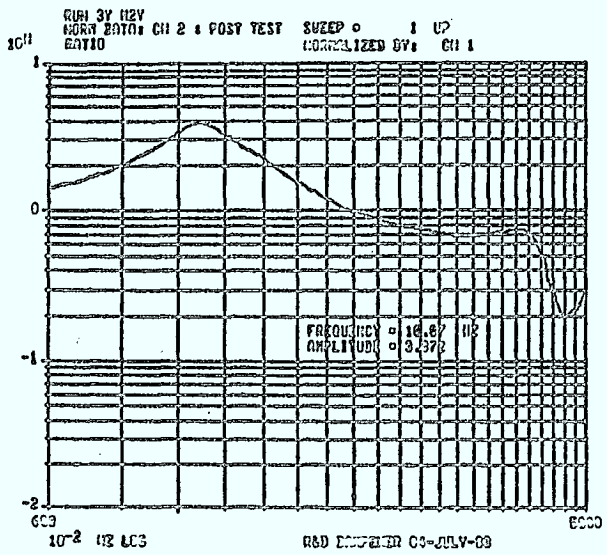

1.0 G

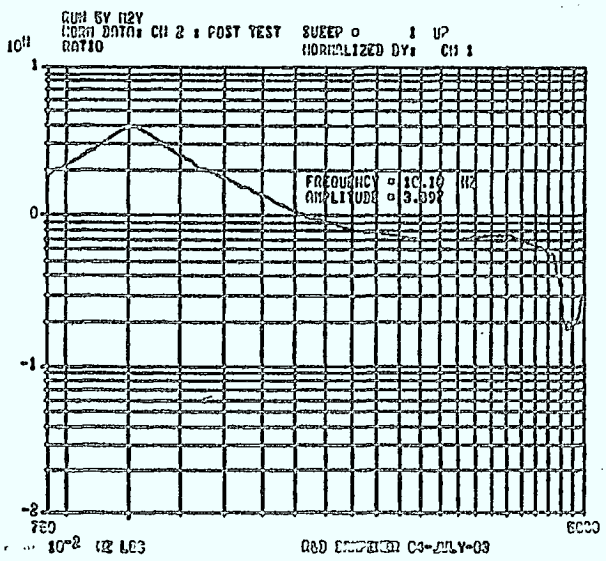

1.5 G

FIGURE 6.2.4-1 SINE SWEEP TEST RESULTS FOR THE TDR UNIT FOR VARIOUS AMPLITUDES ACCELERATION

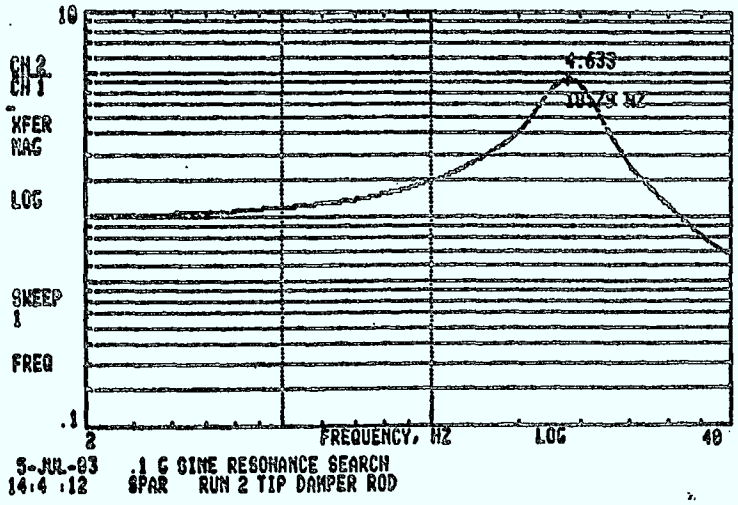

0.1 G

BASE ACCELERATION AMPLITUDE

0.5 G

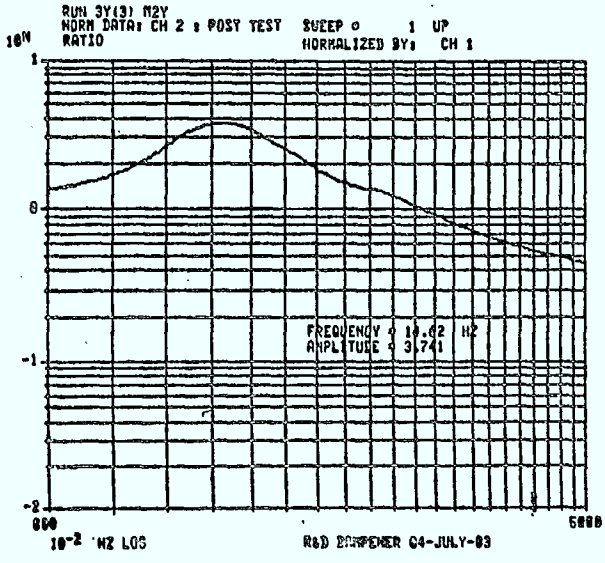

1.5 G

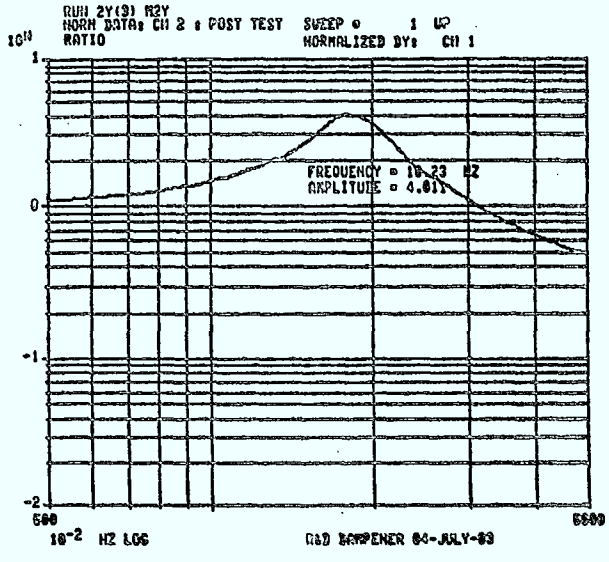

FIGURE 6.2.4-2 SINE SWEEP TEST RESULTS FOR THE TDR PRETEST BONDED UNIT

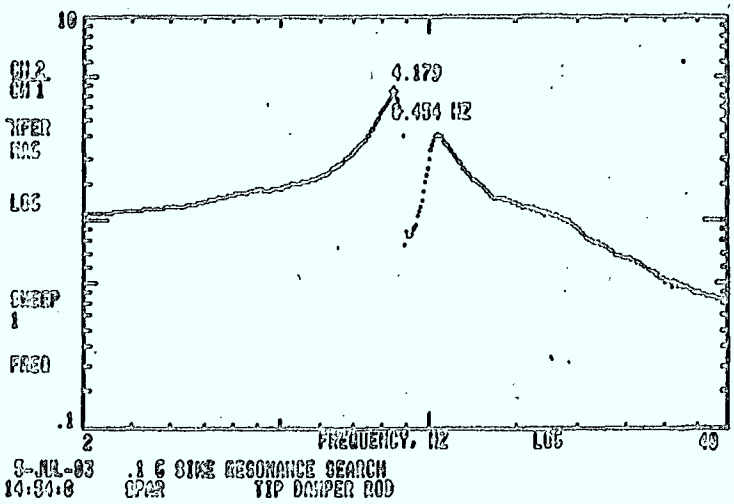

BASE ACCELERATION AMPLITUDE

0.1 G

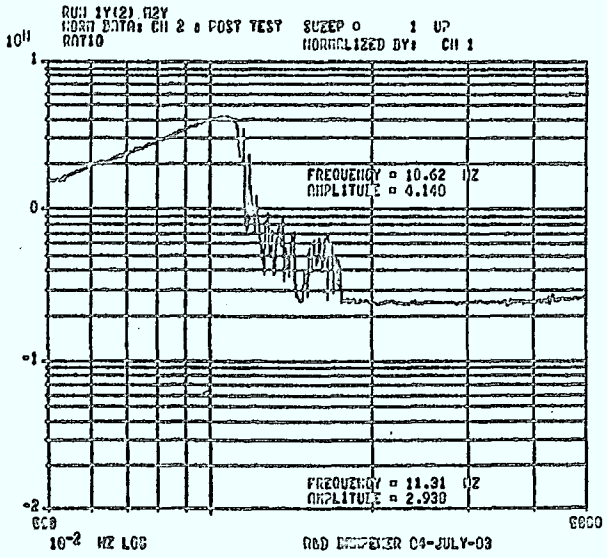

0.5 G

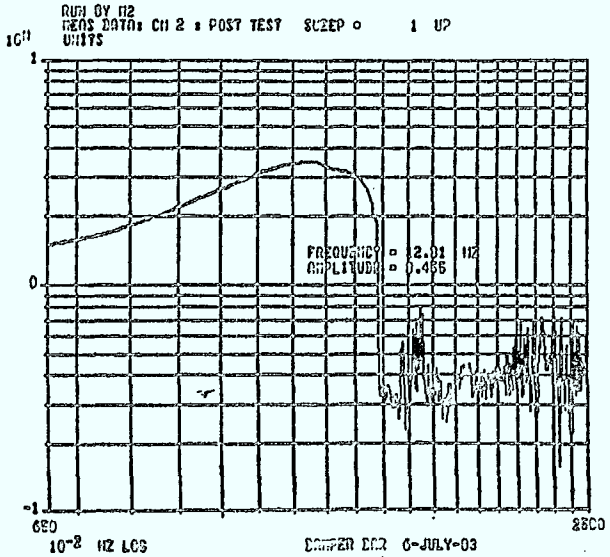

1.0 G

FIGURE 6.2.4-3 SINE SWEEP TEST RESULTS FOR THE TDR PRETEST GREASED UNIT

Tables 6-2.3, 6-2.4 and 6-2.5 are used to evaluate the equivalent viscous damping ratio, ζ, damping factor c and damping energy per cycle with respect to various damper inputs and strokes.

TABLE 6-2.3

TDR TEST RESULTS (AT RESONANCE)

Tip Mass = 0.55 kg

INPUT g LOAD	AMPLI-FICATION FACTOR Q	NATURAL FREQ. ν Hz	DAMPING RATIO	DAMPING COEFF. N/(m/s)	DAMPING ENERGY E J/CYCLE	INPUT AMP. (X) mm	DAMPER STROKE S mm
0.1	4.365	12.35	.118	10.04	1.23E-3	0.16	1.1
0.6	4.016	11.016	.129	9.79	.052	1.23	7.41
1.0	3.878	10.78	.133	9.94	.145	2.1	12.3
1.5	3.897	10.10	.133	9.27	.375	3.65	21.2

TABLE 6-2.4

TDR PRETEST BONDED UNIT RESULTS (AT RESONANCE)

Tip Mass = .19 kg

INPUT g LOAD	AMPLI-FICATION FACTOR Q	NATURAL FREQ. w Hz	DAMPING RATIO	DAMPING COEFF. N/(m/s)	DAMPING ENERGY E J/CYCLE	INPUT AMP. (X) mm	DAMPER STROKE S mm
0.1	4.633	18.79	.11	5.0	2. E-4	0.07	.5
0.6	4.011	18.23	.129	5.6	4.5E-3	0.37	2.25
1.5	3.741	14.67	.139	4.9	6.0E-2	1.73	9.5

TABLE 6-2.5

TDR PRETEST GREASED UNIT RESULTS (AT RESONANCE)

Tip Mass = 0.19 kg

INPUT g LOAD	AMPLI-FICATION FACTOR Q	NATURAL FREQ. ν Hz	DAMPING RATIO	DAMPING COEFF. N/(m/s)	DAMPING ENERGY E J/CYCLE	INPUT AMP. (X) mm	DAMPER STROKE S mm
0.1	4.179	8.179	.123	2.42	9.4E-4	.371	2.3
0.5	4.14	10.62	.125	3.18	1.4E-2	1.1	6.9
1.0	.455	12.31	.151	4.5	3.5E-2	1.6	8.1

7.0 ASTROMAST TEST RESULTS

The astromast used in the solar array model has been tested (both statically and dynamically) by CRC personnel. The results of this test are covered in Ref. 1.

The astromast testing was done prior to that of the solar array. A great deal of practical information on testing techniques was gained and made use of for the solar array test (see Section 7.2). The effects of accelerometer cables, accelerometer mass and various excitation techniques were examined. As in the case of solar array results, random excitation produced slightly lower resonance values than sine.

Table 7 summarized the astromast test results, as well as the FEM predictions done by the University of Sherbrooke (Ref.7).

7.1 Astromast - Solar Array Comparison

The addition of the solar array blanket to the astromast had two gross effects. One was to lower the frequency, the other was in increase the damping, for the fundamental modes.

These two factors had significant effects on the test philosophy. The lower frequency of the solar array precluded any testing using the electromechanical shaker (the shaker low frequency limit is about 5 Hz), but meant that the step relaxation method could be used to excite the modes of interest for the solar array.

The increased damping of the solar array (lower Q-factor) allowed for higher acceleration inputs to the structure, without fear of breaking the astromast. As a result, the signal to noise ratio for the hydraulic shaker testing was improved for the solar array.

The mass of the solar array was 3 to 4 times that of the astromast. The decrease in frequency was slightly more than expected by the mass change, but much of the additional mass was concentrated at the tip (i.e., higher mass moment of inertia).

The Q factor for the solar array first mode was about 8; for the astromast, the value was about 45.

The damping values for the astromast increase with frequency, while for the solar array they tend to remain about the same, or possibly decrease slightly.

TABLE 7

ASTROMAST DYNAMIC RESULTS

MODE	TEST RESULTS DAMPING (% CRITICAL)	TEST RESULTS FREQUENCY (Hz)	ANALYTICAL RESULTS FEM (Hz)	ANALYTICAL RESULTS VARIATIONAL Model (Hz)
Bending 1	2-3	1.8-1.88	1.76	2.16
Bending 2	3	11.8-11.95	12.9	17.0
Bending 3	6	28	34.7	51.5
Torsion 1	1	10.7	7.63	12.2
Torsion 2	2	32	25.0	41.0
Torsion 3	8.8	46	47.0	

A difference in the two structures of important significance with respect to applicable parameter estimation techniques was the degree of structural linearity.

The Polyreference parameter estimation technique requires the structure be stationary and linear. The linearity can be tested using a reciprocity check. The FRF at point i with reference (excitation) j should be the same as that of point j with reference (excitation) i.

Figure 7-1(a) is the reciprocity check for the astromast. Figure 7-1(b) is the reciprocity check for the solar array. Clearly linearity of the astromast is a reasonable assumption, while that for the solar array is not.

7.2 Applicability of Test Techniques

The astromast testing was used as a baseline to evaluate the transducers used, their placement techniques and the allowable input amplitudes to the astromast structure.

The astromast test established that the best response and control accelerometers to use for the test were the Endevco piezoresistive accelerometers. Their mass is 5 grams. The mass loading effects were evaluated for the astromast and this is discussed in Section 7.2.1.

An astromast is a very fragile structure. The maximum deflection allowable was 2 inches. To ensure that the astromast was not overloaded, the maximum tip deflection was to be limited to a nominal one inch value. Such low amplitudes meant that the noise levels of the test environment were significant with respect to the input levels. Section 7.2.2 discusses the input/noise ratio.

7.2.1 Mass Loading Effects (Ref. 1) -The effects of the accelerometers, as well as the accelerometer cables were checked (independently). The effect of two accelerometers was checked and found to have no effect on astromast FRF up to about 60 Hz.

The effects of the accelerometers on the astromast were evaluated by placing dummy masses at accelerometer locations. The effect of three accelerometers, below 10 Hz was not discernable. At 12 Hz there was a .7% shift in frequency and 5% in amplitude.

The effect of the accelerometers on the solar array would have been much less than that of the solar array (array was 4 to 5 times heavier than the astromast). The accelerometers placed on the blanket were an exception to this. A cursory examination of the effect was made by examining the FRF's of the TDR, with and without accelerometers on the blanket. Figure 7-2.1 is an overlay,

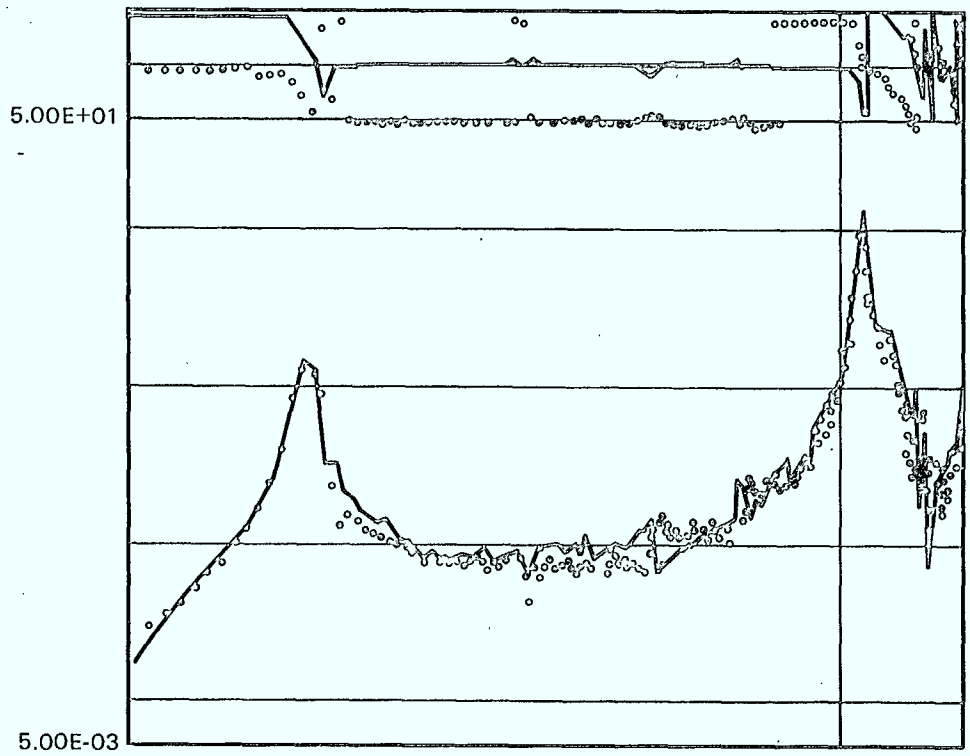

FIGURE 7.1a ASTROMAST RECIPROCITY CHECK

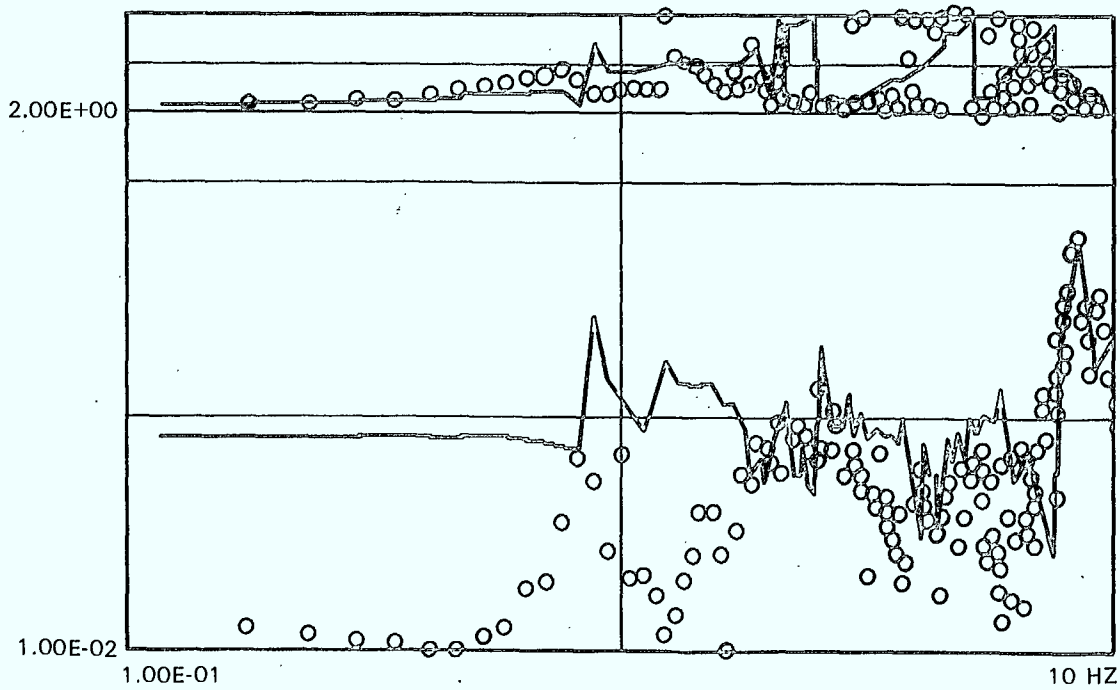

FIGURE 7.1b SOLAR ARRAY RECIPROCITY CHECK

FREQRESP-BODE
4Z- 4X- NO. 0

showing the effect. The frequencies do not shift appreciably, though there is some evidence of small amplitude changes around 1 Hz. The effect of the accelerometers on the blanket shape would no doubt be more pronounced, but there was no way of evaluating it.

7.2.2 Input Acceleration Level - Noise Ratio -The hydraulic shaker was deemed unsuitable for the astromast testing, though it was used extensively for the solar array test. The astromast had slightly higher fundamental frequencies, so it could be tested using an electromechanical shaker. The reason that the hydraulic shaker was not used for the astromast testing was the signal to noise ratio. The hydraulic shaker was the source of the noise. The Q-factor of the astromast was so high (45) that the input amplitudes had to be very low to avoid breaking the structure. For the sine sweep, the amplitude was .004 g's. The Q-factor of the solar array was significantly lower (8), thereby improving the signal to noise ratio, amplitude of sine = .008 g's).

8.0 DISCUSSION OF ERRORS

The concept of error in this section has been expanded to include the nonlinear nature of the structure. Modal Analysis is a linear analysis. Many of the characteristics of the solar array do not conform to this assumption and are grouped in the error analysis.

The solar array model tested introduced complications which would not actually exist in a solar array. The tension level, maintained by the TDR was not held constant under vibrations or temperature changes, as it would be for an actual solar array. The non-constant tension may have been the source of the travelling wave phenomenon observed (described in Section 8.4).

There were blanket modes in the test model that may not exist for a solar array. These were the 'clapping modes'. In a conventional solar array, the out of plane hanger rod stiffness is orders of magnitude higher than that of the test model. This type of mode was not present in the analytical modelling because the blanket sections were assumed to maintain straight lines across the width.

The actual experimental errors present during the test are discussed in Section 8.1 and 8.2.

The most important type of error to consider was the environmental error introduced by testing the structure on earth, when its operating environment would be space. The aerodynamic and gravity errors are discussed in Section 8.3. The aerodynamic error discussion applies only to the array testing done in air - most of the testing was done in vacuum. The effects of air testing are discussed more fully in Section 9.0.

8.1 Noise Levels

There were various sources of noises present in the experiment. The hydraulic shaker was tested and a low frequency noise found to be present (see Figure 2-3.2). This source of noise was included in both the input and output responses, thereby limiting its effect.

The accelerometers were checked for noise response and found to be virtually noise free.

While the structure was being tested in air, the noises from the environment (a vibration test lab) were kept to reasonable limits by testing when obvious noise sources were minimized (vacuum pumps turned off, no other vibration tests being conducted at the time). The effects of breezes exciting the structure were very low, because the structure was inside the vacuum chamber, with only a door open (7' x 7').

While testing in vacuum, external noise sources were eliminated, except for noise transmitted from outside the vacuum chamber, through the hydraulic shaker. This type of noise did exist (pushing on the chamber wall registered as a response from the accelerometers) but as it would have existed for the input and output responses (and was small), it was not a problem.

The largest and most significant error existed in the structure itself. Some of the connections were designed as pin connections. The connections were not precision connections and acted as noise sources - introducing amplitude dependent local modes. The fact that these noise sources appeared in output values only and were not totally independent of the excitation, made them important. (Non-coherent noise sources get 'averaged out' by the ensemble averaging done in the FFT analysis).

8.2 Coherence

The ordinary coherence function (discussed in Section 3.1.1) provides a measure of the linear response of a structure to a known input. Figures 8-2.1, 8-2.2 and 8-2.3 are examples of FRF and coherence functions obtained for random, step and sine test data.

At resonance, the coherence would be expected to rise slightly. Though this does not appear to be the case, it was discovered that the reason is simply a case of insufficient frequency points taken in this region - the FRF is not affected.

The coherence function for the Step Relaxation test had errors in the calculation (the software was in a development phase) and should only be considered as the trend of the test.

8.3 Environmental Effects: Air and Gravity

The effects of testing in air rather than vacuum are discussed in Section 9.0. The tests done in air had a potential error. The air tests were done while the structure was mounted in the vacuum chamber. The intention of this was to eliminate problems due to change of mounting boundary conditions and to save time (assembling and dismounting the structure was a difficult procedure, due to its size and the fragility of the astromast).

Subsequent to testing, it became apparent that the first natural frequency of the structure had increased, rather than decreased, as had been expected. It could be that the air, trapped in the vacuum chamber, acted to artificially stiffen the structure. Subsequent to the test results, analytical results have indicated that for some modes, blanket damping does have the effect of increasing frequency. The test results indicate increases of 5% to 10%, while the analytical results indicate only 2%.

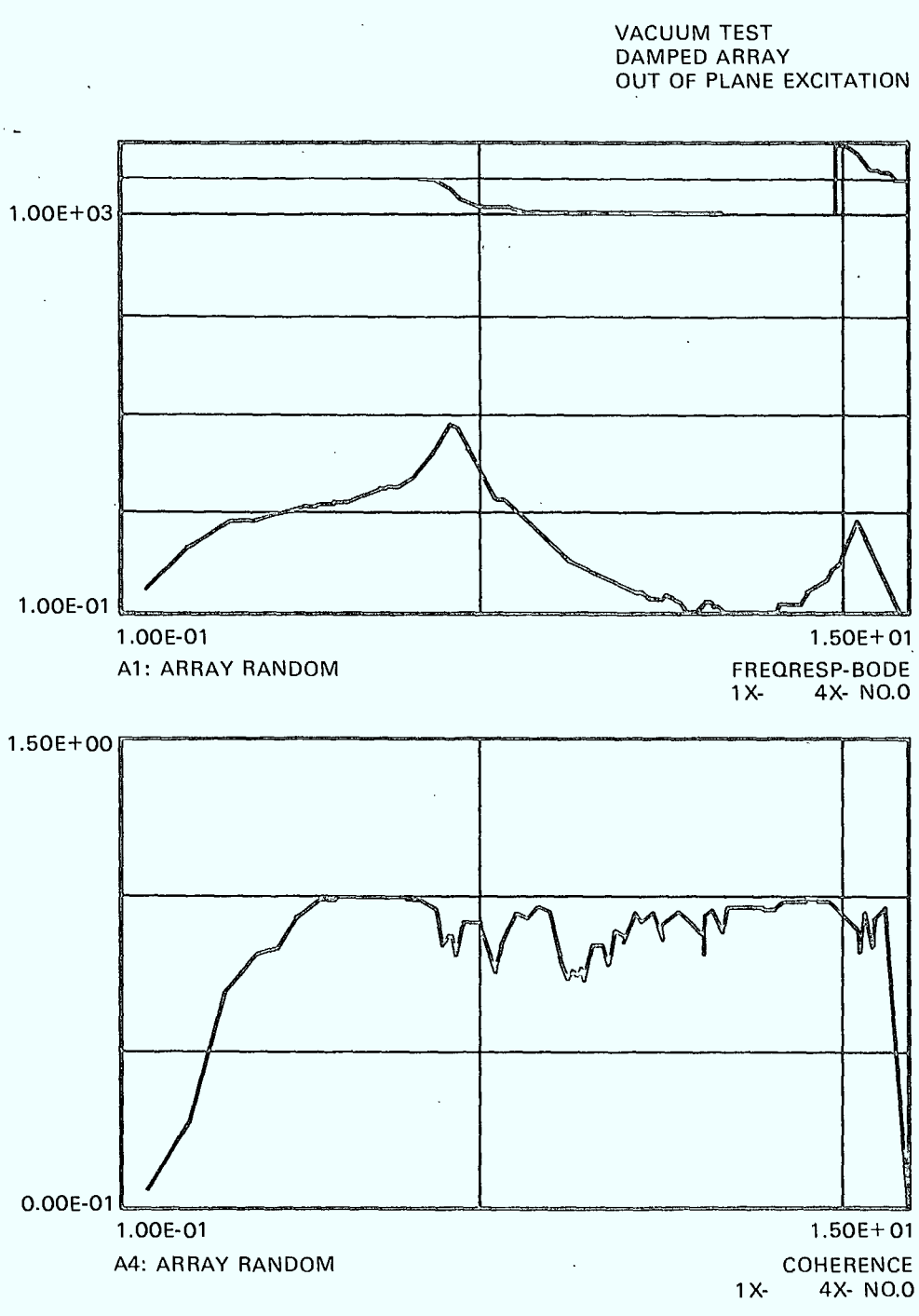

FIGURE 8.2-1 RANDOM EXCITATION FREQUENCY RESPONSE AND COHERENCE FUNCTIONS

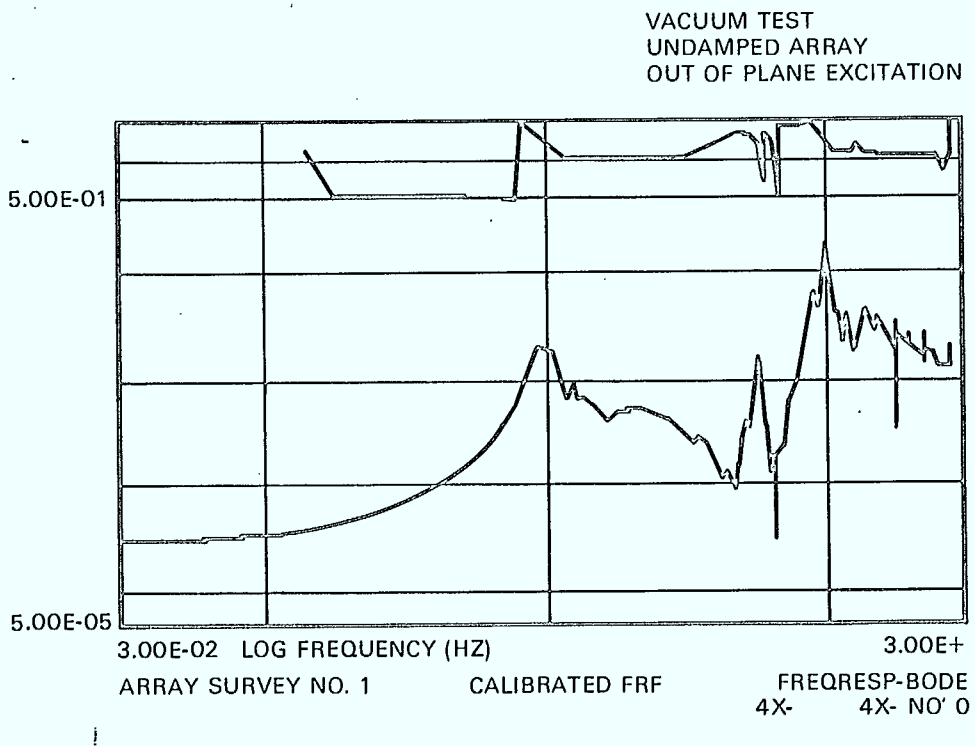

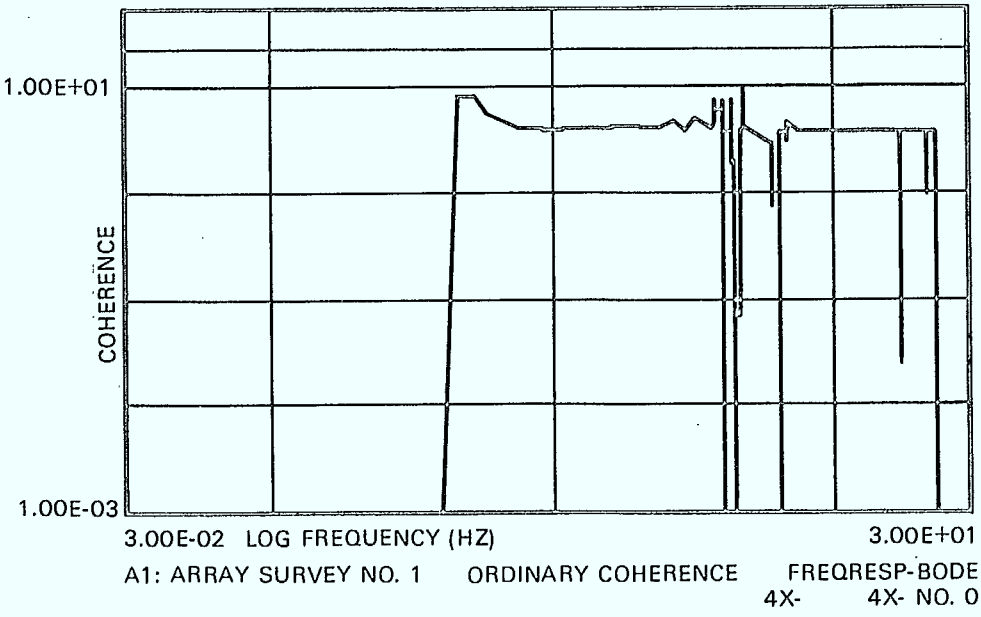

FIGURE 8.2-2 STEP RELAXATION EXCITATION FREQUENCY RESPONSE AND COHERENCE FUNCTIONS

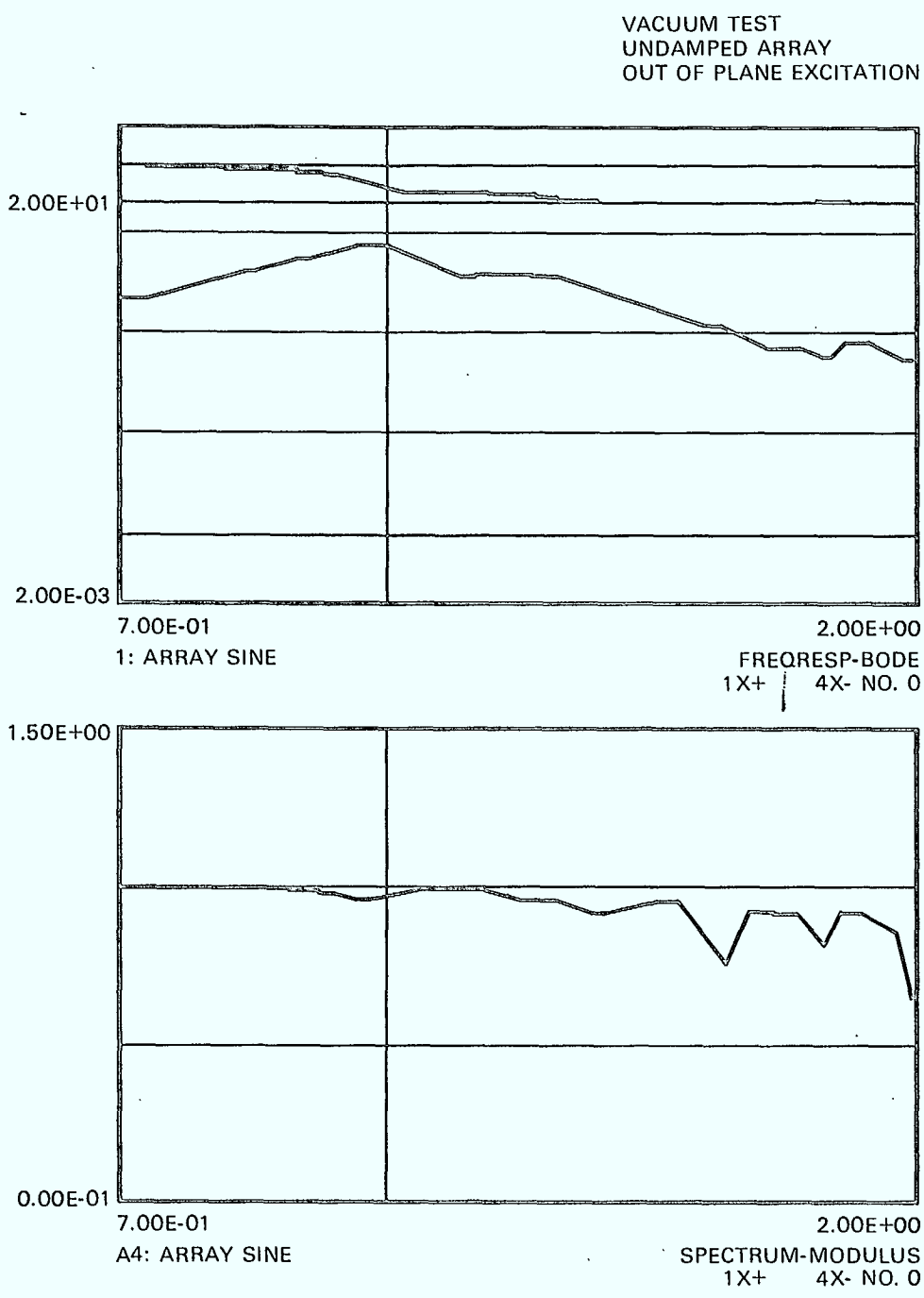

FIGURE 8.2-3 SINE SWEEP EXCITATION FREQUENCY RESPONSE AND COHERENCE FUNCTIONS

The effects of testing in a gravity environment have been calculated by the analytical model (Ref. 4). Table 8-3 lists the results calculated for 1-g and 0-g cases.

The effect of gravity was to stabilize the structure, since it was mounted upside down. The in-plane mode is almost unaffected by the presence of gravity (1%). The out-of-plane and twist modes are very sensitive to gravity due to the tension levels being gravity dependent. These strong effects of gravity make analytical models extremely important - until such time as solar arrays can be tested in space.

In addition to stabilizing the structure, gravity has the effect of changing the blanket tension with respect to length (due to the blanket self weight).

Figure 8-3 illustrates the effect.

8.4 Blanket Effects

The blanket is the main component of a solar array that non-standard structural behaviour can be attributed to. Its structural characteristics are amplitude dependent. The solar array model tested compounds the amplitude dependence. Under vibration, the tension level in the blanket was altered. In a conventional solar array the tension level would remain constant.

During the testing, the presence of a travelling wave was observed. It seemed to start at the tip end of the blanket and travel up the structure. A short time after the wave reached the tip, another wave would start and move up again. Accurate estimate of the wave size and speed was not possible, but the approximate speed was of the order of 5 in/sec with a wavelength of 2-4 inches.

A similar phenomenon occurs in pipe flow (e.g., pressure wave as a valve is opened) or in pile driving. It is a linear phenomenon, but not easily handled using mode superposition (the technique assumed for modal analysis). The wave shape and propagation must be treated as the sum of all of the mode shapes in the axial and out of plane directions.

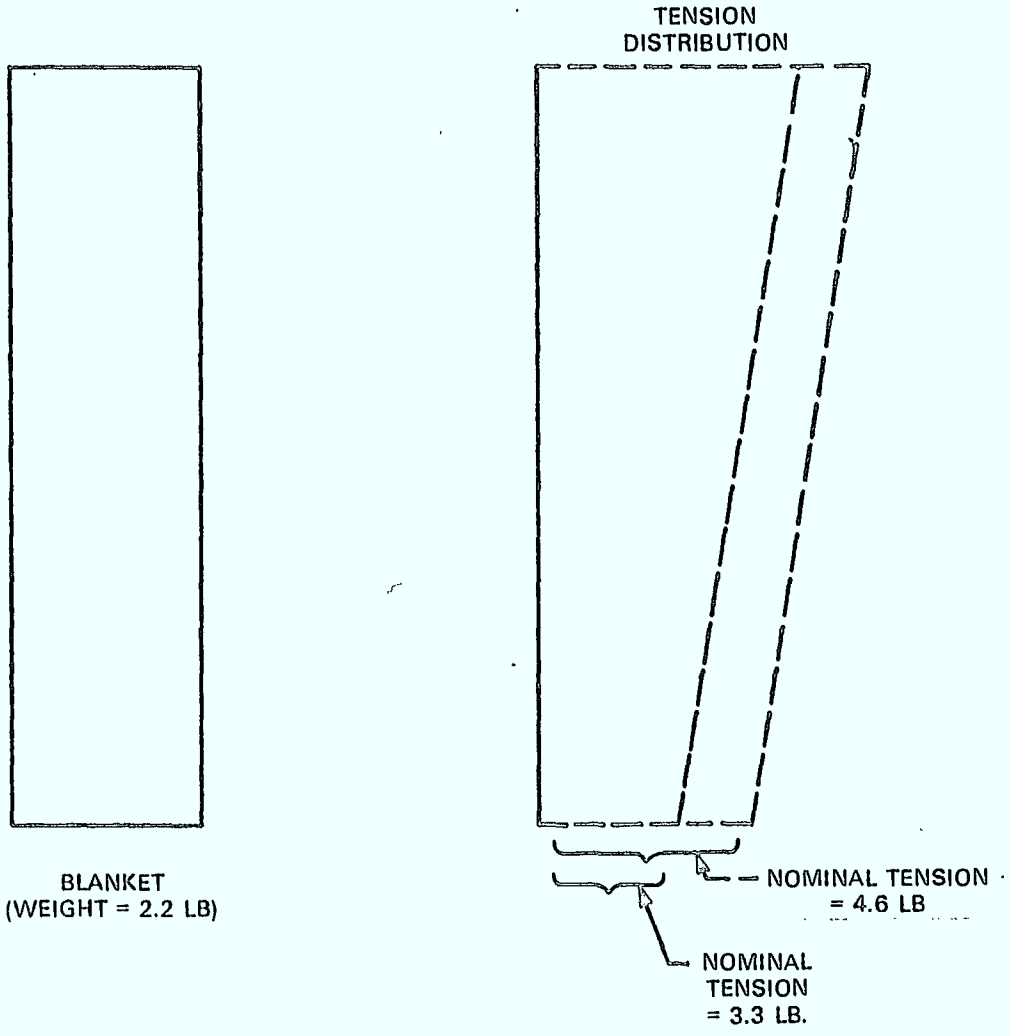

FIGURE 8-3 EFFECT OF GRAVITY ON BLANKET TENSION

RANDOM, BASE EXCITATION
OUT OF PLANE TEST
UNDAMPED TDR CONFIGURATION

O O O ACCELEROMETERS ON BLANKET
——— NO ACCELEROMETERS ON BLANKET

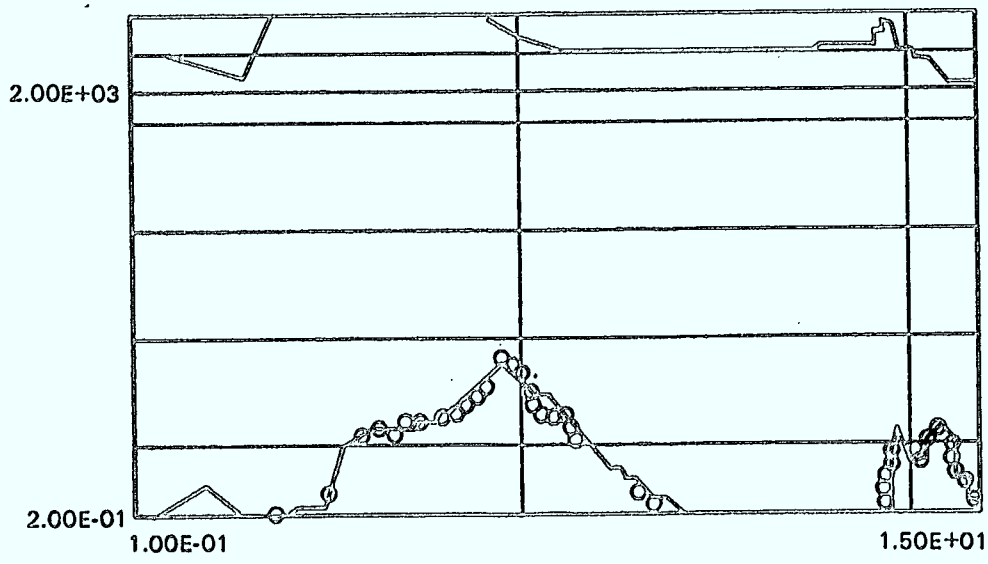

SOLAR ARRAY PROJ.
VACUUM WITH ACC. ON BLANKET

FREQRESP-BODE
1X+ 5X+ NO. 0

FIGURE 8-4: BLANKET ACCELEROMETER EFFECT

TABLE 8-3

EFFECTS OF GRAVITY ON ARRAY MODEL
(BASED ON ANALYTICAL MODEL)
DAMPED CONFIGURATION

	Frequency (Hz)	
	Earth Gravity	No Gravity
Out of plane - 1	0.92	0.77
Out of plane - 2	1.28	1.03
Out of plane - 3	2.46	1.70
In plane - 1	1.29	1.27
In plane - 2	10.3	10.31
In plane - 3	15.3	15.2
Twist - 1	1.52	1.16
Twist - 2	2.2	1.97
Twist - 3	3.5	2.53

9.0 EFFECTS OF AIR - (Reference. 14)

Testing a solar array in vacuum conditions is not only time consuming and expensive, for solar arrays being built today, it is impossible. L-SAT size arrays are larger than existing vacuum chambers. It is for this reason that the effects of testing an array in air have been examined.

The results of step relaxation testing done in air are included in Section 9.1. Section 9.2 compares the air and vacuum test results.

There are two effects of testing in air that were expected to alter the vacuum test results. One was the 'added mass' effect of entrained air. The other effect was increased damping due to the air drag. Both of these effects were expected to lower the resonant frequencies of the structure.

Note: The following calculations are approximate, intended only to provide numerical trends.

The equation of motion for 'Still Air' Free Vibrations is:

$$m_o \ddot{y} + 2 m_o \zeta_o \omega_o \dot{y} + k y = -\rho V C_I \ddot{y} + \tfrac{1}{2} \rho C_D A |\dot{y}| \dot{y} \qquad (9.1)$$

where

m_o = structural mass

ζ_o = damping ratio, vacuum

w_o = undamped natural frequency, vacuum

V = structure, volume

C_I = added mass coefficient

ρ = fluid density (air)

C_D = drag coefficient

A = frontal area

this can be rewritten as

$$m \ddot{y} + 2m \zeta_A \omega_A \dot{y} + k y = \tfrac{1}{2} \rho C_D A |\dot{y}| \dot{y} \qquad (9.2)$$

= .89 i.e., the frequency in air should have been about 10% lower than in vacuum.

The drag of the structure is proportional to velocity squared (as shown in Equation 9.1) if the Reynolds Number is sufficiently high (assume 1.E4). Taking

Re No. $= \frac{\omega D^2}{\nu}$ with characteristic dimension, D = astromast diameter plus blanket offset (13"), as a minimum.

for the lowest mode $\omega = 2\pi$

$$\text{Re No.} = \frac{2\pi X\ (13/12)^2}{1.64 \times 10^{-4}}$$

$$= 4.5 \times 10^4$$

In the modal analysis processing, the drag value would appear as additional damping. To estimate the magnitude of this effect, consider the first out of plane bending mode. Assume

$C_D = 1$

$A = 4 \times 20 = 80$ ft.

$f_o = 1$ Hz.

$x = Q \times 1" \times f_o$

$= 8 \times .083 \times 1$

$= .66$ ft/sec

Drag Force $= 1/2\, \rho\, \dot{y}^2\, C_D\, A$

$= .5 \times .00238 \times .66^2 \times 1 \times 80$

$= .041$ lb.

The damping force, in vacuum can be estimated as

$$\text{Damping Force} = 2m\dot{wy}$$
$$= 2 \times .4 \times .05 \times 2 \times .66$$
$$= .165 \text{ lb.}$$

where

$m = .4$ slugs
$\omega = .05$

Thus the air drag effect could be expected to add about 25% to the damping value. For higher frequencies, this value can be expected to decrease because amplitudes of oscillations will decrease, as will the effective drag area. The increase in damping will not be large enough to show an appreciable change in the damped natural frequency.

9.1 Solar Array Testing in Air

In plane and out of plane testing of the undamped structure configuration was done using the step relaxation method of excitation. The results are listed in Tables 9-1.1 to 9-1.3. Table 9-1.1 results are based on the MPLUS computer estimates. Table 9-1.2 results are the result of estimating resonances (manually) from all of the FRF's and averaging them. Table 9-1.3 combines the MPLUS and statistical estimates.

9.2 Comparison of Air and Vacuum Results

Table 9-2.1 is a comparison of the air and vacuum test results from the step relaxation testing of the undamped solar array configuration. Figure 9-2.1 overlays FRF's from air and vacuum tests.

The principal unexpected results was the apparent increase in frequency for the fundamental modes, in air. Comparison between other modes indicates almost no effect due to the air, on the resonant frequency.

The damping values for the out of plane modes are significantly higher in the air tests. For the in plane results the effect appears only for the first mode. For the mode at about 12.5 - 13 Hz., the damping seems to have decreased.

In addition to the step relaxation tests, a partial random test on the damped configuration was done in air. There were only 3 points measured, for an out of plane test. Table 9-2.2 compares these results to the equivalent vacuum case.

A study on the effects of blanket damping, being done by CRC personnel is now in progress. As described in Section 4.2 of this report, preliminary results show that for some modes, blanket damping does have the effect of increased some natural frequencies.

TABLE 9-1.1

MPLUS Results
T = 3.3 lb.
Air

TEST TYPE	DATA QUALITY	EXCITATION DIRECTION	FREQUENCY	DAMPING	DESCRIPTION OF MODE
Step	Good	In plane	1.011	.097	1st in-plane/torsion mode.
Step	Good	In plane	4.63	.032	
Step	Good	In plane	5.941	.074	
Step	Good	In plane	9.621	.017	
Step	Good	In plane	11.302	.015	
Step	Good	In plane	12.861	.025	
Step	Good	Out of plane	1.058	.118	1st out of plane bending.
Step	Good	Out of plane	5.675	.022	
Step	Good	Out of plane	9.243	.055	
Step	Good	Out of plane	9.873	.012	
Step	Good	Out of plane	13.09	.007	

TABLE 9-1.2

Spectral Peaks
T = 3.3 lb.
Air

In-Plane Excitation

TEST TYPE	# SAMPLES	AVERAGE FREQUENCY	SAMPLE STANDARD DEVIATION	FREQUENCY RANGE	DESCRIPTION OF MODE
Step	5	.948	.0147	.934-.962	In plane/torsion - predominantly in-plane + TDR_Z.
Step	4	5.875	.062	5.802-5.948	In-plane/torsion; torsion.
Step	6	9.531	.084	9.462-9.600	In-plane/torsion, torsion + TDR_Z.
Step	3	11.19	.134	10.964-11.416	
Step	5	12.64	.022	12.62-12.661	In-plane/torsion; torsion.

TABLE 9-1.2 - continued

Spectral Peaks
T = 3.3 lb.
Air

Out-Of-Plane Excitation

TEST TYPE	# SAMPLES	AVERAGE FREQUENCY	SAMPLE STANDARD DEVIATION	FREQUENCY RANGE	DESCRIPTION OF MODE
Step	6	1.064	.033	1.037-1.091	Out of plane + some in-plane + TDR_Z.
Step	6	5.571	.026	5.550-5.592	Out of plane + some in-plane + TDR_Z.
Step	6	9.738	.086	9.667-9.809	Out of plane + some in-plane + TDR_Z.
Step	4	12.958	.059	12.89-13.03	

TABLE 9.1.3

SUMMARY OF RESULTS
DAMPED TDR AIR TEST

SPAR

EXCITATION DIRECTION	TEST TYPE	FREQUENCY RANGE (HZ)	DAMPING	MODE SHAPE DESCRIPTION
IN PLANE	STEP	.95-1.0	.07-.10	1ST IN PLANE/TORSION-PREDOMINANTLY IN PLANE
IN PLANE	STEP	4.6	.03	-
IN PLANE	STEP	5.85-5.95	.07	
IN PLANE	STEP	9.5-9.6	.017	
IN PLANE	STEP	11.2-11.3	.015	
IN PLANE	STEP	12.65-12.90	.025	
OUT OF PLANE	STEP	1.055-1.065	.112-.118	1ST OUT OF PLANE BENDING (SOME IN PLANE AS WELL)
OUT OF PLANE	STEP	5.57-5.68	.022	
OUT OF PLANE	STEP	9.2	.055	
OUT OF PLANE	STEP	9.75-9.90	.012	
OUT OF PLANE	STEP	13.0-13.1	.007	

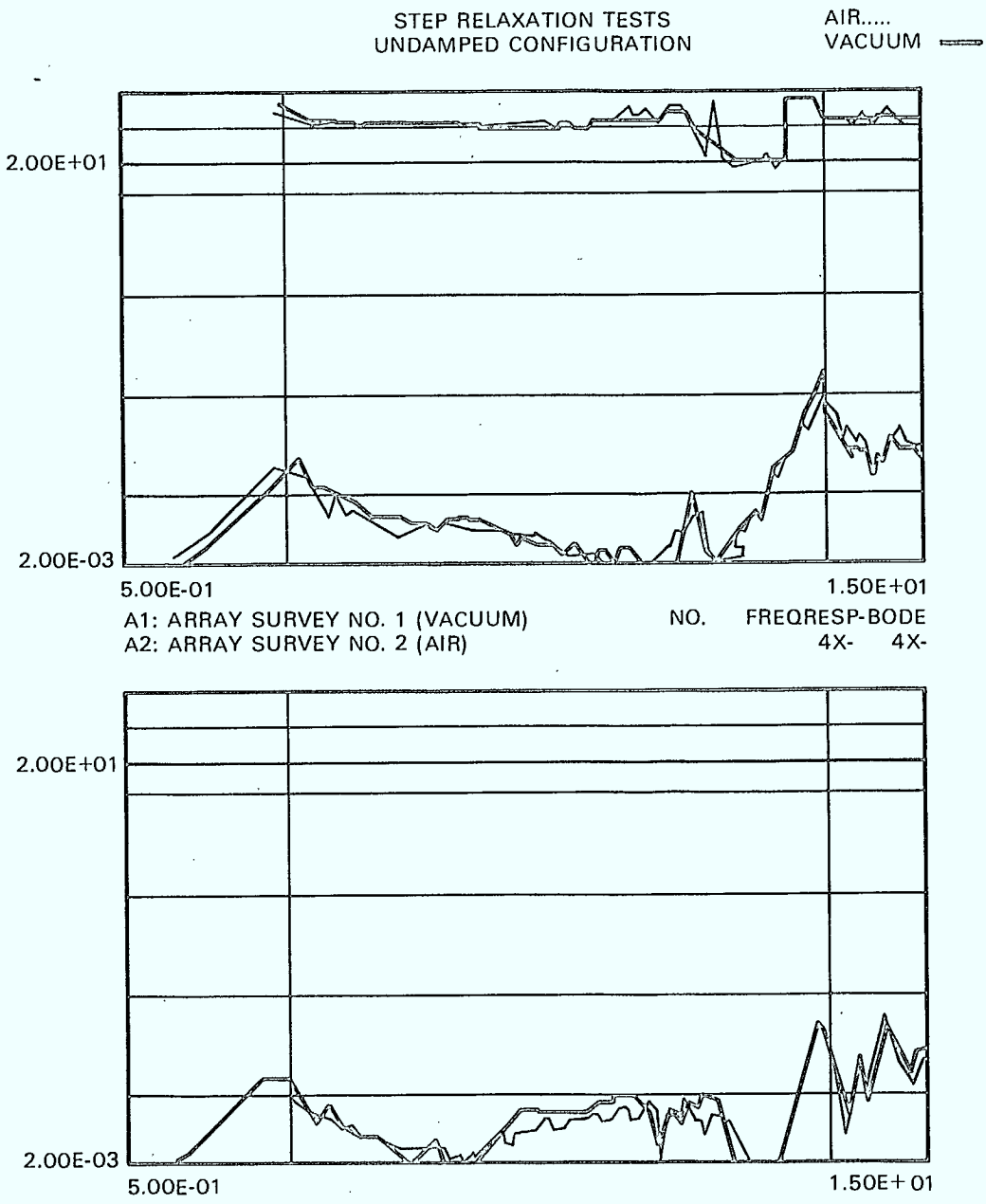

FIGURE 9.2-1 FRF OVERLAY OF AIR AND VACUUM RESULTS

TABLE 9-2.2

COMPARISON OF AIR AND VACUUM DATA* (1st MODE)

RANDOM, OUT OF PLANE EXCITATION

DAMPED CONFIGURATION, t = 4.6 lb

ACCELEROMETER LOCATION	FREQUENCY		DAMPING	
	AIR	VACUUM	AIR	VACUUM
5z, TDR	.93	.97	.058	.048
9x, Blanket	.856	.83	.178	.127
10x, Blanket	.89	.84	.134	.120

* Data estimated manually from FRF's
Damping estimated using Half Power Method

10.0 DISCUSSION AND CONCLUSIONS

One of the intents of the modal testing of a solar array was to establish its linearized structural characteristics. The testing has done more to highlight non-linearities than it has to provide realistic linear results. The global resonant frequencies and damping values vary along the structure. They vary with the type of testing done (frequencies of random tests seem to be lower, but this is anticipated, even for more linear structures).

Three types of excitation were investigated: base random, base sine sweep and step relaxation. No one technique was able to excite all modes. Frequency and damping values varied for each type of testing. The sine test results indicated the highest frequencies and the lowest damping values. Random test frequency results are generally lower. The sine sweep seemed to miss the least modes, but it was only performed for a limited frequency range. The step relaxation technique seemed well suited to a solar array type structure, but more excitation points should have been used.

Most of the testing was done in vacuum conditions. As has been mentioned, this may not be possible for solar arrays currently being built. For this reason, testing in air and extrapolating to vacuum becomes very desirable. The time to test in vacuum is prohibitively long as well. The actual testing for an air set-up and test was about one hour (after the structure had been assembled) - for a vacuum test it was 3 to 4 hours. The improvement to the test results would be enormous if it were to be possible to spend the extra (2 to 3 hours/test) time testing more transducer locations. As long as the transducers (accelerometers) must be mounted to the array, it will not be possible to instrument for a complete configuration at one time. Thus the same test must be repeated several times - in a vacuum environment this is very time consuming.

The ability to measure the vibrations in a non-contact manner would improve the quality of the results, as well as potentially reduce testing time. Even ignoring the mass loading effects - the condition of test stationarity is difficult to realize if the test must be repeated several times (to gather enough data points).

The testing that was done in air has been compared to the vacuum results. It had been expected that the most significant aerodynamic effect would be to lower the resonant frequencies. This did not seem to be the case - in fact, the fundamental frequencies increased slightly. A CRC analytic study in process confirms that blanket damping can cause some natural frequencies to increase. The damping values for the out of plane modes doubled, while the in plane increased slightly.

Many of the results obtained from these group of tests need more examination before modal analysis can be expected to characterize the structure to a data quality sufficient for analytical techniques (substructure analysis).

The structure tested - a solar array - cannot be adequately treated by the sophisticated linear parameter estimation techniques of commercial modal analysis software. The spectral analysis portion of the software is valuable to solar array testing. A combination of spectral analysis, visual mode shape information and old fashioned techniques such as log decrement decay would have improved mode shape and damping estimates.

The modal analysis results are incomplete with respect to mode shapes - more measurement points would be needed to adequately describe the mode shapes (1 or 2 tranducers for every m^2 of blanket would be desirable if non-contact ones were available). The effects of testing the structure in air are not what one would have expected. More work on the aerodynamic effect is planned (Masters Thesis, of S. Draisey).

The excitation techniques - base excitation and step relaxation have been used. It turns out that base excitation is not properly treated by the commercial software analysis packages. In the next phase of this contract, work will be done to allow for proper analysis of base excitation. The step relaxation technique was advanced significantly on the astromast testing, just prior to this contract. It has been established as a useful means of exciting the low frequency components of a flexible structure. To extend its useful range, a multiple excitation type of step relaxation should be developed (to allow for high energy input content in regions of higher frequency).

The damper designed within this contract did not prove to be suitable for the test model. The possible benefit of significantly reducing solar array frequencies to increase the damping characteristics needs investigation.

If the Canadian aerospace industry is to remain competitive in the integration and test field, modal analysis experience is required. The first phase of this contract made a significant step towards establishing a modal analysis capability.

BIBLIOGRAPHY

[1] Y. Soucy and F.R. Vigneron, "Identification of Structural Properties of an Astromast".

[2] F.R. Vigneron, "Comparison of Test Configurations for Modal Parameter Identification", Technical Memorandum DSM-29, Space Mechanics Directorate, Department of Communications, May 1983.

[3] F.R. Vigneron, "A Structural Dynamics Model for Flexible Solar Arrays of the Communications Technology Satellite", Communications Research Centre Report No.1268, April 1975.

[4] K.W. Lips, "Mode Shapes and Modal Frequencies for the Experimental Solar Array via Continuum Modelling", Memorandum to F. Vigneron, File DSM 5440-2, October 4, 1983, Department of Communications, Ottawa.

[5] G. Hok, "Responses of Linear Resonant Systems to Excitation of a Frequency Varying Linearly with Time", Journal of Applied Physics, August 1948, Vol.19.

[6] T.D. Harrison, "Communications Technology Satellite Deployed Solar Array Dynamics Tests", CRC Report No.1264, January 1975.

[7] Massoud, Beliveau and Bourassa, "Identification Methods for Determination of Structural Properties of Satellite Substructure", University of Sherbrooke, 1983.

[8] S. Draisey, "Modal Survey Test - Solar Array - Test Plan/Procedure", SPAR-TP.201, February 1983.

[9] F. Rimrott, "Development of Methods for Modal Test of Large Lightweight Space Structures", SPAR-P.879, Issue B, June 1982.

[10] Modal Plus-7 Manual, Structural Dynamics Research Corporation.

[11] Mutch, Vigneron, Vold, "The Dynamic Analysis of a Space Lattice Structure via the Use of Step Relaxation Testing", to be presented at the 1984 IMAC Conference.

[12] Clough and Penzien, Dynamics of Structures. McGraw-Hill, 1975.

[13] Bendat and Piersol, Random Date: Analysis and Measurement Procedures. Wiley-Interscience, 1971.

[14] R.D. Blevins, Flow Induced Vibration. Van Nostrand Reinhold Company, 1977.

APPENDIX H

Hilbert Transform

Subroutine to Calculate Hilbert Transform

```
SUBROUTINE HLD1        74/74   OPT=1                    FTN 4.6+43

 1                SUBROUTINE HLD1
                  COMMON/HIL81/A,X,Y
                  DIMENSION B(19),W(5)
                  DATA M/19/,M1/9/,M2/5/,LOC/0/,W/0.62421036,0.17695171,
 5               10.07470435,0.02874678,0.0072805927
                  IF(LOC.NE.0)GO TO 10
                       DO 5 I=1,M
                       B(I)=0.
                5      CONTINUE
10              10     LOC=LOC+1
                  IF(LOC.GT.M)LOC=1
                  B(LOC)=A
                  SUM=0.
                  K=LOC-M1
15                IF(K.LT.1)K=K+M
                       DO 15 I=1,M2
                       J1=K-2*I+1
                       IF(J1.LT.1)J1=J1+M
                       J2=K+2*I-1
20                     IF(J2.GT.M)J2=J2-M
                       SUM=SUM+(B(J1)-B(J2))*W(I)
               15      CONTINUE
                  X=B(K)  <- shifted function (by 10 steps)
                  Y=SUM   <- Hilbert transform of shifted function
25                RETURN
                  END
```

The accuracy of this routine is dependant on the choise of samples per cycle of the function. Optimum are from 3 to 8.

```
      PROGRAM HTFV(INPUT,OUTPUT,TAPE4=INPUT,TAPE5=OUTPUT)
      COMMON/HILB1/A,X,Y
      DIMENSION B(100),W(50)
      DATA PI/3.1415927/
      DMP(XI,XO)=ALOG(XI**2+XO**2)
      WRITE(5,4)
    4 FORMAT(1H1,60H      A     TH          Y=HILB     X=SHIFT A   TRUE RESULT
     1 CALC     )
            DO 10 II=1,200
            I=II-1
            TH=FLOAT(I)*2.0*PI/7.
            A=COS(TH)*EXP(-.006*I)
            T=SIN(TH)*EXP(-.006*I)
            CALL HLB1
      TRD=DMP(A,T)
      CAL=DMP(X,Y)
      WRITE(5,6)A,TH,Y,X,TRD,CAL
    6       FORMAT(1H , 4F10.4,2E10.4)
   10 CONTINUE
      STOP
      END
```